Climate Change Impacts on Climate Variables for a Deep Geological Repository (Ignace Study Area)

NWMO-TR-2020-04 **December 2020**

Andre Schardong, Patrick Breach, Janya Kelly, Sean Capstick

Golder Associates Ltd

nwmo

NUCLEAR WASTE MANAGEMENT ORGANIZATION

SOCIÉTÉ DE GESTION DES DÉCHETS NUCLÉAIRES

Nuclear Waste Management Organization
22 St. Clair Avenue East, 6th Floor
Toronto, Ontario
M4T 2S3
Canada

Tel: 416-934-9814
Web: www.nwmo.ca

Climate Change Impacts on Climate Variables for a Deep Geological Repository (Ignace Study Area)

NWMO-TR-2020-04

December 2020

Andre Schardong, Patrick Breach, Janya Kelly, Sean Capstick

Golder Associates Ltd

Document History

Title:	Climate Change Impacts on Climate Variables for a Deep Geological Repository (Ignace Study Area)		
Report Number:	NWMO-TR-2020-04		
Revision:	R001	Date:	December 2020
Golder Associates Ltd			
Authored by:	Andre Schardong and Patrick Breach, Golder Associates Ltd		
Verified by:	Janya Kelly, Golder Associates Ltd		
Approved by:	Sean Capstick, Golder Associates Ltd		
Nuclear Waste Management Organization			
Reviewed by:	Helen Leung, Jeremy Chen and Melissa Mayhew		
Accepted by:	Paul Gierszewski		

Revision Summary		
Revision Number	**Date**	**Description of Changes/Improvements**
R000	2020-06-15	Initial issue
R001	2020-12-07	Inclusion of additional climate variables

ABSTRACT

Title: **Climate Change Impacts on Climate Variables for a Deep Geological Repository (Ignace Study Area)**
Report No.: **NWMO-TR-2020-04**
Author(s): Andre Schardong and Patrick Breach
Company: Golder Associates Ltd
Date: December 2020

The Nuclear Waste Management Organization (NWMO) completed a literature review on climate change impacts and developed a preferred method to assess the climate change impacts on probable maximum precipitation (PMP). The objective of this study is to apply the preferred method to assess the climate change impacts on the PMP and Intensity-Duration-Frequency (IDF) amounts for a case study (Ignace study area) during currently planned Deep Geological Repository (DGR) implementation periods for used fuel. Additional climate variables including monthly temperature and precipitation statistics, WMO climate indices, potential evapotranspiration, drought index, wind speed and relative humidity have been included to support further assessments at the Ignace study area. Daily timeseries for the current climate and future projections have been developed to support climate change impact studies at the site.

The results have been presented for a range of global climate models within the ensemble and are expressed in terms of percentiles, so that the level of acceptable risk can be selected by using the desired percentile. Climate extreme projections for the 2050s and 2080s are indicating a future that is likely to be wetter, which is consistent with the current and future climate projections. Both the 1-day PMP values and the 1-day rainfall events are projected to increase during the 2050s and 2080s at the 50^{th} percentile level.

There is a level of inherent uncertainty when projecting future climate; however, the approach taken in this study aims to address this uncertainty by relying on a multi-model ensemble and providing percentiles. The estimated percent changes to precipitation through the PMP and IDF curves has been described in terms of percentiles, allowing for different levels of acceptable risk. The selection of future projections for a climate change risk assessment should be based on the balance between the extra investment and consequential risks.

Based on Golder's experience in climate change projections, the proposed approaches are considered best guidance for the industry.

TABLE OF CONTENTS

LIST OF TABLES

Page

LIST OF FIGURES

Page

GLOSSARY OF TERMINOLOGY AND ABBREVIATIONS

Term/Acronym	Definition
AD	Anderson-Darling
AHCCD	Adjusted and Homogenized Canadian Climate Data
AMS	Annual Maximum Series
AR5	Fifth Assessment Report
BCCAQ	Bias Correction/Constructed Analogues with Quantile mapping reordering
CC	Climate Change
CCCR	Canada's Changing Climate Report
CDF	Cumulative Density Function
CMIP	Climate Model Intercomparison Project
CS	Climate Station
CSA	Canadian Standards Association
DAD	Duration-Area Depth
DGR	Deep Geologic Repository
ECCC	Environment and Climate Change Canada
ECMWF	European Centre for Medium-Range Weather Forecasts
ECP	Extended Concentration Pathways
EQM	Equidistant Quantile Matching
EV1	Extreme-Value Type 1 Distribution (Gumbel)
EV2	Extreme-Value Type 1 Distribution (Fréchet)
EV3	Extreme-Value Type 1 Distribution (Weibull)
GCM	Global Climate Model
GEV	Generalized Extreme Value
IDF	Intensity-Duration-Frequency
IPCC	Intergovernmental Panel on Climate Change
KS	Kolmogorov-Smirnov

Term/Acronym	Definition
LOCA	Localized Constructed Analogues
LP3	Log-Pearson Type 3
MERRA	Modern-Era Retrospective analysis for Research and Applications
MNRF	Ministry of Natural Resources and Forestry
MTO	Ministry of Transportation Ontario
NASA	National Aeronautics and Space Administration
NWMO	Nuclear Waste Management Organization
OFAT	Ontario Flow Assessment Tool
OMNR	Ontario Ministry of Natural Resources
PDF	Probability Density Function
PE3	Pearson Type 3
PMP	Probable Maximum Precipitation
PPT	Precipitation
PWC	Precipitable Water Content
PWM	Probability Weighted Moment
QDM	Quantile Delta Mapping
RCP	Representative Concentration Pathway
RCS	Regional Climate Station
RM	Ratio Method
SRES	Special Report on Emissions Scenarios
UNEP	United Nations Environment Program
WCRP	World Climate Research Program
WMO	World Meteorological Organization

1. INTRODUCTION

A changing climate within Ontario's watersheds may present physical risks to infrastructure if designs do not consider the impacts of these changes. Golder Associates Ltd. (Golder) was retained to apply the developed methodology by the Nuclear Waste Management Organization (NWMO) in Wood (2019) to assess the impacts of climate change on probable maximum precipitation (PMP) events for two study areas for a Deep Geologic Repository (DGR) for used fuel. In addition to the assessment of future PMP events, future Intensity-Duration-Frequency (IDF) values are estimated for 100-year and 500-year return periods, and additional climate variables including seasonal, annual, and monthly temperature and precipitation statistics are calculated along with derived climate variables including rain and snow, snow depth, potential evapotranspiration, drought index, and qualitative information for wind speed and relative humidity.

Previous studies undertaken within the Ontario Power Generation's DGR Project for low and intermediate level radioactive waste at the Bruce nuclear site have evaluated the potential for flooding to impact the operations of the DGR based on the current climate (AMEC 2011). In the future, projected higher temperatures may change the capacity of the atmosphere to hold water, potentially resulting in more frequent and intense storms. This projected change in climate may increase vulnerabilities to potential climate extremes at the two DGR study areas (i.e., Ignace and South Bruce) for used fuel. Siting the potential placement of the DGR within these two study areas must consider the range of credible storms within the watershed to appropriately design the associated storm water management system. Therefore, the first step towards potential placement of the DGR is to understand how the projected changes in climate may impact PMP and IDF values at the study areas using the method developed in Wood (2019).

This report documents the climate change impacts on IDF, PMP, and additional climate variables in the Ignace study area. The approach and methodology are summarized first to characterize the current and future climate conditions in the Ignace study area (Section 2). Detailed descriptions of the data sources and approaches used for both the climate baseline and future climate projections are provided in Appendix A. Next, for the baseline and future climate conditions, IDF, PMP, and additional climate variable values are estimated respectively in Section 3 and Section 4. Detailed statistics for PMP and IDF estimates are given in Appendix B, while daily current and future climate timeseries for the additional climate variables are provided in Appendix C. A qualitative climate assessment for considering the projected changes in PMP, IDF, and additional climate variables beyond the year 2100 is given in Section 5. Uncertainty of climate change projections and recommendations on how to use the data are discussed in Section 6 and Section 7, respectively. Finally, conclusions and recommendations are provided in Section 8.

2. APPROACH AND METHODOLOGY ON PMP, IDF, AND ADDITIONAL CLIMATE VARIABLE ANALYSES

Understanding what the current climate conditions of the study area are and understanding how they are projected to change under future climate change is fundamental to the following approach. The discussion of climate vulnerability is focused around rainfall events, namely PMP and IDF values with different return periods and durations. Contextual climate information is also provided for additional climate variables. The approach follows the key steps in Figure 1. The following sections provide high level overviews of the methodologies used to develop the current climate and future projected climate datasets used in this assessment. More detailed information on each methodology is provided in Appendix A.

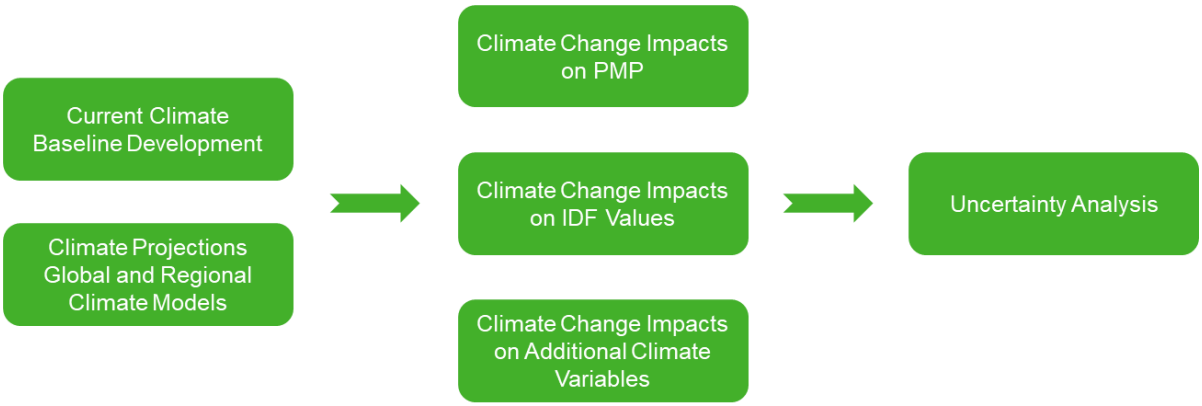

Figure 1: High Level Step-Wise Approach

2.1 CURRENT CLIMATE METHODOLOGY ON PMP, IDF, AND ADDITIONAL CLIMATE VARIABLE ANALYSES

Understanding the current climate and current climate trends is important when evaluating current design parameters. Where available, the climate baseline is grounded in observations from local climate observation stations. The baseline is established using available local climate stations and/or publicly available nearby regional climate stations infilled with reanalysis data whenever possible (to meet data completeness requirements, such as only considering observations where at least 90% observations are available in any given year or month). Before infilling, the reanalysis data are compared and correlated to available regional climate stations.

Reanalysis data from Version 2 of the National Aeronautics and Space Administration's (NASA's) Modern-Era Retrospective analysis for Research and Applications (MERRA-2) and the European Centre for Medium-Range Weather Forecasts (ECMWF) Re-Analysis (ERA5) data are used to represent current climate or to infill the missing data from observations. R-squared (R^2) statistics is calculated between MERRA-2 and ERA5 and is used to complete missing historical observed dataset. The R^2, also known as coefficient of determination, provides a measure of how well observed outcomes are replicated by the regression line fitted. It ranges from 0 to 1, 1 being a perfect fit.

Using the daily current climate baseline precipitation, the PMP is calculated according to Hershfield Method (Chapter 4 in WMO 2009a) and the DAD (duration-area-depth) curves discussed in Appendix A of this report. A second method (the Transposition method) relies on observations of significant storms nearby the study area and is accomplished by construction of DAD curves. Using the same daily current climate baseline precipitation, IDF values are then calculated for various durations (1-day through 120-day) and return periods (1 in 100 years and 1 in 500 years). PMP is calculated for 1-day, 2-day, and 3-day durations. The IDF values for the current climate are calculated by adjusting a statistical distribution to the Annual Maximum Series (AMS) based on daily observed data. The AMS is a record of the largest 1-day rainfall for each year in a series and is calculated by extracting the maximum value of the daily precipitation series for each year. Three statistical distributions (Gumbel, Generalized Extreme Value – GEV, Pearson/Log-Pearson Type 3) are tested against the available data and the parameters are estimated using the method of L-moments (Hosking and Wallis 1997), following the approach adopted by Environment and Climate Change Canada - ECCC (ECCC 2019).

Annual and monthly temperature and precipitation statistics are calculated by resampling the daily current climate dataset. Derived variables including rain, snow, snow depth, drought index, WMO climate indices, and potential evapotranspiration use precipitation and temperature values from the current climate dataset. Rain, snow and snow depth are calculated using methods adopted by ECCC, drought index is calculated using the Standardized Precipitation and Evapotranspiration Index (SPEI) method of Vincente-Serrano et al. (2010), WMO Indices are calculated using the methods of WMO (2009b), and potential evapotranspiration is calculated using the Hargreaves method (Hargreaves and Samani 1985). A high-level flowchart with the analyses conducted is presented in Figure 2.

The detailed description of the methods is presented in Appendix A.2.

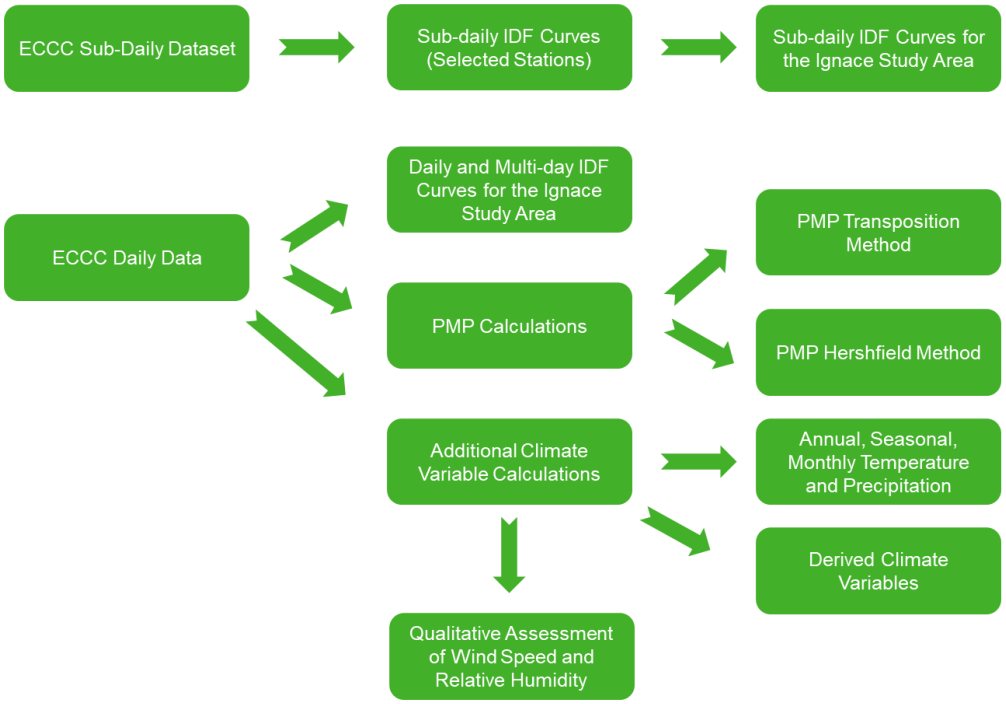

Figure 2: High-Level Summary of Evaluation of Current Climate on PMP, IDF, and Additional Climate Variable Analyses

2.2 FUTURE CLIMATE METHODOLOGY ON PMP, IDF, AND ADDITIONAL CLIMATE VARIABLE ANALYSES

The approach to evaluating future climate impacts on precipitation uses the state of science and publicly available climate projections to complete the climate change impact assessment on the PMP and the IDF values. The range of projected future climate depends on the emission scenario used to project the future climate conditions as well as selected global climate model (GCM). Since no one model or climate scenario can be viewed as completely accurate, the Intergovernmental Panel on Climate Change (IPCC) recommends that climate change assessments use as many models and climate scenarios as possible, or a "multi-model ensemble". For this reason, the multi-model ensemble approach is used here to describe the probable range of results using percentile levels. Changes to both PMP and IDF curves are expressed as percent changes from the model baseline. For the additional climate variables, temperature-based statistics and the WMO indices are expressed as absolute changes while all other variables are expressed as percentage changes.

For this study, Golder developed methods to extract climate data (precipitation and temperature) from the multi-model ensemble for model baseline (1950-1993), the mid-century (2041- 2070), and end-of-century (2071 through to 2100) time periods for the PMP and IDF. The baseline period of 1950 to 1993 was selected based on a combination of data availability constraints (observed data from relevant climate stations has data only until the year 1993), as well as the need for a long observation period to allow for more accurate analysis of precipitation extremes in the form of PMP and IDF curves. The future time periods of 2041 to 2070 (2050s) and 2071 to 2100 (2080s), chosen to be a length of 30 years (minimum number of years needed to represent a climate normal as recommended by the World Meteorological Organization (WMO)), represent the changes in climate for mid-century and end of century time periods and are applicable to the site characterization, construction and operational periods. Currently, downscaled climate projections only extend out to the year 2100, making the 2071 to 2100 time period the furthest point into the future for detailed assessment. A qualitative assessment is provided for time periods beyond 2100 to cover the monitoring and decommissioning periods for the project. Emission scenarios RCP 2.6, RCP 4.5, and RCP 8.5 from the IPCC Fifth Assessment Report (AR5) (IPCC 2013) are used to describe the model baseline, mid-century and end-of-century time periods. The qualitative assessment past 2100 relies on projections available in literature.

Daily downscaled climate projections for precipitation and minimum and maximum temperature are obtained for the multi-model ensemble. This ensemble consists of statistically downscaled climate scenarios that correspond to a particular GCM for a given Representative Concentration Pathway (RCP). These daily time-series are then used in conjunction with methods for estimating PMP, snowfall, and moisture to establish initial ranges for PMP-related variables (based on literature values and results from historic analysis of PMPs), including precipitable water and moisture content, and rainfall. Ranges for previously identified ancillary factors (such as snowpack and snowmelt) are also established. The ranges are then presented as percent changes between the baseline period and the selected future periods across all GCMs and RCPs.

Using the historic data and GCM ensemble results, projections for future IDF values are developed. These projections can be used to understand aspects of the PMP storm (including sub-daily rainfall distribution) and how the PMP storm compares to more frequent design storms typically used in non-critical infrastructure design. These IDF values are done using two methods currently used by Golder to estimate the changes to IDF distributions: (1) Quantile Delta Mapping (QDM) method and; (2) the Ratio Method (RM).

A high-level flowchart with the PMP and IDF analyses conducted and presented in this report are presented in Figure 3. The future projected changes in PMP are calculated using the moisture maximization method and the Hershfield method. The moisture maximization method is not used for current climate conditions, since it produces an analogous vapour pressure result (rather than an absolute rainfall depth value), and can only be used to estimate the change in PMP (i.e., based on change in vapour pressure) rather than provide an absolute value. Comparing the modelled future climate to model baseline produces changes in specific humidity, so it can be used to estimate percent change in PMP depths between baseline and future conditions. Ensemble statistics in terms of percentiles are calculated across the results from both methods. The daily rain and snowmelt projected changes are calculated using the same methodology as for the current climate but applied to all ensemble members and presented using percentiles across the ensemble.

In Figure 4, the analyses conducted for the additional climate variables and how they relate to one another are presented. Future change in rain, snow, snow depth, WMO climate indices, and potential evapotranspiration are derived from both precipitation and temperature values from the downscaled climate projections. The drought index is estimated using the Standardized Precipitation and Evapotranspiration Index (SPEI), which incorporates precipitation projections and potential evapotranspiration derived from the temperature projections. Qualitative analyses are carried out for wind speed and relative humidity, as these variables are not included in the statistically downscaled model ensemble. Published values applicable to the Ignace study are used to infer how these variables may change in the future.

The detailed description of the methods for future climate is presented in Appendix A.3.

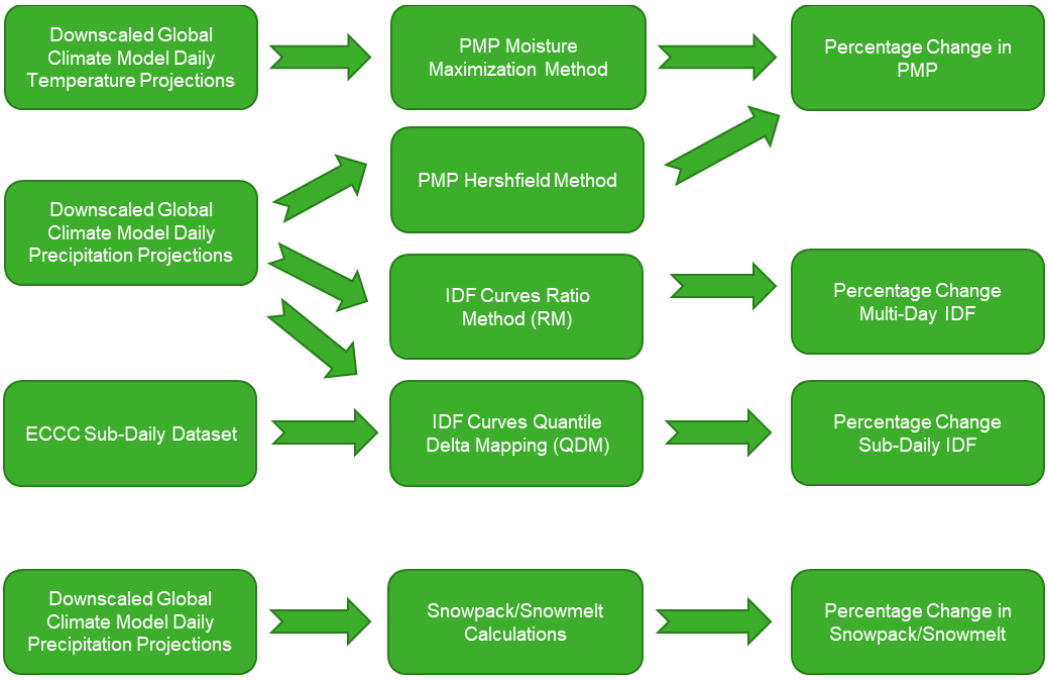

Figure 3: High-Level Summary of Evaluation of Future Climate on PMP and IDF Estimates

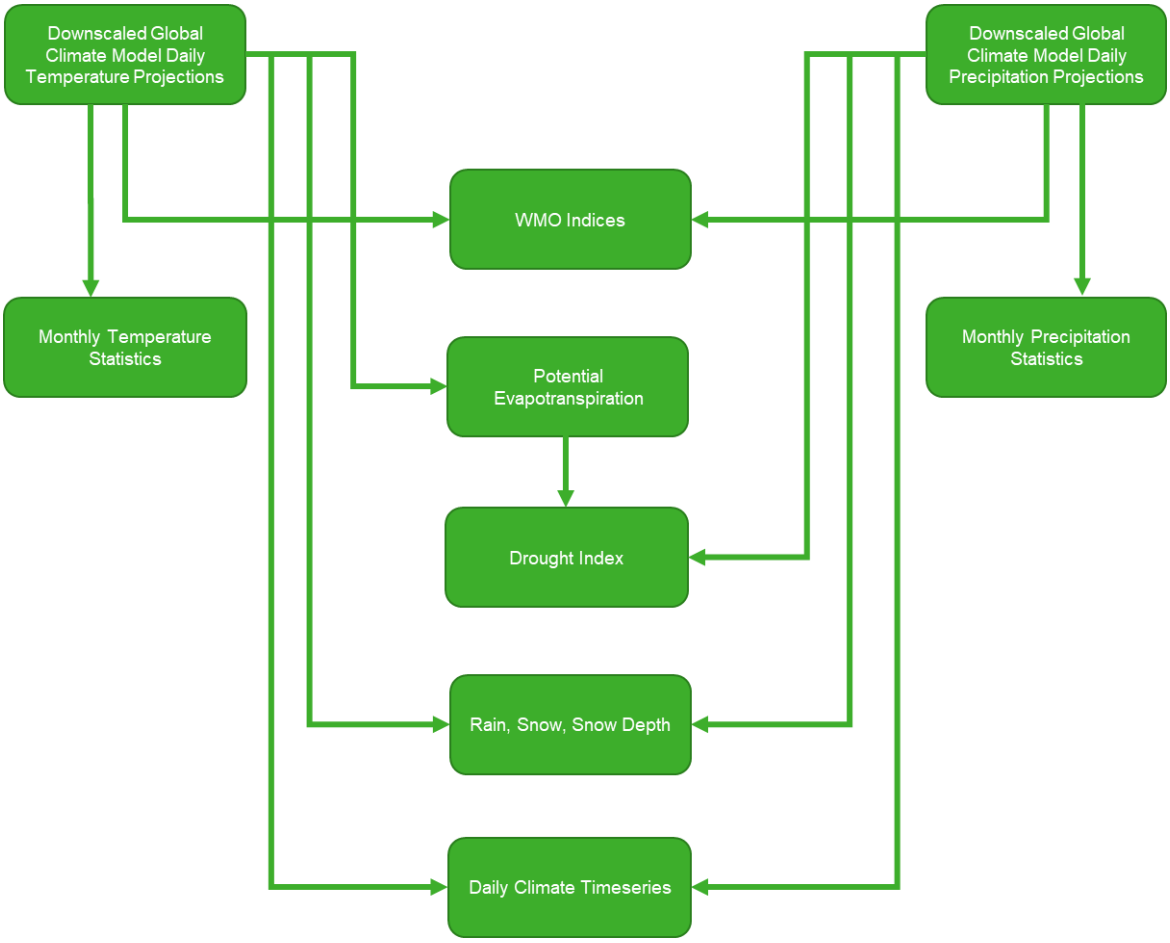

Figure 4: High-Level Summary of Evaluation of Future Climate on Additional Climate Variable Estimates

3. ANALYSES OF CURRENT CLIMATE ON PMP, IDF, AND ADDITIONAL CLIMATE VARIABLES

The following sections outline the development of the climate baseline and calculations of the baseline IDF curves, PMP, and additional climate variables. The baseline was developed using the high-level described in Section 2.1. The detailed description of the methods is presented in Appendix A.2. Select tables presented in this section are coloured using a gradient to aid in the visual representation of the values. The colour gradients provide a relative indication of the highest (red) and lowest (green) values with transitional colours in between. Colours cannot be compared between tables, as the colour scale is relative for each.

3.1 CLIMATE BASELINE DEVELOPMENT

The current climate baseline was developed using publicly available regional climate stations using the methodology presented in Appendix A.2.

The following sections describe the three climate datasets used for the various analyses in this report:

1) Daily dataset to screen for significant storms for the Transposition method and the construction of the DAD curves as used in Wood (2019).
2) Daily infilled dataset at the Ignace study area for the analysis of daily and multi-day IDF curves, the PMP statistical (Hershfield) method, and the analysis of rainfall on snow and snowpack.
3) Data from the ECCC Engineering Database for the calculation of the sub-daily IDF curves.

3.1.1 Daily Climate Dataset

The main criteria for the climate stations selected were the length of record (minimum 30 years of data), proximity to the study area, and the availability of continuous precipitation data. Other criteria are listed in Appendix A.2. All publicly available stations within about 100 km from the study area were considered for the analysis of regional storms. The candidate stations with daily data for the Ignace study area were collected from Environment and Climate Change Canada (ECCC 2019). The list of the selected stations is presented in Table 1 and the location of the stations relative to the study area is provided in Figure 5. These stations were primarily used to screen for significant storms in the study area and to assist in calculating the DAD curves. The data available for the DAD analysis are less critical, since the interest is in specific (large) events.

Two of the stations listed, Ignace - 6033690 and Ignace TCPL 58 - 6033697 located in the center of the study area, were analyzed further to create a consolidated baseline for the Ignace study area. Although these stations only provide data up to 1993, together they provide 81 years of continuous data, allowing for more reliable estimates of extreme rainfall statistics including PMP and IDF. The geographical siting of the other stations was deemed to be too dissimilar to the Ignace area to be considered for correlation (e.g., differences in factors such as distance from the site, elevation difference, proximity to water bodies). Due to the localized nature of precipitation, these factors are considered important in order to develop a more reliable current climate dataset.

Table 1: Climate Station Properties

Station Name	Climate ID	Latitude and Longitude	Elevation (masl [2])	Distance from Ignace Study Area (km)	Years Available	Notes
ATIKOKAN (AUT) [3]	6020LPQ	48.76, -91.63	389.3	73.5	2000-2019	Used to screen for large storms and Sub-daily IDF
ATIKOKAN	6020379	48.75, -91.62	395.3	74.6	1966-1988	Used to screen for large storms
DRYDEN	6032117	49.78, -92.83	371.9	93.4	1914-1997	Used to screen for large storms
DRYDEN A [1]	6032119	49.83, -92.75	412.7	90.9	1970-2005	Used to screen for large storms
DRYDEN REGIONAL	6032125	49.83, -92.74	412.7	90.3	2010-2019	Used to screen for large storms
IGNACE	6033690	49.42, -91.65	446.5	0.7	1889-1971	Used to screen for large storms and define the baseline at Ignace study area, PMP estimates and daily IDF Curves
IGNACE TCPL 58	6033697	49.48, -92	473	25.5	1969-1993	Used to screen for large storms and define the baseline at Ignace study area, PMP estimates and daily IDF Curves
KENORA RCS [3]	6034073	49.79, -94.38	412.7	200.5	2008-2019	Used to screen for large storms and Sub-daily IDF
MARTIN TCPL 60	6035002	49.28, -91.23	470.6	34.9	1969-1984	Used for screen large storms
MINE CENTRE	6025203	48.77, -92.62	342.9	100.7	1914-2005	Used for screen large storms
SIOUX LOOKOUT A [1, 3]	6037775	50.12, -91.9	383.1	79.8	1938-2013	Used to screen for large storms and Sub-daily IDF
SIOUX LOOKOUT A	6037776	50.11, -91.91	383.1	78.9	2013-2019	Used to screen for large storms
GERALDTON A [1, 3]	6042716	49.78, -86.93	348.4	343.6	1981-2015	Used to screen for large storms
GRAHAM A	6042975	49.27, -90.58	503.2	80.1	1948-1967	Used to screen for large storms
QUORN	6046811	49.42, -90.9	444.7	55.0	1915-1960	Used to screen for large storms
THUNDER BAY CS [3]	6048268	48.37, -89.33	199.4	206.7	2003-2019	Used to screen for large storms and Sub-daily IDF
UPSALA (AUT)	6049095	49.03, -90.47	488.5	96.8	1973-2019	Used to screen for large storms
UPSALA	6049096	49.05, -90.47	483.7	95.8	1947-1972	Used to screen for large storms
UPSALA TCPL 62	6049098	49.03, -90.52	492.9	93.6	1970-1986	Used to screen for large storms
WIARTON A [1, 3]	6119500	44.75, -81.11	222.2	954.1	1947-2014	Used to screen for large storms and Sub-daily IDF

Notes: [1] Stations available in the AHCCD dataset.
[2] Meters above sea level.
[3] Included in the Engineering Dataset for Sub-Daily IDF curves analysis – See Table 4.

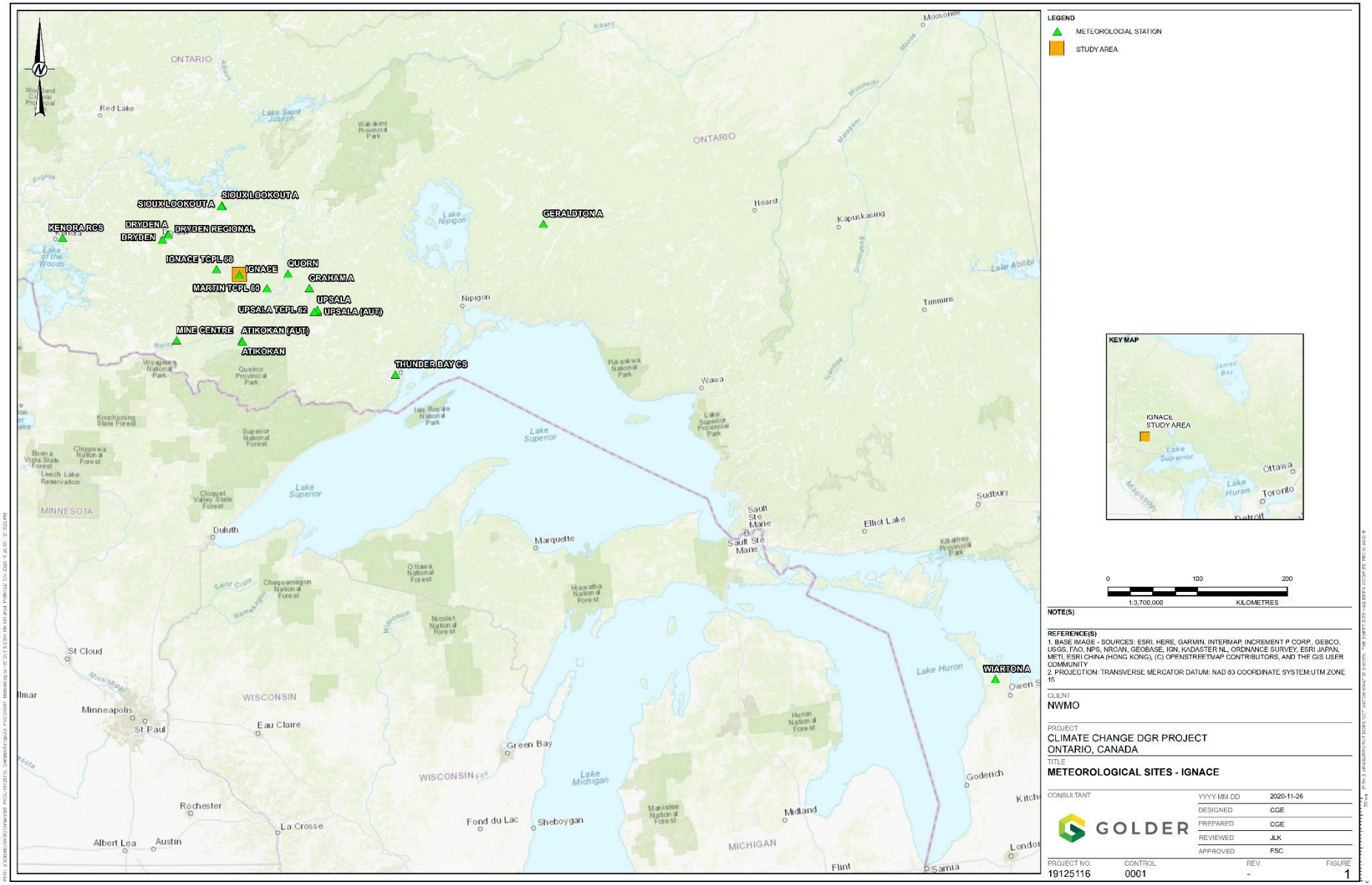

Figure 5: Map of Ignace Study Area Location and Regional Climate Stations

A third subset of stations was selected from the ECCC Engineering Database for the sub-daily IDF curves as noted in Table 1 (notes column) and listed separately in Table 4. The selected stations for sub-daily IDF analysis are discussed in Section 3.1.3.

Some of the stations listed in Table 1 are available in the daily precipitation AHCCD dataset from Environment and Climate Change Canada (ECCC 2019). For the investigations of candidate storms for the calculation of the PMPs and the DAD curves, the data from the AHCCD were compared to the original (raw) records from ECCC and the higher value was selected if concurrent records are found.

3.1.2 Daily Infilled Dataset Series for the Ignace Study Area

A daily dataset was defined for the Ignace study area using stations Ignace (6033690) and Ignace CPL 58 (6033697) to calculate the daily and multi-day IDF curves, the PMP Hershfield method, and the rainfall on snow analysis.

The Ignace (6033690) station has long records dating back to 1889 and ending in 1971. Only years and months with at least 90% of the data available were considered. Another nearby station, Ignace TCPL 58 (6033697), was also considered using the same data completeness criteria.

After applying the data completeness criteria, 54 years of the data were available for the analysis. Of those, four years (1916, 1950, 1955 and 1959) have missing data higher than 5% (less than 10%) and were removed from the series given that some of the months did not meet the completeness criteria. The year 1891 was also removed due to missing temperature data.

Infilling for the Ignace (6033690) station was not possible, as the reanalysis data from MERRA-2 and ERA5 are only available from 1979 and 1981 onwards. For Ignace TCPL 58 (6033697) station, ERA5 and MERRA-2 were both tested against the concurrent period from 1979 and 1981 to 1993. MERRA-2 presented a better agreement with observations from Ignace TCPL 58 (6033697) station, with R-squared (R^2) statistics for a linear regression of 0.82, while ERA5 was lower at 0.63. (The infilling process is discussed in Appendix A.2.1).

For Ignace TCPL 58 (6033697) station, data records were available from 1969 to 1993. After applying the data completeness analysis, only 12 years of data were available. The data completeness levels were below 90% for the years 1984 to 1993. Some of the missing records during the wet months from May to October were infilled using reanalysis data (MERRA-2) with the regression equations presented in Table 2. The MERRA-2 reanalysis data are available past 1992 up to present; however, no observations are available from the stations at the Ignace area to support the extension of the data series only using the modelled data.

Given the proximity of the two stations and similar elevation and latitude, a combined series was created after infilling procedure to represent the Ignace study area resulting in a lengthy series with records from 1914 to 1992. The annual maximum of the daily total precipitation of the combined series is presented in Figure 6 and Table 3.

The dashed gray trend line in Figure 6 represents the combined series and the solid black trend line represents Ignace (6033690) station. The trends align well, validating the use of the combined longer series. Although more recent observations are missing, the series has 72 years of valid records that were used for the extreme precipitation analysis (daily and multi-day IDF curves, PMP Hershfield (statistical) method, and the rainfall on snow analysis) presented in the following sections.

Table 2: Correlation between Ignace TCPL 58 Station and MERRA-2 Data during 1981-1992

Climate Variable	Percentage Infilled [(1)]	Daily R^2	Infilling Equation
Daily Maximum Temperature	7%	0.97	Infilled=0.960 x MERRA-2
Daily Minimum Temperature	7%	0.97	Infilled=0.956 x MERRA -2
Daily Mean Temperature	7%	0.99	Infilled=0.967 x MERRA -2
Daily Total Precipitation	8%	0.82	Infilled=0.733 x MERRA -2

Note: [(1)] Observations from Ignace TCPL 58 station are available from 1969 through to 1993. MERRA-2 is available from 1981.

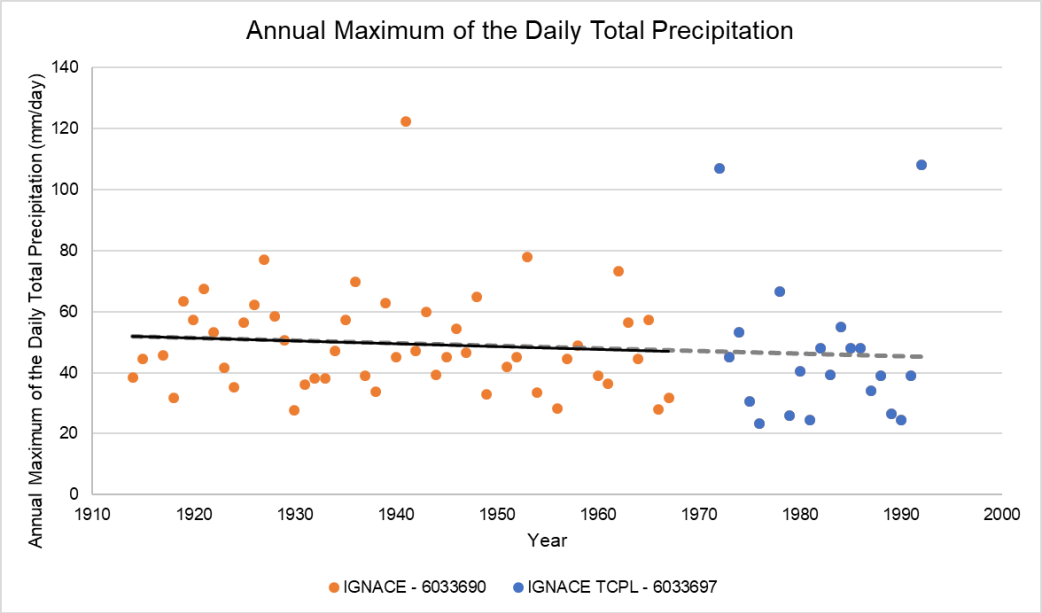

Figure 6: Annual Maximum of the Daily Total Precipitation Series for Ignace and Ignace TCPL 58

Table 3: Annual Maximum of the Daily Total Precipitation Series for Ignace and Ignace TCPL 58

Year	PPT (mm)	Year	PPT (mm)	Year	PPT (mm)	Year	PPT (mm)
1914	38.4	1933	38.1	1952	45.2	1976	23.4
1915	44.5	1934	47.0	1953	78.0	1978	66.7
1917	45.7	1935	57.2	1954	33.5	1979	26.0
1918	31.8	1936	69.9	1956	28.2	1980	40.4
1919	63.5	1937	38.9	1957	44.5	1981	24.5
1920	57.2	1938	33.8	1958	49.0	1982	48.0
1921	67.6	1939	62.7	1960	38.9	1983	39.4
1922	53.3	1940	45.2	1961	36.3	1984	55.0
1923	41.7	1941	122.4	1962	73.2	1985	48.1
1924	35.1	1942	47.2	1963	56.4	1986	48.0
1925	56.4	1943	59.9	1964	44.5	1987	34.0
1926	62.2	1944	39.4	1965	57.4	1988	39.0
1927	77.0	1945	45.2	1966	27.9	1989	26.6
1928	58.4	1946	54.4	1967	31.8	1990	24.4
1929	50.5	1947	46.5	1972	106.9	1991	39.0
1930	27.7	1948	64.8	1973	45.2	1992	108.0
1931	36.1	1949	33.0	1974	53.3	---	---
1932	38.1	1951	41.9	1975	30.5	---	---

Note: (1) PPT denotes the annual maximum daily total precipitation (mm).

3.1.3 IDF Engineering Dataset

The list of stations used to support the analysis of the sub-daily IDF curves (Section 3.2) was obtained directly from the ECCC IDF Engineering Database (ECCC 2019). The stations were selected based primarily on the distance from the Ignace study area and the length of records of at least 30 years. The stations used are listed in Table 4. It is worth noticing that some of the stations Geraldton A, Thunder Bay CS and Wiarton A are located farther from the Ignace area.

The data from the ECCC IDF Engineering are provided in the form of preprocessed annual maximum series (AMS) for selected sub-daily durations and they are verified by ECCC for quality assurance (ECCC 2019).

Table 4: Stations from the Engineering Data Set for Sub-daily IDF Curves

Name	Climate ID	Years Available	Elevation (masl)	Latitude and Longitude	Distance from Ignace Study Area (km)
ATIKOKAN (AUT)	6020LPQ	1967-2007	389	48.76, -91.63	73.5
KENORA RCS	6034073	1966-2011	412	49.79, -94.38	200.5
SIOUX LOOKOUT A	6037775	1963-2007	383	50.12, -91.9	79.8
GERALDTON A	6042716	1952-2007	348	49.78, -86.93	343.6
THUNDER BAY CS	6048268	1952-2012	199	48.37, -89.33	206.7
WIARTON A	6119500	1976-2007	222	44.75, -81.11	954.1

3.2 BASELINE IDF CURVES

IDF curves were calculated using the selected stations in the baseline development for selected return periods including 100-year and 500-year return periods. The IDF curves were compared to other available IDF calculations for the region, including historical precipitation trends. Two distinct analyses are presented in the next sections. The first analysis (Sections 3.2.1 to 3.2.3) using the sub-daily ECCC Engineering Database is an interpolated sub-daily IDF curves from selected stations for the Ignace study area and includes a comparison to other sources. The second analysis using the Annual Maximum of the Daily Total Precipitation time series (Section 3.1.2) calculates the daily and multi-day IDF curves for the Ignace study area (Section 3.2.4).

3.2.1 Sub-Daily IDF Curves for the Selected Stations

For each of the selected stations listed in Table 4, three statistical tests including the Anderson-Darling, Chi-squared and Kolmogorov-Smirnov tests were used to select the best statistical distribution to fit the data from the four distributions- Gumbel (EV1), Generalized Extreme Value (GEV), Pearson Type 3 (PE3), and Log-Pearson type 3 (LP3) as described in Appendix A.2.2.3. This approach ensures that the most suitable distribution is used for each of the station to fit the IDF curves, i.e., better fitted to the observations. Table 5 presents the results of each statistical test for each of the five stations. The table shows how many times the distribution was selected for each of the sub-daily durations. The most frequent distribution was then used for that specific station for all sub-daily durations and the selected return periods including 100 and 500-years. The summary of the IDF curves for selected return periods, including 100 and 500-year, is presented in Table 6. The colour scale assists in the reading of the results and the analysis of the magnitude of the projections. The scale is presented for each of the sub-daily durations and grouped for the five stations. The cell space filled by the colour bars are relative to the correspondent precipitation amounts and proportional to the maximum for that duration. The GEV distribution was the most often selected for three of the stations, the Log-Pearson Type 3 for two stations, and the Gumbel and Pearson Type 3 for one station each. For Wiarton A station, the GEV and LP3 distributions yielded inconsistent estimates for 2, 6 and 12- hours durations compared to the 24-hour duration for higher return periods (greater than 100-years), and therefore, the Gumbel distribution was used. A detailed analysis of the raw data ordered from ECCC would be required to analyze sub-daily durations of 2, 6 and 12 hours, which is out of the scope of this study.

Table 7 through Table 12 present the detailed IDF curve calculations for stations near the Ignace study area.

Table 5: Best Distribution for Each Climate Station (Number of Times Selected for the Sub-Daily Durations)

Station	Distributions			
	GEV	EV1	PE3	LP3
6020LPQ - ATIKOKAN (AUT)	3	1	0	5
6037775 - SIOUX LOOKOUT A	3	4	1	1
6042716 - GERALDTON A	5	1	2	1
6034073 - KENORA RCS	1	0	5	3
6048268 - THUNDER BAY CS	5	0	2	2
6119500 - WIARTON A	6	0	0	3

Table 6: IDF Curves Summary – Rainfall Accumulation (mm)

Station	Duration	Return Period (years)						
		10	20	50	100	500	1000	2000
ATIKOKAN (AUT)	5 min	12.3	13.9	16.0	17.7	21.8	23.7	25.7
SIOUX LOOKOUT A	5 min	13.7	15.9	18.6	20.7	25.5	27.5	29.6
WIARTON A	5 min	10.7	12.1	13.8	15.2	18.3	19.6	20.9
THUNDER BAY CS	5 min	12.1	14.1	16.7	18.7	23.7	25.9	28.1
KENORA RCS	5 min	14.9	16.5	18.4	19.7	22.4	23.5	24.6
GERALDTON A	5 min	10.3	11.4	12.7	13.6	15.2	15.8	16.4
ATIKOKAN (AUT)	10 min	17.2	18.8	20.7	22.1	25.2	26.5	27.8
SIOUX LOOKOUT A	10 min	20.0	23.2	27.3	30.3	37.4	40.4	43.5
WIARTON A	10 min	15.2	17.0	19.4	21.3	25.4	27.2	29.0
THUNDER BAY CS	10 min	17.7	20.3	23.8	26.3	32.3	34.9	37.5
KENORA RCS	10 min	20.8	23.2	26.1	28.1	32.6	34.4	36.1
GERALDTON A	10 min	15.8	18.0	20.8	22.8	27.4	29.3	31.2
ATIKOKAN (AUT)	15 min	22.4	24.9	28.1	30.5	36.1	38.5	41.0
SIOUX LOOKOUT A	15 min	23.2	26.8	31.5	34.9	43.0	46.4	49.9
WIARTON A	15 min	19.2	21.6	24.8	27.1	32.6	34.9	37.3
THUNDER BAY CS	15 min	21.9	25.7	30.9	35.0	45.6	50.6	55.8
KENORA RCS	15 min	26.2	29.8	34.3	37.6	44.8	47.9	50.9
GERALDTON A	15 min	19.5	22.3	25.8	28.3	33.9	36.3	38.6
ATIKOKAN (AUT)	30 min	28.3	31.5	35.8	39.1	47.1	50.8	54.5
SIOUX LOOKOUT A	30 min	29.7	34.3	40.2	44.7	55.0	59.5	63.9
WIARTON A	30 min	25.7	29.1	33.5	36.8	44.5	47.8	51.1
THUNDER BAY CS	30 min	29.3	34.5	41.7	47.4	61.9	68.6	75.8
KENORA RCS	30 min	35.3	40.7	47.7	52.8	64.2	69.1	73.9
GERALDTON A	30 min	23.8	26.1	28.6	30.1	33.1	34.1	35.0
ATIKOKAN (AUT)	1 hr	34.2	38.0	43.0	46.9	56.4	60.8	65.4
SIOUX LOOKOUT A	1 hr	34.9	40.1	46.7	51.8	63.3	68.3	73.3
WIARTON A	1 hr	35.2	40.5	47.4	52.6	64.5	69.6	74.7
THUNDER BAY CS	1 hr	37.5	45.6	57.8	68.5	99.2	115.6	134.3
KENORA RCS	1 hr	45.2	52.5	61.7	68.5	83.6	90.0	96.3
GERALDTON A	1 hr	29.7	33.4	37.9	41.1	48.0	50.7	53.4
ATIKOKAN (AUT)	2 hr	43.0	48.3	55.7	61.5	76.5	83.6	91.2
SIOUX LOOKOUT A	2 hr	46.1	53.4	62.7	69.7	86.0	92.9	99.9
WIARTON A	2 hr	46.1	53.4	62.8	69.9	86.2	93.2	100.2
THUNDER BAY CS	2 hr	45.2	54.8	69.7	82.9	122.0	143.3	168.0
KENORA RCS	2 hr	61.9	76.2	95.2	109.5	143.0	157.5	171.9
GERALDTON A	2 hr	34.7	39.4	45.6	50.4	62.1	67.3	72.6
ATIKOKAN (AUT)	6 hr	62.4	75.1	94.6	111.7	161.5	188.2	218.8
SIOUX LOOKOUT A	6 hr	59.1	67.9	79.2	87.7	107.3	115.7	124.1
WIARTON A	6 hr	57.5	65.6	76.0	83.8	102.0	109.7	117.5
THUNDER BAY CS	6 hr	56.8	68.7	87.4	104.5	156.6	185.9	220.5
KENORA RCS	6 hr	81.1	98.9	122.8	140.9	183.2	201.4	219.7
GERALDTON A	6 hr	47.0	55.4	68.6	80.6	117.6	138.5	163.2
ATIKOKAN (AUT)	12 hr	76.1	91.8	115.8	136.8	197.6	230.2	267.4
SIOUX LOOKOUT A	12 hr	66.9	76.3	88.6	97.8	119.0	128.2	137.3
WIARTON A	12 hr	64.6	73.7	85.4	94.2	114.5	123.3	132.0
THUNDER BAY CS	12 hr	67.4	80.9	101.5	119.6	172.1	200.4	232.7
KENORA RCS	12 hr	97.3	118.0	145.3	165.9	213.8	234.4	255.0
GERALDTON A	12 hr	55.8	65.2	79.9	93.0	132.2	153.9	179.2
ATIKOKAN (AUT)	24 hr	80.4	96.0	119.7	140.5	200.5	232.6	269.3
SIOUX LOOKOUT A	24 hr	75.2	85.7	99.1	109.2	132.6	142.6	152.6
WIARTON A	24 hr	69.7	77.9	88.5	96.5	114.9	122.8	130.7
THUNDER BAY CS	24 hr	75.8	92.5	119.8	145.3	226.7	274.4	332.1
KENORA RCS	24 hr	105.7	126.1	152.6	172.4	217.8	237.2	256.5
GERALDTON A	24 hr	70.7	82.7	100.5	115.6	157.8	179.5	203.8

Table 7: IDF Curves for 6020LPQ ATIKOKAN (AUT) – Gumbel Distribution (mm)

Return Period (years)	5min	10 min	15 min	30min	1h	2h	6h	12h	24h
2	8.4	12.6	15.6	20.0	24.7	30.4	37.0	44.5	49.2
5	10.7	15.4	19.8	24.9	30.4	37.8	50.9	61.9	66.4
10	12.3	17.2	22.4	28.3	34.2	43.0	62.4	76.1	80.4
20	13.9	18.8	24.9	31.5	38.0	48.3	75.1	91.8	96.0
50	16.0	20.7	28.1	35.8	43.0	55.7	94.6	115.8	119.7
100	17.7	22.1	30.5	39.1	46.9	61.5	111.7	136.8	140.5
200	19.4	23.4	32.9	42.5	50.9	67.7	131.3	160.7	164.1
500	21.8	25.2	36.1	47.1	56.5	76.5	161.5	197.7	200.5
1,000	23.7	26.5	38.5	50.8	60.8	83.6	188.2	230.2	232.6
2,000	25.7	27.8	41.0	54.5	65.4	91.2	218.8	267.4	269.3

Table 8: IDF Curves for 6037775_SIOUX_LOOKOUT_A - Gumbel Distribution (mm)

Return Period (years)	5min	10 min	15 min	30min	1h	2h	6h	12h	24h
2	8.1	11.8	13.9	17.6	21.4	27.2	36.2	42.1	48.0
5	11.5	16.7	19.5	24.9	29.5	38.6	50.0	57.0	64.4
10	13.7	20.0	23.2	29.7	34.9	46.1	59.1	66.9	75.3
20	15.9	23.2	26.8	34.3	40.1	53.4	67.9	76.3	85.7
50	18.6	27.3	31.5	40.2	46.7	62.7	79.2	88.6	99.1
100	20.7	30.3	34.9	44.7	51.8	69.7	87.7	97.8	109.2
200	22.8	33.4	38.4	49.1	56.7	76.7	96.1	106.9	119.3
500	25.5	37.4	43.0	55.0	63.3	86.0	107.3	119.0	132.6
1,000	27.5	40.4	46.4	59.5	68.3	92.9	115.7	128.2	142.6
2,000	29.6	43.5	49.9	63.9	73.3	99.9	124.1	137.3	152.6

Table 9: IDF Curves for 6119500 WIARTON A – Gumbel Distribution (mm)

Return Period (years)	5 min	10 min	15 min	30 min	1h	2h	6h	12h	24h
2	7.1	10.3	12.8	16.7	21.3	27.1	36.3	40.9	48.2
5	9.3	13.3	16.7	22.1	29.7	38.5	49.1	55.2	61.1
10	10.7	15.2	19.2	25.7	35.2	46.1	57.5	64.6	69.7
20	12.1	17.0	21.6	29.1	40.5	53.4	65.6	73.7	77.9
50	13.8	19.4	24.8	33.5	47.4	62.8	76.0	85.4	88.5
100	15.2	21.3	27.1	36.8	52.6	69.9	83.8	94.2	96.5
200	16.5	23.0	29.5	40.1	57.7	76.9	91.7	103.0	104.4
500	18.3	25.4	32.6	44.5	64.5	86.2	102.0	114.5	114.9
1,000	19.6	27.2	34.9	47.8	69.6	93.2	109.7	123.3	122.8
2,000	20.9	29.0	37.3	51.1	74.7	100.2	117.5	132.0	130.7

Table 10: IDF Curves for 6048268_THUNDER BAY CS – GEV Distribution (mm)

Return Period (years)	5 min	10 min	15 min	30 min	1h	2h	6h	12h	24h
2	7.2	10.8	13.1	17.0	20.9	25.8	33.9	39.9	44.8
5	10.1	15.0	18.3	24.2	30.2	36.5	46.4	55.2	61.5
10	12.1	17.7	21.9	29.3	37.5	45.2	56.8	67.4	75.8
20	14.1	20.3	25.7	34.5	45.6	54.8	68.7	80.9	92.5
50	16.7	23.8	30.9	41.7	57.8	69.7	87.4	101.5	119.8
100	18.7	26.3	35.0	47.4	68.5	82.9	104.5	119.6	145.3
200	20.8	28.9	39.4	53.4	80.6	98.2	124.5	140.2	176.0
500	23.7	32.3	45.6	61.9	99.2	122.0	156.6	172.1	226.7
1,000	25.9	34.9	50.6	68.6	115.6	143.3	185.9	200.4	274.4
2,000	28.1	37.5	55.8	75.8	134.3	168.0	220.5	232.7	332.1

Table 11: IDF Curves for 6034073 KENORA RCS – PE3 Distribution (mm)

Return Period (years)	5 min	10 min	15 min	30 min	1h	2h	6h	12h	24h
2	10.0	13.7	16.3	20.9	25.8	29.2	40.7	49.0	55.6
5	13.1	18.1	22.3	29.5	37.5	47.7	63.4	76.6	84.8
10	14.9	20.8	26.2	35.3	45.2	61.9	81.1	97.3	105.7
20	16.5	23.2	29.8	40.7	52.5	76.2	99.0	118.0	126.1
50	18.4	26.1	34.3	47.7	61.7	95.2	122.8	145.3	152.6
100	19.7	28.1	37.6	52.8	68.5	109.5	140.9	165.9	172.4
200	20.9	30.1	40.8	57.8	75.1	123.9	159.1	186.6	192.0
500	22.4	32.6	44.8	64.2	83.6	143.0	183.2	213.8	217.8
1,000	23.5	34.4	47.9	69.1	90.0	157.5	201.4	234.4	237.2
2,000	24.6	36.1	50.9	73.9	96.3	171.9	219.7	255.0	256.5

Table 12: IDF Curves for 6042716 GERALDTON A – GEV Distribution (mm)

Return Period (years)	5 min	10 min	15 min	30 min	1h	2h	6h	12h	24h
2	6.7	9.8	12.0	16.2	19.2	23.0	31.0	37.3	45.0
5	9.0	13.4	16.6	21.1	25.7	29.9	39.8	47.5	59.5
10	10.3	15.8	19.5	23.8	29.7	34.7	47.0	55.8	70.7
20	11.4	18.0	22.3	26.1	33.4	39.4	55.4	65.2	82.7
50	12.7	20.8	25.8	28.6	37.9	45.6	68.6	79.9	100.5
100	13.6	22.8	28.3	30.2	41.1	50.4	80.6	93.0	115.7
200	14.3	24.8	30.8	31.5	44.2	55.4	94.8	108.2	132.5
500	15.2	27.4	33.9	33.1	48.0	62.1	117.6	132.2	157.8
1,000	15.8	29.3	36.3	34.1	50.7	67.3	138.5	153.9	179.5
2,000	16.4	31.2	38.6	35.0	53.4	72.6	163.2	179.2	203.8

3.2.2 Spatial Interpolation to the Ignace Study Area

The stations located at the study area do not have short duration (sub-daily) rainfall records. A spatially interpolated (linearly scaled with distance) IDF curve was calculated using the station results from the two closest stations to the study area, 6020LPQ ATIKOKAN (AUT) and 6037775 – SIOUX LOOKOUT A (Table 4). The resulting sub-daily IDF is presented in Table 13. The results agree with the values calculated for other stations in the region. The 24-hour, 100-year return period precipitation is estimated at 125.5 mm and the 500-year return period at 167.9 mm.

Table 13: Spatially Interpolated IDF Curves for the Ignace Study Area (mm)

Return Period (years)	5 min	10 min	15 min	30 min	1 h	2 h	6 h	12 h	24 h
2	8.3	12.2	14.8	18.8	23.1	28.9	36.6	43.3	48.6
5	11.1	16.1	19.6	24.9	30	38.2	50.5	59.5	65.4
10	13	18.5	22.8	28.9	34.5	44.5	60.8	71.6	77.9
20	14.8	20.9	25.8	32.8	39	50.7	71.6	84.4	91
50	17.3	23.8	29.7	37.9	44.8	59	87.2	102.7	109.8
100	19.1	26	32.6	41.8	49.2	65.5	100.2	118.1	125.5
200	21	28.2	35.5	45.7	53.7	72	114.4	134.9	142.6
500	23.6	31	39.4	50.9	59.7	81	135.5	160	167.9
1,000	25.5	33.2	42.3	54.9	64.4	88.1	153.5	181.3	189.5
2,000	27.6	35.3	45.2	59	69.2	95.3	173.4	205	213.3

3.2.3 Comparison with Other Sources

The above stations were compared with publicly available external tools and portals to confirm the results presented in the previous section were in line with other sources. The following sources were used in the comparison:

- **IDF_CC Tool**: The tool used Gumbel and GEV distribution with the method of moments and L-moments respectively to calculate the baseline values. The tool only calculates return periods up to 100-year.
- **MTO Lookup tool**: The tool used Gumbel with the method of moments to calculate the baseline values for the IDF curves. The tool only calculates return periods up to 100-year and uses an interpolation methodology.

Only select return periods and 24-hour durations were used for comparison, as presented in Table 14. The estimates generated by Golder are in line with the IDF tool, with a higher projection for Atikokan (AUT) and Kenora RCS, and similarly for the other stations. The comparison with the MTO tool shows larger variations that may be attributed to the spatial interpolation of the MTO tool. The projected values are shown not to change significantly from one station to the others.

Table 14: IDF Curves Comparison with Other Sources – 100-Year Return Period for 24-Hour Duration

Station	Golder	IDF_CC Tool		MTO IDF Tool	
	(mm)	(mm)	(%)	(mm)	(%)
6020LPQ - ATIKOKAN (AUT)	140.5	114.5	22.6%	130.9	7.3%
6037775 - SIOUX LOOKOUT A	109.2	113.0	-3.4%	128.1	-14.7%
6119500 - WIARTON A	96.5	95.9	0.6%	127.3	-24.2%
6048268 - THUNDER BAY CS	145.3	145.4	-0.1%	121.3	19.7%
6034073 - KENORA RCS	172.4	158.6	8.7%	133.0	29.6%
6042716 - GERALDTON A	115.6	115.7	-0.1%	118.4	-2.3%
Ignace study Area (1)	125.5	—	—	128.6	-2.5%

Note: (1) Interpolated IDF curve calculated in Section 3.2.2.

3.2.4 Daily and Multi-Day IDF Curve for the Ignace Study Area

The data source for this analysis is the daily baseline time series defined in Section 3.1.2. The daily and multi-day IDF curves were calculated for the same return periods used for the IDF curves in the previous section. Based on the goodness of fit tests, the Pearson Type 3 distribution was selected to calculate the curves. The results are shown in Table 15 for selected durations up to 120-days. The 1-day IDF curve is converted to 24-hours duration (using the 1.13 ratio recommended by the World Meteorological Organization 2019). Daily rainfall can be calculated for two different periods: 24-hour rainfall and 1-day rainfall. The 24-hour rainfall is calculated as the maximum rainfall during a moving block of 24 hours, while the 1-day rainfall is calculated as the maximum rainfall during the period from midnight of one day to midnight of the next. Due to the differences in the method of calculation, there are typically differences in the values, with the 24-hour rainfall often being higher (moving block allows for greater capture of storms). As seen in Table 16, the interpolated IDF curve (calculated in Section 3.2.2) shows good agreement, with higher differences for longer return periods due to uncertainties in the extrapolation.

Table 15: Daily and Multi-day IDF Curves for the Ignace Study Area (mm)

Return Period (years)	1-Day	2-Day	3-Day	4-Day	5-Day	6-Day	7-Day	10-Day	20-Day	30-Day	50-Day	75-Day	90-Day	120-Day
2	44.3	54.8	64.1	69.6	74.5	77.8	82.8	95.8	135.8	167.4	220.9	291.6	332.7	407
5	61.6	78	89	95.6	100.7	104.6	110.4	126.9	168.9	203.6	264.3	350.1	398.8	486.1
10	73.4	94.1	105.2	112.1	117.2	122	128.1	147	188.2	224	288.1	382.1	434.8	530.2
20	84.7	109.6	120.4	127.5	132.4	138.2	144.4	165.7	205.3	241.5	308.1	409.2	465.3	567.9
50	99.1	129.5	139.5	146.6	151.2	158.5	164.7	189.1	225.8	262.1	331.3	440.6	500.4	612
100	109.8	144.3	153.4	160.5	164.7	173.2	179.5	206.2	240.2	276.3	347.1	462	524.3	642.3
200	120.4	158.8	166.9	173.9	177.9	187.7	193.8	222.8	253.8	289.6	361.8	481.9	546.6	670.6
500	134.1	177.9	184.5	191.3	194.8	206.3	212.2	244.2	271.1	306.2	379.9	506.4	574	705.8
1,000	144.4	192.1	197.6	204.2	207.2	220.2	225.8	260.1	283.6	318.2	392.8	523.9	593.5	731.1
2,000	154.6	206.3	210.4	216.8	219.5	233.8	239.3	275.8	295.8	329.7	405.1	540.6	612.1	755.4

Table 16: Comparison of the IDF Curves at Ignace Study Area

Return Period (years)	Daily to 24-Hours [(1)] (mm)	Interpolated to Ignace Study Area, 24-Hours (mm)
2	50.1	48.6
5	69.6	65.4
10	82.9	77.9
20	95.7	91.0
50	112.0	109.8
100	124.1	125.5
200	136.0	142.6
500	151.5	167.9
1,000	163.1	189.5
2,000	174.7	213.3

Note: [(1)] Converted to 24-hours duration using the 1.13 WMO ratio.

3.3 BASELINE PMP CALCULATIONS

Using the stations listed in Table 1 that were involved in the baseline development, DAD curves and PMP values were calculated for the desired duration periods (1-day, 24-hour, 2-day, and 3-day). The PMP values were calculated specifically for the Ignace study area using the precipitation series defined in Section 3.1.2 and Figure 5 of this report for the Hershfield method and cross validated using two different methods, the PMP Hershfield and the Transposition (DAD curves).

3.3.1 Historical storms for the Transposition Method

All periods for the stations (Table 1) were screened for large events, including the most recent observations. The periods covered by the stations is from the early 1900s to 2019. All precipitation events higher than 100 mm/day were preselected and screened. One event registered at Ignace (6033690) station in September 1941, and two other stations were investigated. The total 1-day precipitation registered at Ignace was 122.4 mm on September 21st, 115.8 mm on September 20 at Sioux Lookout A Station (6037775), and 106.7 mm at Quorn Station (6046811). The 3-day accumulation from September 19th to 21st, 1941 was registered as 138.4, 134.8 and 129.8 mm, respectively.

The second major event in the study area was registered on June 2002; a large storm was registered on the northern region of Northwestern Ontario, parts of Manitoba and Minnesota (USA). This storm was named the 49th Parallel storm and it was the largest recorded for some of the stations including Mine Centre and Atikokan AUT. The amount recorded from June 8th to 11th, 2002, was 293.2 mm at Mine Centre (6025203) and 194.0 mm in Atikokan AUT (6020LPQ). Other stations farther north also registered significant amount on the same days, Sioux Lookout A (6037775) with 90.8 mm (92.88 mm from the AHCCD dataset) in the three days, Dryden A (6032119) with 113.1mm. Other stations farther away from the study area, such as Geraldton A (6042716) and Wiarton A (6119500) only registered 43.8 mm, and 9.1mm, respectively for this event.

According to Murphy et al. (2003), severe flooding, record precipitation, and high river flows were registered from the above-mentioned storm. A series of Mesoscale Convective Systems (MCS) moved through southern portions of northwestern Ontario, southeastern Manitoba, and northern Minnesota from the evening of June 8, 2002 through the morning hours of June 11, 2002. The highest rainfall rates occurred on June 9th and 10th associated with intense thunderstorms that were continuously generating and moving across the area from the Roseau River to just southwest of Upsala, Ontario and resulted in a swath having rainfall accumulations in the 200-400 mm range (Figure 1 in Murphy et al. 2003).

No significant storm events where registered on the stations from 2002 to present (based on the observations screened). The storm registered on September 1941 was deemed to not be large enough to affect the PMP in the study compared to the 49th parallel event. The DAD curve is constructed for this specific storm and compared to the results from the site specific Hershfield method for the study area.

3.3.2 Estimates of PMP with the Hershfield method

For the estimate of the PMP using the Hershfield method as described by the World Meteorological Organization (WMO 2009a), the daily baseline time series prepared for the Ignace study area as described in Section 3.1.2 was used. The results using the baseline time series were compared to the calculations from the DAD curves for the Transposition method in the next section. The 1-day PMP value found was 364.3 mm (Table 17), which is equivalent to 411.7 mm for the 24-hour duration PMP using the 1.13 conversion factor (from daily to 24-hour rainfall events) recommended by the WMO. The 2-day and 3-day PMP values for the same location were calculated as 482.2 mm and 510.1 mm, respectively.

Table 17: PMP Summary for Statistical Method for the Ignace Study Area

Duration	PMP (mm)
1-Day	364.3
24-Hour (1)	411.7
2-Day	482.2
3-Day	510.1

(1) Converted from daily to 24-hour duration using the 1.13 ratio recommended by the WMO (2009a).

3.3.3 Development of DAD Curves in Estimate of PMP with the Transposition Method

The DAD curves were developed using the Transposition method described in Appendix A.2.3. For the development of the DAD curves for the Ignace study area, the focus was on the 49th Parallel storm in June 2002. This storm was the most intense observed near the Ignace area, based on the records extracted from the stations listed in Table 1. Additionally, previous analysis conducted by OMNR (2006) concluded that the 49th Parallel storm was found to be larger than the Timmins and Hazel events for all durations above 12 hours and comparable to the Hazel event and comparable for smaller durations.

The DADs were constructed for 1-day, 2-day and 3-day, and the areal average determined the envelopment curves. Figure 7 presents the curves constructed for 1-day, 2-day and 3-day from the data collected from the stations listed in Table 1 and the data points are given in Table 18. The dots in Figure 7 represent the total precipitation for each of the events registered on the stations screened and the area of influence for the corresponded rainfall amounts using the method described in Appendix A.2.3.1. The dashed lines represent the envelopment for both durations (1-day and 3-day) as indicated. The resulting DAD curves show little change in total precipitation from 25 km^2 to 1,000 km^2. This is due to the nature of the 49th Parallel storm in the region, which produced a line of mesoscale convective systems passing over the area resulting in a large storm radius.

The original DAD curves were constructed as shown in Figure 7. The original DAD curves and consequent PMP values were multiplied by the maximization factor (used to maximize the screened observed storm) and transposition factor (used to transpose the values of the PMP to the Ignace study area), using the precipitable water content as described in Appendix A.2.3.2. The maximization factor was estimated for Mine Centre Station as 2.21 (following the methodology described in Appendix A.2.3.2), using the 12-hours persistent dew point map from Figure 3.6 in OMNR (2006) for the month of June and the maximum daily mean temperature as a proxy for the dew point of the 49th Parallel storm of June 2002. The transposition factor (as defined in Appendix A.2.3.2) was estimated as 0.92, also using the map from Figure 3.6 in OMNR (2006); the approximate values of the 12-hours, 100-year return period dew point temperature were extracted for the locations of Mine Centre station and the Ignace study area. The storm maximization for the 1-Day PMP was then calculated as 2.033 (2.21 x 0.92) to obtain the adjusted DAD curve and PMP for Ignace (Table 20). For the 2- and 3- Day PMP, the maximization delta of the 1-Day PMP was added to the original 2- and 3-Day DAD curve (Table 19).

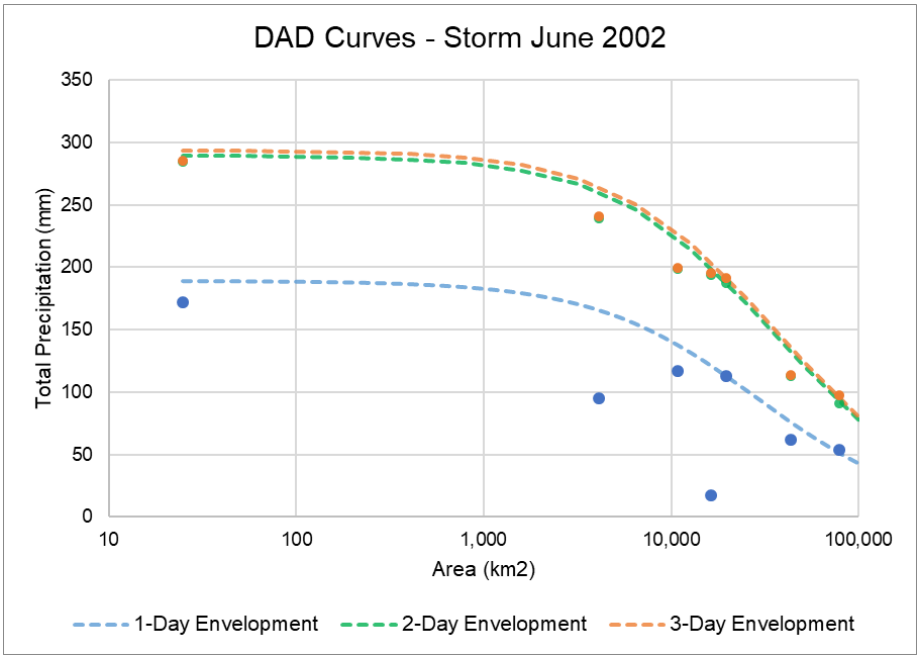

Figure 7: DAD Curves for 49th Parallel Storm, 1-, 2- and 3-Day Duration (Non-Maximized Storm)

Table 18: Data Points Used to Obtain the DAD Curves

Station / Points	Area (km²)	2002-06-09 1-Day	2002-06-09 and 10 2-Day	2002-06-09 to 11 3-Day
		PPT [1] (mm)	PPT (mm)	PPT (mm)
6020LPQ	16,367.4	17.6	194.0	195.8
Midpoint 6025203 to 6020LPQ	4,091.8	94.8	239.4	240.6
6025203	25.0	172.0	284.8	285.4
6032119	43,446.8	61.6	113.1	114.0
Midpoint 6025203 to 6032119	10,861.7	116.8	199.0	199.7
6037775	78,442.0	54.0	90.8	97.5
Midpoint 6025203 to 6037775	19,610.5	113.0	187.8	191.5

[1] PPT = Total Precipitation

Table 19: Original DAD Curves for the 49th Parallel Storm

Area (km²)	PMP (mm)		
	1-Day	2-Day	3-Day
25	188.8	289.6	293.7
100	188.4	289	293.1
500	186.4	286.7	290.8
1,000	183.9	283.6	287.7
2,000	179.1	277.6	281.8
5,000	170.3	266.4	270.7
10,000	154.9	246.6	250.9

Table 20: Adjusted DAD Curves for the Ignace Study Area

Area (km²)	PMP (mm)			
	1-Day	2-Day	3-Day	24-hour [1]
25	383.9	484.7	488.8	433.9
100	383	483.6	487.7	432.7
500	379.1	479.3	483.4	428.3
1,000	374	473.6	477.8	422.6
2,000	364.2	462.7	466.9	411.6
5,000	346.2	442.3	446.6	391.2
10,000	314.9	406.6	411	355.9

[1] Converted to 24-hour using 1.13 ratio recommend by the WMO (2009a).

3.3.4 PMP Comparison

The estimated 1-Day PMP value from the DAD curves for 1,000 km^2 (374.0 mm) in the Transposition method is slightly higher than that obtained by the Hershfield method (364.3 mm) (Table 21). The values of the PMP calculated were compared with other sources, including OMNR (2006), for validation. The PMP values were calculated by OMNR as an average by group of watersheds in Ontario as opposed to specific locations or specific storms. The Ignace study area is located in the English/Lake St. Joseph watershed and the 24-hour PMP is estimated at 436 mm. This is in line with the estimated calculation of 422.6 mm in Table 20.

If the Agimak River into Sandbar Lake is considered, the Ignace study area is only 126 km². If the watershed for Agimak River into Barrel Lake is considered, the Ignace study area is approximately 812 km² using the Ministry of Natural Resources and Forestry (MNRF) Ontario Flow Assessment Tool (OFAT; MNRF 2020). Therefore, if the largest area is considered, the Ignace study area would be below 1,000 km².

Table 21 : PMP Comparison for the Ignace Study Area

Duration	PMP (mm)		
	Golder – Transposition (1)	Golder - Hershfield	OMNR (2006)
24-hour	422.6	411.7	436
1-day	374	364.3	—

(1) For watershed areal extent of 1000 km^2.

3.3.5 Sub-Daily PMP Estimates

The hourly precipitation data are not available from ECCC and therefore the sub-daily PMP was estimated using ratios obtained for the IDF curves for the sub-daily durations, from 5 minutes to 12 hours as described in Appendix A.2.3.3 (Table 22). The ratios were calculated using 24-hour duration and 100-year return period from the IDF curve calculated for the Ignace study area in Section 3.2.2. The 100-year return period is selected since it provides a more realistic and reliable estimate among sub-daily durations than higher return periods. The ratios were applied to the 24-hours PMP values obtained by the Hershfield method (Section 3.3.2) and the Transposition method (Section 3.3.3); the results are presented in Table 23 and Table 24. As noted in the previous sections, the values of the sub-daily PMP calculated by the Hershfield methods are similar to the values from the Transposition method for areas up to 1,000 km^2. There are some uncertainties associated with the approach used to come up with the sub-daily values, since the actual sub-daily storm distribution may differ from the storm distribution derived using the adopted method.

Table 22: Conversion Ratios from 24-hour to Sub-daily PMP

Duration	5-min	10-min	15-min	30-min	1-hour	2-hour	6-hour	12-hour
Ratio	0.152	0.208	0.260	0.333	0.392	0.522	0.798	0.941

Table 23: Estimated Sub-Daily PMP Values for the Ignace Study Area – Hershfield Method

Duration	PMP (mm)
5-Min	62.7
10-Min	85.4
15-Min	107.0
30-Min	137.0
1-Hour	161.5
2-Hour	214.7
6-Hour	328.7
12-Hour	387.4
24-Hour	411.7
1-Day	364.3

Table 24: Estimated Sub-Daily PMP Values for the Ignace Study Area – Transposition Method

Area (km^2)	PMP (mm)									
	1-Day	24-Hour	12-Hour	6-Hour	2-Hour	1-Hour	30-Min	15-Min	10-Min	5-Min
25	383.9	433.9	408.3	346.4	226.3	170.2	144.4	112.8	90	66.1
100	383	432.7	407.3	345.6	225.8	169.8	144.1	112.5	89.8	66
500	379.1	428.3	403.2	342	223.5	168.1	142.6	111.4	88.9	65.3
1,000	374	422.6	397.7	337.4	220.4	165.8	140.7	109.9	87.7	64.4
2,000	364.2	411.6	387.3	328.6	214.7	161.5	137	107	85.4	62.7
5,000	346.2	391.2	368.2	312.4	204.1	153.5	130.2	101.7	81.2	59.6
10,000	314.9	355.9	334.9	284.1	185.6	139.6	118.5	92.5	73.8	54.2

3.4 RAINFALL ON SNOW

The analysis of rain on snow included the combined effect of precipitation as rainfall and the melting of accumulated snow. This analysis was conducted for the Ignace station using the baseline daily total precipitation and daily temperature time series defined for the Ignace study area as described in Section 3.1.2 in Table 3. The rain on snow requires the concurrent daily total precipitation and temperature data from the Ignace station. The procedure used for the calculation of the rainfall on snow results presented in this report follows the methodology adopted by ECCC (Louie and Hogg 1980), and the steps adapted are detailed in Appendix A.2.4. A snowpack accumulation and snowmelt model (Pysklywec et al. 1968) were used to estimate the depth of equivalent rainfall converted from the snowpack accumulation for the Ignace study area. A probability distribution (Gumbel) was used to calculate the estimates for selected return periods and presented in Table 25. The 1-day snowpack accumulation was calculated with the same distribution are presented in Table 26. The rain on snow projections can assist hydrological modeling to determine flood assessments, dam safety assessments, storage requirements and others. For shorter durations, i.e., the 1-day 100-year return period rain on snow event is calculated at 87 mm, indicating that extreme rainfall events are predominant over the snowmelt events based on the analysis of the historical observations. Longer duration events, however, 20-days or more and high return periods (100-year or more), may be useful for hydrological analysis when volumetric capacity is an important variable to consider.

Table 25: Rainfall on Snow Projections for the Ignace Study Area (mm)

Return Period (years)	1-Day	2-Day	3-Day	4-Day	5-Day	6-Day	7-Day	10-Day	20-Day	30-Day	50-Day	75-Day	90-Day	120-Day
2	38	54.2	69.5	83.5	96.2	106.5	117	146.8	208.3	245.7	295.7	328	332.7	342.3
5	51.1	71.8	91.6	110.5	128.5	144.4	160.9	206.8	300.8	354	412.8	449.9	453	455.5
10	59.8	83.5	106.2	128.4	150	169.5	190	246.5	362	425.7	490.4	530.6	532.7	530.4
20	68.2	94.7	120.2	145.5	170.5	193.6	217.9	284.6	420.7	494.5	564.8	608.1	609.2	602.3
50	79	109.2	138.3	167.7	197.2	224.8	254	334	496.7	583.5	661.2	708.3	708.1	695.4
100	87	120.1	151.9	184.4	217.1	248.2	281	371	553.7	650.2	733.3	783.3	782.3	765.1
200	95.1	130.9	165.5	200.9	237	271.5	308	407.8	610.4	716.7	805.3	858.2	856.1	834.6
500	105.7	145.1	183.3	222.8	263.2	302.2	343.6	456.4	685.3	804.4	900.1	956.9	953.6	926.2
1,000	113.8	155.9	196.8	239.3	283	325.4	370.5	493.1	741.9	870.7	971.8	1031.5	1027.3	995.5
2,000	121.8	166.7	210.3	255.9	302.8	348.6	397.3	529.9	798.4	937	1043.5	1106	1100.9	1064.7

Table 26: 1-Day Snowpack Accumulation for the Ignace Study Area (mm)

Return Period (years)	2	5	10	20	50	100	200	500	1,000	2,000
1-Day	207.1	301.3	363.6	423.4	500.8	558.7	616.5	692.8	750.4	808.0

3.5 BASELINE ADDITIONAL CLIMATE VARIABLES

To provide more context for the extreme rainfall projections in Sections 3.2 and 3.3, additional climate variables were analyzed for the Ignace study area. These include annual and monthly temperature and precipitation statistics from which seasonal variation can be inferred. Derived climate variables are also provided, including WMO indices, rain and snow, snow depth, potential evapotranspiration, drought index, and qualitative information for wind speed and relative humidity. The information for wind speed and relative humidity variables may be interpreted qualitatively, as alternative datasets were used due to limited available data for the Ignace study area. The period of 1914 to 1992 is used to maintain consistency with the period used for PMP and IDF estimates (Section 3.3 and 3.2), although this may impact estimates of trends in the WMO indices. Additional climate variables provided for the study area will allow for further understanding of the current climate conditions and may be used to support additional studies relating to site hydrology and ecology, for example.

3.5.1 Precipitation and Temperature

Daily precipitation and mean temperature variables are used to estimate annual and monthly mean, minimum, and maximum statistics, highlighting the climate variation over a year at the site. Annually, the average total precipitation for the Ignace study area is 747.6 mm, ranging from 409.9 mm to 1166.2 mm. The wettest months of the year occur from June to September with a range of 88.7 mm to 94.7 mm of mean monthly total precipitation (Table 27). April has the potential to be the driest month with a minimum total of 0 mm occurring in 1980, while the month of September holds the historical maximum of 275.6 mm occurring in 1941.

Mean temperature was used for the calculation of the annual and monthly statistics (Table 28). The annual average temperature was calculated as 1.2°C ranging from -1.13°C to 4.6°C. The warmest month on average is the month of July with a mean temperature of 18.2°C, and the coldest is the month of January with a mean temperature of -18.5°C. The coldest monthly temperature occurred in February 1914 with a minimum monthly temperature of -25.9°C in 1914, while the warmest monthly temperature occurred in July with a maximum monthly temperature of 21.5°C in 1936. Observations for the most recent decade at the Ignace study area are not included (see Section 3.1), however the warmest years on record have been experience during this time globally (IPCC 2018). Therefore, it is possible that the warmest months at the Ignace study may not be captured in the baseline period.

Table 27: Mean, Minimum, and Maximum of Monthly Total Precipitation for the Baseline Period from 1914 to 1992 (mm)

Month	Mean	Minimum	Maximum
January	39.6	2.5	157.5
February	35.2	5.0	86.4
March	40.1	5.0	114.4
April	48.9	0.0	113.1
May	59.8	1.3	165.6
June	94.7	36.9	216.4
July	97.4	21.3	213.9
August	88.7	21.9	208.3
September	91.9	11.1	275.6
October	55.0	14.6	139.2
November	53.9	5.1	147.3
December	44.2	1.7	111.8
Annual	747.6	409.9	1166.2

Table 28: Mean, Minimum, and Maximum of Monthly Mean Temperature for the Baseline Period (°C)

Month	Mean	Minimum	Maximum
January	-18.5	-25.5	-11.1
February	-15.6	-25.9	-6.2
March	-8.3	-15.1	-1.3
April	1.5	-2.8	8.4
May	9.5	4.5	13.9
June	15.0	11.7	19.0
July	18.2	14.6	21.5
August	16.6	13.7	20.6
September	10.9	7.2	13.9
October	4.4	-1.3	10.7
November	-5.3	-10.7	-0.6
December	-14.9	-21.4	-8.0
Annual	1.2	-1.13	4.6

Additional daily climate variables including rain, snow, snow depth, and potential evapotranspiration are added to the current climate baseline dataset. Rain, snow, and snow depth are derived from daily precipitation and temperature variables from the current climate baseline, using the methods adopted by the ECCC (see Appendix A.3.4). The resulting daily timeseries for the current climate baseline including precipitation, temperature, rain, snow, snow depth, and potential evapotranspiration are provided in Appendix C.

3.5.2 WMO Climate Indices

The World Meteorological Organization's (WMO's) Expert Team on Climate Change Detection and Indices (ETCCDI; WMO 2009b) recommends using 27 climate extreme indices as a means of summarizing daily temperature and precipitation statistics, focusing primarily on aspects of climate extremes. They have been developed to allow consistent comparison of climate conditions on an international basis. For the following assessment, the WMO climate indices were calculated for the current climate baseline period using the 27 indices, as described in Appendix A. Two analyses for the WMO indices are completed. In the first, the minimum, maximum, mean and median values for each of the 27 indices are calculated over the entire period (Table 29). In the second, the long-term averages and trends are calculated based on the annual values of each of the indices (Table 30).

Table 29: WMO Indices for Current Climate Extremes

ID	Indicator Name	Units	Min	Max	Mean	Median
CDD	Consecutive dry days	Days	10.0	43.0	23.1	21.0
CSDI	Cold spell duration indicator	Days	0.0	9.0	1.3	0.0
CWD	Consecutive wet days	Days	2.0	10.0	5.2	5.0
DTR	Diurnal temperature range	ºC	9.6	13.8	11.8	11.8
FD0	Frost days	Days	173.0	233.0	201.8	202.0
GSL	Growing season Length	Days	128.0	211.0	168.0	166.5
ID0	Ice days	Days	94.0	146.0	122.3	124.0
PRCPTOT	Annual total wet-day precipitation	mm	404.2	1160.8	747.6	737.0
R10	Number of heavy precipitation days	Days	12.0	41.0	24.2	24.0
R20	Number of very heavy precipitation days	Days	2.0	17.0	7.9	8.0
R95p	Very wet days	mm	0.0	347.1	116.4	89.9
R99p	Extremely wet days	mm	0.0	367.5	56.2	46.1
R30MM	Number of days above 30 mm	Days	0.0	10.0	2.7	2.5
RX1day	Max 1-day precipitation amount	mm	24.4	122.4	49.6	45.5
Rx5day	Max 5-day precipitation amount	mm	32.8	154.0	80.6	74.9
SDII	Simple daily intensity index	mm/day	5.3	12.5	7.7	7.4
SU25	Summer days	Days	5.0	63.0	34.7	34.5
TN10p	Cool nights	% of Days	0.3	20.5	9.5	8.9
TN90p	Warm nights	% of Days	4.4	22.2	9.8	9.6
TNn	Minimum of daily minimum temperature	ºC	-48.9	-33.9	-41.0	-40.9
TNx	Maximum of daily minimum temperature	ºC	16.7	24.4	19.9	19.8
TR20	Tropical nights	Days	0.0	4.0	0.7	0.0
TX10p	Cool days	% of Days	3.5	17.4	9.7	10.0
TX90p	Warm days	% of Days	2.7	21.8	9.9	9.4
TXn	Minimum of daily maximum temperature	ºC	-37.2	-20.6	-27.7	-27.8
TXx	Maximum of daily maximum temperature	ºC	29.4	41.7	32.7	32.2
WSDI	Warm spell duration indicator	Days	0.0	20.0	3.9	0.0

Table 30: Long-term Averages and Trends of WMO Indices for Current Climate Extremes

Climate Indices	Units	Mean	Decadal Trend	Statistical Significance
Consecutive dry days	Days	23.1	+0.1	not statistically significant
Cold spell duration indicator	Days	1.3	0.0	no apparent trend
Consecutive wet days	Days	5.2	+0.2	significant at the 99th percentile
Diurnal temperature range	ºC	11.8	-0.4	significant at the 99.9th percentile
Frost days	Days	201.8	-2.3	significant at the 99.9th percentile
Growing season length	Days	168.0	+0.4	not statistically significant
Ice days	Days	122.3	+0.2	not statistically significant
Annual total wet-day precipitation	mm	747.6	-22.8	significant at the 99th percentile
Number of heavy precipitation days	Days	24.2	-1.2	significant at the 99.9th percentile
Number of very heavy precipitation days	Days	7.9	-0.3	significant at the 90th percentile
Very wet days	mm	57.5	-4.5	significant at the 99.9th percentile
Extremely wet days	mm	56.2	0.0	no apparent trend
Number of days above 25 mm	Days	2.7	0.0	no apparent trend
Max 1-day precipitation amount	mm	49.6	-1.5	significant at the 90th percentile
Max 5-day precipitation amount	mm	80.6	-0.6	not statistically significant
Simple daily intensity index	mm/day	7.7	-0.3	significant at the 99.9th percentile
Summer days	Days	34.7	-1.8	significant at the 95th percentile
Cool nights	% of Days	9.5	-1.6	significant at the 99.9th percentile
Warm nights	% of Days	9.8	+0.5	significant at the 99th percentile
Min Tmin	ºC	-41.0	+0.8	significant at the 99.9th percentile
Max Tmin	ºC	19.9	+0.2	significant at the 90th percentile
Tropical nights	Days	0.7	0.0	no apparent trend
Cool days	% of Days	9.7	-0.1	not statistically significant
Warm days	% of Days	9.9	-0.4	significant at the 90th percentile
Min Tmax	ºC	-27.7	0.0	no apparent trend
Max Tmax	ºC	32.7	-0.2	not statistically significant
Warm spell duration indicator	Days	3.9	0.0	no apparent trend

As shown in Table 29, the number of heavy precipitation days (R10) (i.e., daily precipitation greater than 10 mm) was approximately 24.2 days per year on average, ranging from 12 to 41 days during the current climate baseline period. Based on the R10 value, there are at a minimum, 12 days in each year corresponding to precipitation greater than 10 mm. Maximum one-day (RX1day) and five-day (Rx5day) precipitation events were 49.6 mm and 80.6 mm on average, corresponding to a 2 to 5 year return period event based on the current climate IDF curves developed in Section 3.2.4. Compared with the monthly total precipitation in Section 3.5.1, the average annual maximum five-day event is greater than what is received in most months on average. This indicates that extreme precipitation amounts are concentrated in a limited number of months in the year. The precipitation during the extremely wet days (R99p) (i.e., the annual total precipitation when daily precipitation is greater than the 99th percentile) could be up to a maximum of 367.5 mm. The number of consecutive dry days (CDD) ranged from 10 days to 43 days per year, with an average of 23.1 days.

The highest (TXx) and lowest (TXn) recorded daily maximum temperature is 41.7°C and -37.2°C, respectively. The highest (TNx) and lowest (TNn) recorded daily minimum temperature is 24.4°C and -48.9°C, respectively. The range of extreme daily temperatures is almost double of that shown in the monthly statistics for mean temperature in Section 3.5.1. This indicates that the daily temperatures show a high degree of variation compared to the monthly averages.

The long-term averages and trends over the current climate baseline period are calculated for the WMO indices using the methodology outlined in Appendix A. For each of the 27 indices, the climate normal, decadal trend, and statistical significance of the trend were calculated. The climate normal is used to establish the current conditions, while the decadal trend indicates the direction and magnitude of how the indices are changing on average over a ten-year period. The analysis assessed the statistical significance at the 90th, 95th, 99th and 99.9th percentile levels. Below the 90th percentile level a trend is deemed to be “not statistically significant”, while trends that are 0 when rounded to the first decimal place are labelled as “no apparent trend”. The long-term averages and trends are presented in Table 30.

Statistically significant trends related to precipitation extremes indicate that over the current climate period, the number of consecutive wet days is increasing, however the number of heavy precipitation days is decreasing along with the annual total precipitation and maximum 1-day precipitation amounts. Significant trends related to temperature extremes indicate that daily minimum temperatures, and warm nights are increasing (days where daily minimum temperature is greater than 90th percentile), while cold nights (days where daily minimum temperature is less than 10th percentile) and summer days (days with greater than 25°C daily maximum temperature) have a decreasing trend. These trends indicate that precipitation is decreasing, but is spread over more consecutive wet days, while temperatures are becoming more mild (fewer frost days, cold nights, summer days, and cool nights).

3.5.3 Potential Evapotranspiration

Estimates of potential evapotranspiration can provide an indication of how much water is lost to the atmosphere through evaporation and transpiration processes at a given location without soil moisture limitations. The Hargreaves equation (Hargreaves and Samani 1985) is selected to provide consistency between the current climate observations and future climate projections. Annual and monthly potential evapotranspiration estimates for the Ignace study area are provided in Table 31. Potential evapotranspiration calculated using the current climate baseline temperatures is provided as a daily time series in Appendix C.

Table 31: Potential Evapotranspiration for the Ignace Study Area on a Monthly Timescale for the Baseline Period from 1914 to 1992

Month	Potential Evapotranspiration (mm)
January	0.0
February	2.5
March	24.0
April	62.5
May	112.8
June	133.7
July	146.6
August	120.7
September	72.6
October	39.4
November	12.8
December	2.0
Annual	729.7

The greatest monthly evapotranspiration rates occur in July at 146.6 mm, which was shown to also have the highest mean temperatures. Most of the evapotranspiration occurs in the late spring and summer months of May to August. The lowest evapotranspiration rates occur in January at an average of 0 mm where temperatures are consistently low for the entire month.

For comparison, Hember et al. (2017) have calculated monthly potential evapotranspiration across North America using six different methods for the period of 1971-2000. The range of results for the Ignace study area estimated from the provided maps ranges from 2.5 mm/day to 4 mm/day for the average daily potential evapotranspiration between May and September. Using the estimates provided in Table 31, the mean daily evapotranspiration rate for this time period corresponds to 3.7 mm/day, which is within the range given by Hember et al. (2017), despite the use of different methods and time periods. The Hargreaves method used in this report only requires temperature climate variables as inputs and is selected to provide a consistent method for future projections. Although it appears to perform well for the South Bruce study area, if a more comprehensive assessment is needed, then the method should be checked against other methods that use additional climate variables to confirm the validity of this approach. For example, Penman-Monteith based methods incorporate the effects of wind speed and relative humidity which are not included here.

Annual potential evapotranspiration (729.7 mm) is slightly lower than annual precipitation (747.6 mm in Table 27), indicating an annual surplus of water for the study area. Actual evapotranspiration would be lower than potential due to ideal conditions not always present (e.g., cloud cover limiting solar radiation input, elevated humidity limiting soil moisture), indicating further surplus.

3.5.4 Drought Index

The drought index is estimated using the standard precipitation and evapotranspiration index (SPEI) of Vincente-Serrano et al. (2010), which is based on the standard precipitation index described in WMO (2012). This method illustrates the number of standard deviations the monthly net precipitation (precipitation less evapotranspiration) is from the median. By using net precipitation, both precipitation and temperature influence the drought index instead of only precipitation. The SPEI is calculated on a monthly timescale using a 12-month calculation interval (see Appendix A.3.6.4). Annual values are not provided for the drought index, as for a given month the calculated value is dependent on the previous twelve months; therefore, an aggregated annual value is not meaningful with this calculation approach. The mean of all the calculated values is 0 and the standard deviation is 1 due to the normalization step of the method.

The distribution of SPEI is provided using a set of percentiles across each calendar month in the current climate baseline (Table 32). The values for SPEI can be interpreted using the classification scheme discussed in Appendix A.2.5.4. SPEI values between -1 and 1 are classified as near-normal, between 1 to 1.49 and -1 to -1.49 are moderately wet and moderately dry, between 1.5 to 1.99 and -1.5 to -1.99 are severely wet and severely dry. Extremely wet and dry conditions are represented by a value of 2 and -2 respectively.

At the 50th percentile, only minor variations in drought occur in a given month. From February to May a slight surplus (positive net precipitation) was found, while the month of September had a small deficit (negative net precipitation. The minimum values reveal that the most significant drought events have occurred in April and May with a value of -2.3, while all other months have also exceeded the threshold for extremely dry conditions (-2 or less). Considering the maximum values, extremely wet conditions (2 or higher) have occurred in all months, with the wettest being November, December, and January.

Table 32: Drought on a Monthly Timescale for the Ignace Study Area

Month	Min	10%	25%	50%	75%	90%	Max	Mean	Std. Dev.
January	-2.1	-1.4	-0.7	0.0	0.6	1.2	2.7	0.0	1.0
February	-2.1	-1.4	-0.6	0.1	0.6	1.1	2.5	0.0	1.0
March	-2.2	-1.5	-0.6	0.2	0.5	1.1	2.6	0.0	1.0
April	-2.3	-1.4	-0.6	0.1	0.5	1.1	2.4	0.0	1.0
May	-2.3	-1.2	-0.6	0.1	0.6	1.3	2.4	0.0	1.0
June	-2.0	-1.3	-0.6	0.0	0.7	1.3	2.1	0.0	1.0
July	-2.0	-1.4	-0.9	0.0	0.6	1.2	2.3	0.0	1.0
August	-2.0	-1.4	-0.7	0.1	0.8	1.2	2.2	0.0	1.0
September	-2.2	-1.4	-0.6	-0.1	0.6	1.0	2.3	0.0	1.0
October	-2.2	-1.2	-0.6	0.0	0.6	1.0	2.4	0.0	1.0
November	-2.0	-1.3	-0.5	0.0	0.6	1.1	2.7	0.0	1.0
December	-2.0	-1.3	-0.6	0.0	0.7	1.2	2.8	0.0	1.0

Note: Percentiles are calculated across calendar months to illustrate the distribution of SPEI values.

3.5.5 Wind Speed and Relative Humidity

Climate normals from ECCC for wind speed and relative humidity are not available for the Ignace study area from the Ignace (6033690) or IGNACE TCPL 58 (6033697) climate stations, however climate normals were available for SIOUX LOOKOUT A (6037775) and ATIKOKAN (6020379) climate stations (ECCC 2020). Both stations are located approximately 75 km away from the site with elevation differences of 63 m and 51 m, respectively. These stations represent the closest observed wind speed and relative humidity estimates to the Ignace study area. Observations are preferred over data that has been spatially interpolated or modelled in reanalysis datasets for wind speed and relative humidity variables, as information from neighboring climate stations can be sparse and wind speed is not well represented in climate models. Distance from the site and elevation difference will also impact the applicability of the numbers. Therefore, the values provided should be interpreted qualitatively for the Ignace study area. The annual and monthly summaries for both climate stations are provided in Table 33 and Table 34.

Table 33: Wind Speed and Relative Humidity Data for SIOUX LOOKOUT A (6037775) Station from 1981-2010 Canadian Climate Normals

Month	Average Wind Speed (km/h)	Maximum Hourly Wind Speed (km/h)	Gust Wind Speed (km/h)	Average Relative Humidity at 6 am (%)	Average Relative Humidity at 3 pm (%)
January	11	48	76	75.9	70.4
February	11.1	48	78	75	62.5
March	11.9	64	76	74.7	53.8
April	12.4	63	91	73.7	45.1
May	12.4	64	83	77.1	47.5
June	11.5	58	107	82.4	51.7
July	10.6	56	102	85.9	53.4
August	10.9	54	100	88.1	54.8
September	12.2	56	90	89.4	61.1
October	12.8	58	96	86.8	67.2
November	12.9	64	89	86.5	75.1
December	11.3	59	111	81	75.8
Annual	11.8	64	111	81.4	59.8

The mean, maximum hourly, and gust windspeed for SIOUX LOOKOUT A (6037775) varies from 10.6 km/h to 12.9 km/h, 48 km/h to 64 km/h, and 76 km/h to 111 km/h respectively across calendar months, measured 10 m from the ground surface (Table 33). The monthly average relative humidity is generally higher in the morning than mid-day, with a range of 73.7% to 89.4% at 6 am and 45.1% to 75.8% at 3 pm.

Compared to SIOUX LOOKOUT A (6037775), the ATIKOKAN (6020379) climate station has slightly lower windspeeds with the mean, maximum hourly, and gust windspeed varying from 7 km/h to 9 km/h, 39 km/h to 58 km/h, and 59 km/h to 93 km/h respectively across calendar months (Table 34). The monthly average relative humidity is generally higher at ATIKOKAN (6020379) with a range of 46% to 75% at 3 pm (relative humidity values for 6 am were unavailable from ECCC). This may be due to the proximity of the ATIKOKAN (6020379) station to Lake Superior compared to SIOUX LOOKOUT A (6037775).

Table 34: Wind Speed and Relative Humidity Data for ATIKOKAN (6020379) Station from 1961-1990 Canadian Climate Normals

Month	Average Wind Speed (km/h)	Maximum Hourly Wind Speed (km/h)	Gust Wind Speed (km/h)	Average Relative Humidity at 6 am (%)	Average Relative Humidity at 3 pm (%)
January	7.2	42	59	—	71.9
February	6.9	42	65	—	67.9
March	8.3	52	69	—	61
April	8.6	44	70	—	47.3
May	8.3	42	78	—	46.2
June	8.2	43	93	—	53.8
July	7.1	45	74	—	55.1
August	6.8	42	85	—	57.6
September	7.8	39	78	—	60.8
October	8.5	58	65	—	63.6
November	7.9	46	78	—	71.8
December	6.9	42	63	—	75.4
Annual	7.7	58	93	—	61

It should be noted that the available climate normals from ECCC (2020) for these stations are associated with different time periods due to data availability. Therefore, any trends that are present in the underlying data series for wind speeds and relative humidity may affect the values provided and their applicability to the Ignace study area. As mentioned previously, the information from these stations represents the best available observed data for the Ignace study area. The values provided for each station should be compared and the most conservative value should be used as either station is located a considerable distance away from the site and has different siting conditions (e.g., elevation, geographic surroundings).

Trend analyses have been conducted using daily mean windspeed timeseries across Canada (Wan et al. 2010). In the region of the Ignace study area, a downward trend was found in the linear trends of homogenized monthly wind speeds for the period of 1953 to 2010. Categorized by season, an upward trend was found for the fall and winter, while downward trends were found for the spring and summer. This indicates that the climate normals for the wind speeds mentioned above are not stationary. Updated climate normals, as they are released, should be reviewed for changes in the wind speed observations provided.

4. ANALYSES OF FUTURE CLIMATE ON PMP, IDF, AND ADDITIONAL CLIMATE VARIABLE ESTIMATES

The following sections build on the current climate descriptions in Section 3 by providing the projected changes under future climate conditions for two future time horizons (2050s and 2080s) relative to the model baseline period of 1950 to 1993. The model baseline is based on projections from the GCMs for the same time period as the observations used to form the current climate baseline. The projected changes in climate are presented as the percentage change from the model baseline with guidance on how to apply the changes to the observed current climate baseline in order to obtain absolute values for future climate. Section 4.1 provides a description of future climate conditions used to estimate the potential changes in IDF curve and PMP estimates, which are later discussed in Sections 4.2 and 4.3. Rain on snow estimates are discussed in Section 4.4, and the additional climate variables are presented in Section 4.5. In all sections, projections are provided in terms of percentiles measured over the 136-member multi-model ensemble. Select tables presented in this section are coloured using a gradient to aid in the visual representation of the values. The colour gradients provide a relative indication of the highest (red) and lowest (green) values with transitional colours in between. Colours cannot be compared between tables, as the colour scale is relative for each.

The following sections focus on the 50th percentile to illustrate general trends, with the remaining percentiles included in Appendix B. Daily future timeseries developed for the additional climate variables are provided in Appendix C. Guidance on applying the percentile changes to the observed current climate basis is provided in Section 4.1.

4.1 FUTURE CLIMATE PROJECTIONS

Climate change has the potential to change future precipitation and temperature regimes that are important inputs for design purposes. Golder has developed a standardized approach to complete climate change assessments, which has been applied in the following sections to aid in the design of deep geological repositories for nuclear waste. The development of a detailed future climate assessment helps support the consideration of climate change in such designs. This climate change assessment report summarizes future projected changes in climate with a focus on extreme precipitation events. Future projected changes in IDF curves, PMP, and the additional climate variables (including annual and monthly temperature and precipitation statistics, WMO indices, rain and snow, snow depth, potential evapotranspiration, drought index, and qualitative information for wind speed and relative humidity) are estimated based on the best available climate science.

The IPCC is generally considered to be the definitive source of information related to past and future climate change as well as climate science. As an international body, the IPCC provides a common source of information relating to emission scenarios, provides third party reviews of models, and recommends approaches to document future climate projections. Periodically, the IPCC issues assessment reports summarizing the most current state of climate science. The Fifth Assessment Report (AR5) (IPCC 2013) represents the most current complete synthesis of information regarding climate change to date. The next assessment report (Sixth Assessment Report) is anticipated in 2022 and will build on the results from AR5. Future climate is typically projected using GCMs that involve the mathematical representation of global land, sea, and atmosphere interactions over a long time period. These GCMs have been developed by different government agencies but share common elements described by the IPCC. The IPCC does not run the models but acts as a clearinghouse for the distribution and sharing of the model forecasts. Future climate projections are made using scenarios that incorporate different representative concentrations pathways (RCPs) to drive the GCM simulations. The RCPs represent different trajectories for radiative forcing due to mainly anthropogenic influence on the climate cycle. The pathways are named after the radiative forcing projected to occur by 2100. Future climate projections are available from about 30 GCMs and four representative concentration pathways (RCP 2.6, RCP 4.5, RCP 6.0, and RCP 8.5) in AR5.

Downscaling procedures allow for GCM model output to be represented at a finer spatial scale which better represents local climate. Statistical downscaling refines GCM projections by incorporating observed data and statistical methods are applied to allow for a better match between local observed climate and historical GCM model output. These methods are then applied to future GCM projections which are assumed to be more representative of local climate. This report focuses on analysis using the statistically downscaled daily data using the Bias Correction/Construction Analogues with Quantile mapping reordering version 2 (BCCAQv2) model from ClimateData.ca (ClimateData 2019), and the Localized Constructed Analogues (LOCA) model from the GDO-DCP archive (Pierce et al. 2014; Reclamation 2013). Climate variables of daily minimum and maximum temperature and precipitation are obtained from these datasets. Three RCP scenarios (RCP 2.6, RCP 4.5, and RCP 8.5) are currently available from ClimateData.ca for the BCCAQv2 model and are used in this report, while only two RCP scenarios (RCP 4.5 and RCP 8.5) are available for LOCA. Details regarding the methodology, number of model projections, and resolution of both the BCCAQv2 and LOCA datasets are included in Appendix A.

Since no one model or climate scenario can be viewed as completely accurate, the IPCC recommends that climate change assessments use as many models and climate scenarios as possible, or a “multi-model ensemble”. For this reason, the multi-model ensemble approach is used to delineate the probable range of results using percentiles. The percentiles are used show the distribution of projected changes. This allows for uncertainty in the projections to be understood, while the 50th percentile is used to illustrate general trends. For critical infrastructure, selection of future projections at higher percentiles and higher return periods should be considered. For example, for critical infrastructure whose failure is considered unacceptable, a 95th percentile could be considered over the typical 50th percentile. The projected changes in climate for the site are calculated using three separate time periods including:

- Model baseline (1950 to 1993) – this time-period represents the current climate conditions for which the changes are estimated using each member of the multi-model ensemble.
- Mid-century (2041 to 2070) – used to represent changes in climate projected for the near future.
- End-of-century (2071 to 2100) – used to represent the furthest projections into the future possible with the available climate model scenarios. Changes in climate are typically greater for this period compared to the mid-century for the RCP4.5 and RCP8.5 scenarios.
- Beyond 2100 - qualitative climate assessment (climate projections beyond 2100 are not currently available from ClimateData.ca) provided using the projected trends from the mid-century and end-of-century periods guided by literature.

Changes in climate for the mid-century and end-of-century future periods are calculated as percentage changes from the model baseline to avoid model bias influencing the results. Absolute values for the future climate projections can be obtained by applying the percentage changes to the observed data for a given percentile level from the multi-model ensemble as outlined in Appendix A (Sections A3.3 and A3.4).

The planned Project phases and how they correspond to the selected time periods are shown in Figure 8. The mid-century period coincides with part of the site characterization, preparation, and construction phase. The mid-century and part of the end of century time periods coincide with the operational period phase. Part of the end of century time period coincides with the extended monitoring period, and the qualitative climate assessment period corresponds with both the extended monitoring and decommissioning period Project phases. The extended monitoring and decommissioning periods extend past the year 2100 up to 2180.

Each of the Project phases coincide with part of the selected climate assessment periods. Percentiles from the multi-model ensembles for mid- and end-of-century may be selected in a way that accounts for how the Project phases and climate periods overlap. For example, a lower percentile may be used to cover the site characterization, preparation, and construction phase, as the mid-century period represents time horizon beyond this project phase. Similarly, a higher percentile may be used for the extended monitoring phase as it takes place after the end-of-century period. The 50th percentile level may be selected from the end-of century climate period to represent the operational project phase. Different percentile levels may be selected from the climate projections based on the level of associated risk for design purposes. For designs that are associated with a high level of risk, the 95th or 99th percentile level may be used. For project phases past 2100, a high percentile from the end-of-century climate period can be used for screening purposes. The qualitative climate assessment provides further guidance on how the climate may change past the year 2100.

The qualitative climate assessment period takes into consideration both the mid-century and end-of-century periods, as well as Extended Concentration Pathways (ECPs). ECPs have been developed by extending the RCP scenarios until the year 2300 using Earth Models of Intermediate Complexity (EMICs). The results of the EMIC extensions are consistent until 2300 with atmospheric-ocean general circulation models used in the IPCC fifth assessment report. Only global values are provided and are not directly applicable to the site; however, they provide qualitative trajectories of changes in temperature and precipitation in the far future.

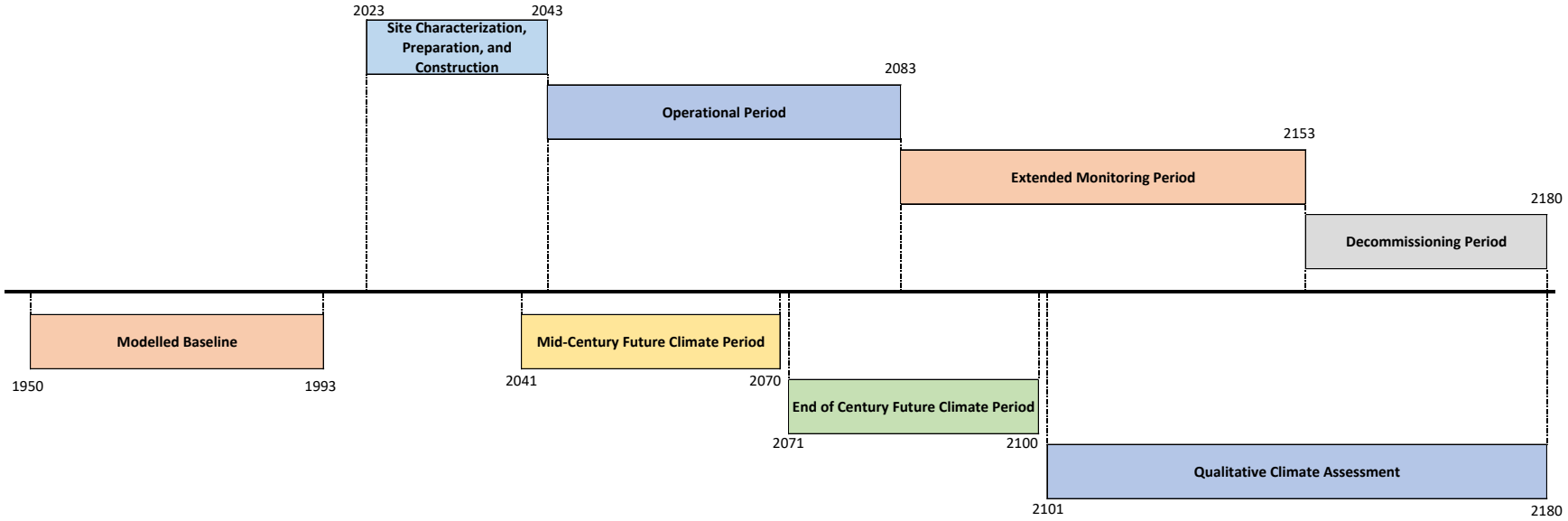

Figure 8: Overview of Project Phases and Selected Future Climate Periods

The future projected changes in PMP are calculated using the Hershfield and moisture maximization methods. Future projected changes in IDF curves for sub-daily, daily, and multi-day durations were estimated using the Equidistant Quantile Mapping (EQM) method and the Ratio method. The same approach for estimating changes in IDF curves is applied to combined daily rain and snowmelt. The ensemble approach is used for all future projections, providing the results for a range of percentiles which takes multiple climate models, emission scenarios, and calculation methodologies into account. Details regarding the methodology for all the analyses provided in this report can be found in Appendix A. The following sections focus on the 50th percentile to illustrate general trends. The remaining percentiles are included in Appendix B.

4.2 CLIMATE CHANGE IMPACTS ON IDF CURVES

The percent changes in IDF conditions (future periods relative to model baseline) were estimated for different durations of extreme rainfall events. Selected results for the 50th percentile for the 2050s and 2080s climatic horizons are summarized in the following sub-sections. Detailed methodology for this section can be found in Section A3.3. Additional results have been included in Appendix B in an Excel spreadsheet format. This format was selected to allow for the results to be more easily accessible and improve the readability of the report.

4.2.1 Percent Changes in Sub-Daily IDF Curves

Sub-daily IDF curves are generally used to size site infrastructure for catchments small enough that runoff from the catchment would peak in less than 24 hours.

Daily rainfall amounts are provided in the climate model ensemble; however, sub-daily rainfall in the future projections are not available. The change in sub-daily rainfall statistics can be inferred by examining the projected changes for the 1-day duration. A summary of the projected changes in 1-day rainfall for the 2-, 5-, 10-, 25-, 50-, 100-, 1000-, and 2000-year return period are presented here for the 2050s and 2080s (Table 35 and Table 36). In the 2050s, the 1-day rainfall amount is projected to increase between 9.5% to 16.8% for the 50th percentile across return periods, while in the 2080s this is projected to increase between 11.8% to 18.1%. Based on these results, daily precipitation is expected to become more intense in the future. This is particularly true in the case of extreme rainfall events due to larger percentage increases shown as return period increases. Changes in sub-daily rainfall durations can be estimated by applying the changes in the 1-day rainfall amounts for the 2050s (Table 35) and 2080s (Table 36) to the observed sub-daily durations (Table 14).

Changes in atmospheric processes driving extreme rainfall will unlikely be uniform in the future climate for sub-daily rainfall durations. However, climate models are not yet able to fully resolve convective processes responsible for generating extreme precipitation amounts on finer spatial scales and contributing to extreme precipitation in larger scale synoptic systems (CSA 2012). Despite this fact, climate projections generally support an increase in short duration rainfall in future climate within Canada (CSA 2012). Therefore, the projected changes in sub-daily rainfall based on the 1-day projected changes should be used with caution. A higher percentile level may be used to account for uncertainty in sub-daily precipitation projections provided here.

Table 35: Summary of the Projected Changes (%) in 1-day Rainfall in 2050s for Ignace Study Area

Statistical indices	Return Period (years)									
	2	5	10	20	50	100	200	500	1000	2000
Minimum	-15.1%	-17.8%	-18.1%	-20.3%	-27.0%	-33.1%	-38.2%	-43.9%	-47.5%	-50.7%
5%	-6.7%	-4.8%	-7.3%	-11.5%	-15.2%	-17.4%	-20.0%	-23.1%	-25.1%	-27.1%
10%	-3.2%	-1.9%	-3.1%	-6.4%	-9.5%	-12.0%	-15.7%	-17.0%	-17.9%	-19.7%
25%	2.7%	4.0%	4.0%	3.6%	1.7%	0.5%	-1.0%	-1.6%	-2.2%	-2.9%
50%	9.5%	11.0%	12.2%	13.2%	14.3%	14.3%	14.4%	15.6%	16.3%	16.8%
75%	15.7%	18.5%	20.9%	24.1%	26.5%	28.7%	31.0%	33.8%	35.7%	37.0%
90%	23.7%	24.8%	30.0%	34.9%	41.8%	46.2%	50.0%	55.3%	59.9%	64.2%
95%	28.8%	29.5%	32.6%	43.4%	54.7%	62.6%	68.7%	76.2%	81.6%	86.5%
99%	32.1%	33.2%	46.1%	60.0%	86.0%	98.9%	108.6%	120.3%	131.0%	140.7%
Maximum	33.7%	37.9%	55.6%	72.1%	91.3%	107.7%	124.5%	144.1%	157.1%	168.9%
Mean	9.7%	11.4%	12.9%	14.3%	16.0%	17.1%	18.0%	19.2%	20.0%	20.7%
Standard deviation	10.3%	10.3%	12.9%	16.5%	21.3%	24.7%	27.7%	31.3%	33.7%	36.0%

Table 36: Summary of the Projected Changes (%) in 1-day Rainfall in 2080s for Ignace Study Area

Statistical indices	Return Period (years)									
	2	5	10	20	50	100	200	500	1000	2000
Minimum	-11.0%	-8.0%	-13.7%	-23.0%	-32.3%	-37.9%	-42.6%	-47.7%	-51.0%	-53.9%
5%	-6.6%	-5.0%	-4.3%	-5.2%	-8.1%	-11.0%	-13.9%	-16.6%	-18.8%	-20.7%
10%	-2.3%	-0.2%	-2.4%	-3.1%	-4.9%	-5.6%	-6.8%	-9.0%	-10.6%	-11.7%
25%	5.6%	7.4%	6.8%	5.4%	3.1%	1.8%	0.9%	-0.6%	-1.5%	-2.1%
50%	11.8%	14.7%	15.6%	16.1%	16.8%	17.8%	17.9%	18.0%	18.1%	18.1%
75%	20.1%	23.6%	26.6%	29.4%	30.3%	31.0%	32.4%	34.8%	35.6%	36.9%
90%	26.6%	31.2%	35.0%	42.7%	53.6%	60.7%	66.7%	73.2%	78.9%	83.2%
95%	31.1%	35.6%	46.2%	57.5%	69.2%	76.0%	83.1%	92.1%	96.7%	100.7%
99%	42.9%	43.4%	58.6%	77.4%	98.7%	112.1%	124.0%	137.6%	146.7%	155.0%
Maximum	47.1%	51.2%	65.1%	89.0%	119.4%	139.6%	157.8%	178.9%	193.1%	205.9%
Mean	12.8%	15.4%	17.2%	18.8%	20.6%	21.8%	22.9%	24.1%	24.9%	25.6%
Standard deviation	11.3%	11.8%	15.0%	19.0%	24.2%	27.7%	31.0%	34.8%	37.4%	39.7%

4.2.2 Percent Changes in Daily and Multi-Daily IDF Curves

Compared to sub-daily IDF values, the multi-day IDF values are used primarily to assess large catchments (where it takes more than 24 hours for flows to peak following a rainfall) and for water management systems (like dewatering and pumping).

The percent changes in daily and multi-day IDF conditions (future periods relative to the model baseline) were estimated for different durations of extreme rainfall events (ranging from 1 day to 120 days). Selected results for the 50th percentile are summarized in Table 37 and Table 38. The methodology is described in Section A.3.3. The remaining percentiles for all the duration periods are presented in Appendix B.

Note that the method used to produce the 24-hour results discussed in Section 4.2.1 (using sub-daily data and interpolating between Atikokan and Sioux Lookout) is different from the method used to produce the 1-day results in this section (fitting a curve to the daily projections for Ignace). The projected changes for the 50th percentile 1-day IDF curves range from 9.5% to 16.8% in the 2050s (Table 37) and 11.8% to 18.1% in the 2080s (Table 38). Generally, the longer durations show a smaller percentage increase (compared to the shorter durations) for both the 2050 and 2080 horizons. This suggests that shorter events are more sensitive to climate change effects, while longer events may be more likely to follow historic patterns.

Projections for the 10-, 20-, and 50-year 24-hour events are available in Canada's Changing Climate report for Ontario using a multi-model ensemble 29 global climate models for comparison (Bush and Lemmen 2019). The report shows that the 24-hour hour event for the 10-, 20-, and 50-year return period is projected to change between 6% to 8.5%, 5.7% to 8.2%, and 4.9% to 8.5% respectively for the period of 2031 to 2050, and 5.3% to 20.5%, 5.1% to 20.1%, and 7.6% to 20.1% respectively for the period of 2081 to 2100 (Bush and Lemmen 2019). It should be noted that these values use global climate models that are not downscaled, have different time periods from those in this report, and present average values from the model ensemble as opposed to 50th percentile shown here. In general, the results shown in Table 37 and Table 38 are slightly higher than the range of projections made in Bush and Lemmen (2019) for the 2050s period and are within the range for the 2080s period.

4.3 CLIMATE CHANGE IMPACTS ON PMP ESTIMATES

PMP values are typically used to assess the safety of critical infrastructure such as dams, where failure of the infrastructure would cause significant damage and/or loss of life. The projected percentage changes in PMP shown here are point projections for the site that are not based on any specific watershed size. Therefore, these projected changes in PMP shown here are the same for the projected DAD curves of the corresponding event duration. Absolute values for future DAD curves can be obtained by applying the percentage changes in PMP to the DAD curves presented for current climate given in Section 3.3.3.

The percent changes in PMP estimates (future periods relative to model baseline) were estimated for future PMP using the Hershfield and Moisture Maximization methods. Both methods provide point estimates of PMP and require the use of annual maximum precipitation series for a given location. The annual maximum precipitation projections for the Ignace study area described in Section 4.1 are used; therefore, the PMP values provided are applicable to the study area and are not associated with a particular watershed or its size.

Table 37: Summary of the 50th Percentile of Projected Percent Changes in Rainfall in the 2050s for Ignace Study Area

Return Period (years)	1-Day	2-Day	3-Day	4-Day	5-Day	6-Day	7-Day	10-Day	20-Day	30-Day	50-Day	75-Day	90-Day	120-Day
2	9.5%	9.3%	9.0%	8.5%	7.9%	7.8%	8.7%	8.1%	6.5%	6.1%	5.2%	5.4%	5.2%	4.5%
5	11.0%	12.3%	11.5%	9.9%	9.8%	10.0%	10.2%	9.7%	8.2%	7.0%	4.6%	3.6%	3.0%	2.9%
10	12.2%	13.5%	13.3%	11.6%	10.7%	10.0%	10.4%	10.1%	7.8%	7.5%	5.1%	3.7%	2.5%	3.0%
20	13.2%	15.7%	16.8%	13.8%	11.2%	9.2%	10.5%	9.6%	7.5%	8.2%	5.7%	4.6%	2.1%	3.1%
50	14.3%	18.7%	19.1%	15.2%	11.6%	10.8%	11.0%	10.0%	10.5%	8.4%	6.7%	4.8%	2.8%	3.8%
100	14.3%	20.9%	20.7%	15.4%	12.1%	11.6%	11.0%	10.2%	11.3%	9.5%	7.1%	5.0%	2.9%	4.0%
200	14.4%	22.1%	21.9%	16.6%	12.5%	12.3%	11.4%	9.6%	11.2%	10.0%	7.4%	6.1%	2.5%	3.7%
500	15.6%	24.0%	23.4%	17.3%	12.9%	12.3%	11.1%	9.6%	10.9%	10.4%	7.6%	6.2%	1.9%	3.7%
1,000	16.3%	24.8%	24.1%	17.8%	13.7%	12.4%	11.2%	9.9%	11.3%	10.6%	7.3%	6.4%	1.8%	3.8%
2,000	16.8%	25.1%	24.6%	18.1%	13.9%	12.8%	11.7%	9.9%	11.7%	10.8%	7.4%	6.7%	1.9%	3.6%

Table 38: Summary of the 50th Percentile of Projected Percent Changes in Rainfall in the 2080s for Ignace Study Area (%)

Return Period (years)	1-Day	2-Day	3-Day	4-Day	5-Day	6-Day	7-Day	10-Day	20-Day	30-Day	50-Day	75-Day	90-Day	120-Day
2	11.8%	11.5%	11.4%	11.2%	12.0%	11.1%	11.3%	10.0%	8.1%	7.6%	5.9%	5.4%	4.4%	3.8%
5	14.7%	15.1%	14.5%	12.6%	12.6%	12.2%	11.9%	10.8%	9.7%	8.7%	6.8%	5.6%	4.9%	4.3%
10	15.6%	18.1%	17.3%	15.3%	14.2%	12.8%	13.2%	11.9%	11.3%	9.9%	7.5%	6.2%	5.6%	4.0%
20	16.1%	19.4%	18.0%	15.9%	14.2%	13.6%	13.9%	13.3%	12.2%	11.0%	6.9%	6.6%	6.1%	4.3%
50	16.8%	22.6%	20.1%	16.4%	15.1%	14.0%	14.4%	14.0%	13.1%	13.0%	8.0%	7.2%	5.9%	4.7%
100	17.8%	23.3%	21.3%	16.5%	14.7%	13.6%	14.4%	15.3%	13.4%	13.6%	9.0%	7.2%	6.5%	5.2%
200	17.9%	24.2%	21.7%	17.0%	14.3%	13.6%	14.9%	16.3%	13.5%	14.4%	9.2%	7.9%	7.0%	5.5%
500	18.0%	25.1%	22.8%	17.4%	14.9%	14.1%	15.0%	17.8%	14.0%	15.2%	9.5%	8.9%	7.1%	5.1%
1,000	18.1%	26.0%	22.5%	17.7%	15.1%	14.2%	15.2%	18.6%	14.6%	15.1%	9.5%	9.1%	8.1%	4.8%
2,000	18.1%	26.6%	23.6%	18.0%	15.0%	14.3%	15.0%	19.3%	14.1%	15.9%	10.1%	9.6%	8.2%	4.8%

Sub-daily climate projections are not available, which are required to generate sub-daily estimates of PMP using these methods. Therefore, PMP is estimated for the 1-, 2-, and 3-day durations (Table 39 and Table 40). The 50th percentile results suggest increases in the 1-day PMP of 18.7% for the 2050s and 25.4% for the 2080s. The results agree with the expectation that as temperature increases under future climate conditions, precipitation is expected to increase as more vapor becomes available in the atmosphere (Kunkel et al. 2013), resulting in a rise in the projected PMP. The range of results for the 1-day PMP (from -27.4% to +103.4% in 2050s and -24.6% and +126.0% in 2080s) suggest that significant flexibility may be required in the future for systems designed for the PMP event.

Table 39: Summary of Selected Percentiles of Projected Percent Changes in PMP Estimates in the 2050s for Ignace Study Area

Percentiles	1-Day	2-Day	3-Day
Minimum	-27.4%	-30.9%	-28.0%
5%	-7.5%	-6.0%	-6.4%
25%	8.6%	11.2%	10.3%
50%	**18.7%**	**18.7%**	**18.5%**
75%	28.3%	30.0%	28.1%
95%	55.8%	54.8%	51.7%
Maximum	103.4%	79.6%	83.7%

Table 40: Summary of Selected Exceedance Probabilities of Projected Percent Changes in PMP Estimates in the 2080s for Ignace Study Area

Percentiles	1-Day	2-Day	3-Day
Minimum	-24.6%	-17.5%	-18.4%
5%	-4.5%	-4.0%	-4.9%
25%	12.4%	13.3%	11.5%
50%	**25.4%**	**27.4%**	**25.7%**
75%	40.2%	44.4%	41.3%
95%	69.8%	73.6%	71.8%
Maximum	126.0%	111.7%	111.4%

Kunkel et al. (2013) used seven GCMs from the CMIP5 to project changes in PMP for the 2050s and 2080s future time periods from the 1971 to 2000 baseline. It was found that ensemble average projected maximum precipitable water changes for Ontario were on the order of 25-35%. The 2080s projection for the 50th percentile in this report is within the range projection in Kunkel et al. (2013); however, the 2050s value is slightly below. Clavet-Gaumont et al. (2017) used an ensemble of 12 RCM runs to project the change in PMP between the periods of 1971 to 2000 and 2041 to 2070 time periods for 5 major Canadian water basins. The 24-, 48-, and 72-hour springtime changes in PMP for the Mattagami river basin (which drains a major portion of northern Ontario) were estimated as 8%, 4%, and 5% respectively, with no consensus in the sign of the change, significantly lower than that of this report as well as Kunkel et al. (2013). The models used and time periods analyzed are different between this study and those in the literature. However, the comparison allows the number to be put into context with the range of those projected previously for a similar area.

Note that the method used to estimate changes in PMP (using the Hershfield and Moisture Maximization methods) is again different from the methods to estimate sub-daily IDF (interpolating changes at Atikokan and Sioux Lookout) and the method used for multi-day IDFs (fitting a curve to the daily projections for Ignace). However, the projected changes in the 50th percentile for 1-day PMP (18.7% in the 2050s and 25.4% in the 2080s; see Table 39 and Table 40) represent the most conservative estimate, as the changes are larger than projected changes for the 50th percentile 1-day IDF curves (9.5% to 16.8% in the 2050s and 11.8% to 18.1% in the 2080s; see Table 37 and Table 38). The larger percent change for the 1-Day PMP event is expected, as the PMP event represents a significantly more extreme event than a return period storm.

Daily rainfall amounts are provided in the climate model ensemble; however, timeseries of sub-daily rainfall in the future projections are not available. Therefore, the same approach used for projecting future sub-daily IDF curves in Section 4.2.1 is also used here. Future sub-daily PMP values can be estimated by applying the percentage changes in the 1-day PMP (Table 39 and Table 40), to the sub-daily PMP values (Table 23) for a given percentile level. This assumes that the changes in sub-daily PMP are the same for the 1-day PMP. Further justification for this approach can be found in Section 4.2.1.

4.4 CLIMATE CHANGE IMPACTS ON RAINFALL ON SNOW

The daily snowpack/snowmelt analysis used the daily precipitation and temperature projections at Ignace (using the same ECCC method as for the baseline climate). These results are used to assess large catchments where peak flooding events may be driven by a combination of rain and melt events (rather than by rain alone, as is assumed the case in IDF and PMP). Previous studies have found that the use of combined rainfall and snowmelt statistics instead of only precipitation can help prevent over or under design, and that the impact of this varies based on the location considered (Yan et al. 2018). The projected changes in the 50th percentile are shown in Table 41 and Table 42 below (future periods relative to the model baseline). For short durations (1 to 3 days), there is a general increase; this is likely the result of larger one-day rainfall events (shown on Table 37 and Table 38 above), which are expected to continue dominating short duration rain-on-snow events. For mid-range durations (6 to 30 days), there is a general downward trend, with larger decreases in the 2080s than in the 2050s, suggesting a general decrease in future snowmelt events which are expected to play a more significant role in the mid-duration rain on snow events. This is also in agreement with an expected decrease in peak snowpack seen in Table 43 (relative to the model baseline from the GCM ensemble over 1950-1993). The longest duration events (120 days) generally match the expected increases in long-duration rainfall (as shown on Table 37 and Table 38) with a range of 5.1% to 6.9% in the 2050s and 2.3% to 5% in the 2080s.

Table 41: Summary of the 50th Percentile of Projected Percent Changes in Rain on Snow Events in the 2050s for Ignace Study Area

Return Period (years)	1-Day	2-Day	3-Day	4-Day	5-Day	6-Day	7-Day	10-Day	20-Day	30-Day	50-Day	75-Day	90-Day	120-Day
2	12.4%	7.4%	3.0%	-0.5%	-2.3%	-3.1%	-4.2%	-6.0%	-6.5%	-5.2%	-2.5%	1.1%	3.3%	6.9%
5	15.0%	10.4%	4.9%	1.7%	-1.4%	-2.9%	-3.0%	-4.5%	-5.3%	-4.3%	-2.4%	0.6%	3.1%	6.2%
10	16.7%	12.2%	6.5%	3.7%	-0.1%	-2.5%	-2.2%	-4.0%	-5.1%	-3.5%	-2.1%	0.8%	3.0%	6.1%
20	18.2%	12.5%	7.7%	5.3%	1.1%	-2.0%	-1.7%	-3.8%	-4.9%	-2.9%	-1.8%	1.1%	3.3%	5.7%
50	19.6%	13.6%	8.9%	6.5%	1.7%	-1.4%	-1.1%	-3.6%	-4.5%	-2.9%	-1.3%	0.9%	3.2%	5.2%
100	20.1%	14.2%	9.5%	6.8%	1.7%	-0.9%	-0.7%	-3.5%	-4.3%	-3.0%	-1.0%	1.4%	3.5%	5.1%
200	20.6%	14.9%	10.1%	7.3%	1.6%	0.1%	-0.1%	-3.2%	-4.0%	-2.4%	-0.7%	1.5%	2.7%	5.1%
500	21.3%	15.5%	11.0%	7.5%	2.1%	0.3%	0.2%	-3.1%	-3.8%	-1.8%	-0.1%	1.8%	3.0%	5.4%
1,000	21.8%	15.8%	11.6%	7.6%	3.0%	0.5%	0.6%	-3.0%	-3.5%	-1.6%	0.0%	1.8%	3.4%	5.3%
2,000	22.2%	16.0%	11.6%	8.0%	3.5%	0.8%	0.5%	-2.7%	-3.2%	-1.3%	-0.1%	1.4%	3.2%	5.2%

Table 42: Summary of the 50th Percentile of Projected Percent Changes in Rain on Snow Events in the 2080s for Ignace Study Area (%)

Return Period (years)	1-Day	2-Day	3-Day	4-Day	5-Day	6-Day	7-Day	10-Day	20-Day	30-Day	50-Day	75-Day	90-Day	120-Day
2	9.2%	4.9%	-1.7%	-6.5%	-9.1%	-10.5%	-12.3%	-13.9%	-15.5%	-12.8%	-9.0%	-5.7%	-3.1%	2.3%
5	12.5%	7.2%	-0.5%	-4.6%	-5.8%	-8.8%	-10.5%	-12.2%	-13.5%	-10.5%	-6.7%	-3.6%	-1.6%	2.6%
10	13.9%	8.9%	1.1%	-3.5%	-6.2%	-8.0%	-8.7%	-11.9%	-13.6%	-9.8%	-6.5%	-3.1%	-0.9%	3.2%
20	14.6%	10.2%	2.0%	-3.2%	-5.9%	-7.7%	-9.1%	-11.9%	-13.7%	-9.4%	-5.7%	-2.7%	-0.9%	3.6%
50	15.7%	11.5%	2.8%	-3.0%	-5.5%	-8.2%	-9.8%	-11.2%	-13.3%	-8.7%	-4.9%	-2.3%	-0.4%	4.5%
100	16.3%	12.6%	2.8%	-2.8%	-5.7%	-8.8%	-9.7%	-11.1%	-12.8%	-8.2%	-4.8%	-2.0%	-0.1%	4.5%
200	16.9%	12.9%	3.4%	-2.4%	-6.0%	-9.0%	-9.5%	-11.0%	-12.5%	-7.5%	-4.7%	-1.0%	0.3%	5.0%
500	17.8%	13.4%	3.9%	-1.8%	-6.3%	-8.9%	-9.8%	-10.3%	-12.2%	-6.4%	-4.7%	-0.4%	0.8%	4.9%
1,000	18.7%	13.7%	4.2%	-1.4%	-6.2%	-8.3%	-9.7%	-10.4%	-12.2%	-6.2%	-4.5%	0.0%	1.4%	4.8%
2,000	19.2%	14.2%	4.4%	-1.2%	-6.2%	-7.7%	-9.5%	-10.7%	-12.1%	-6.0%	-4.4%	0.3%	1.7%	4.6%

Table 43: Percent Change in Peak Snowpack Accumulation for the Ignace Study Area (50th Percentile)

Return Period (years)	2	5	10	20	50	100	200	500	1,000	2,000
Baseline to 2050s	-8.3%	-7.5%	-6.5%	-5.5%	-4.3%	-3.0%	-2.1%	-1.9%	-1.4%	-1.1%
Baseline to 2080s	-13.8%	-10.5%	-8.8%	-7.2%	-6.0%	-5.5%	-4.4%	-3.8%	-3.4%	-2.7%

4.5 CLIMATE CHANGE IMPACTS ON ADDITIONAL CLIMATE VARIABLES

Analysis of climate variables in addition to extreme rainfall provides contextual climate change information for the Ignace study area. These include projected changes in annual and monthly temperature and precipitation statistics from which seasonal variation can be inferred. Derived climate variables including rain and snow, snow depth, potential evapotranspiration, drought index, and qualitative information for wind speed and relative humidity. The information provided for wind speed and relative humidity may be interpreted qualitatively, as downscaled climate projections for these variables are limited. Daily future climate timeseries are provided to facilitate additional studies relating to climate change impacts at the Ignace study area.

4.5.1 Projected Changes in Precipitation and Temperature Statistics

Statistically downscaled projections of daily total precipitation and mean temperature variables are used to estimate the change in monthly mean, minimum, and maximum statistics from the model baseline to future periods. Changes in precipitation are provided as percentage changes from the current climate baseline, while changes in temperature are provided as absolute values in degree Celsius. This is typically done to facilitate the application of projected changes to the baseline values (Anandhi et al. 2011).

Annual total precipitation is projected to increase by 6.8% in the 2050s and 9.4% in the 2080s, indicating an upward trend in total precipitation on an annual scale at the 50th percentile (Table 44 and Table 45). In the 2050s, monthly total precipitation at the 50th percentile is projected to increase for all months except July and August which are projected to change by -1.1% and -4.4% respectively (Table 44). The largest projected increase at the 50th percentile is found in the month of December at 18.6%. The total range of projected monthly changes in precipitation for the multi-model ensemble corresponds to -38.8% in August and 72.2% in December. In the 2080s, the months of July and August also project decreasing precipitation of -1.9% and -8.7% at the 50th percentile while all other month project increasing precipitation amounts (Table 45).

The seasonal variation in projected changes (projected decrease in summer months and greatest projected increase in December) have been confirmed with those provided by the Ontario Climate Data Portal for the 2050s and 2080s time periods for the Ignace study area using a 1986 to 2005 baseline period (OCDP 2020). The reason for the projected decrease in summer precipitation is a consequence of overall surface drying and changes in atmospheric circulation as a result of climate change (Collins et al. 2013). Under the RCP4.5 scenario, for months of July and August, the OCDP values show a projected decrease in precipitation of -22% and -26%, while in December a 34% increase is projected for the 2050s. The difference in values between those reported here are due to the use of a different multi-model ensemble as well as different baseline periods. The range of projected changes for monthly total precipitation in Table 44 and Table 45 across calendar months is illustrated in Figure 9. Similarly, Bush and Lemmen (2019) show a median annual increase across Ontario of 5.5 % (0.4% to 11.1%, 25th and 75th percentile respectively) for RCP2.6 and 6.6% (1.8% to 12.4%, 25th and 75th percentile respectively) for RCP8.5, for the period from 2031 to 2050. This is generally lower than the projected increases for the Ignace study area but reflect differences the regions covered and the future time periods considered. The period from 2081 to 2100 shows increases of 5.3% (-0.1% and 10.8% for the 25th and 75th percentiles) for RCP 2.6 and 17.3% (8.5% and 26.1% for the 25th and 75th percentiles) for RCP8.5, which encompasses most of the monthly median values in Table 44 and Table 45.

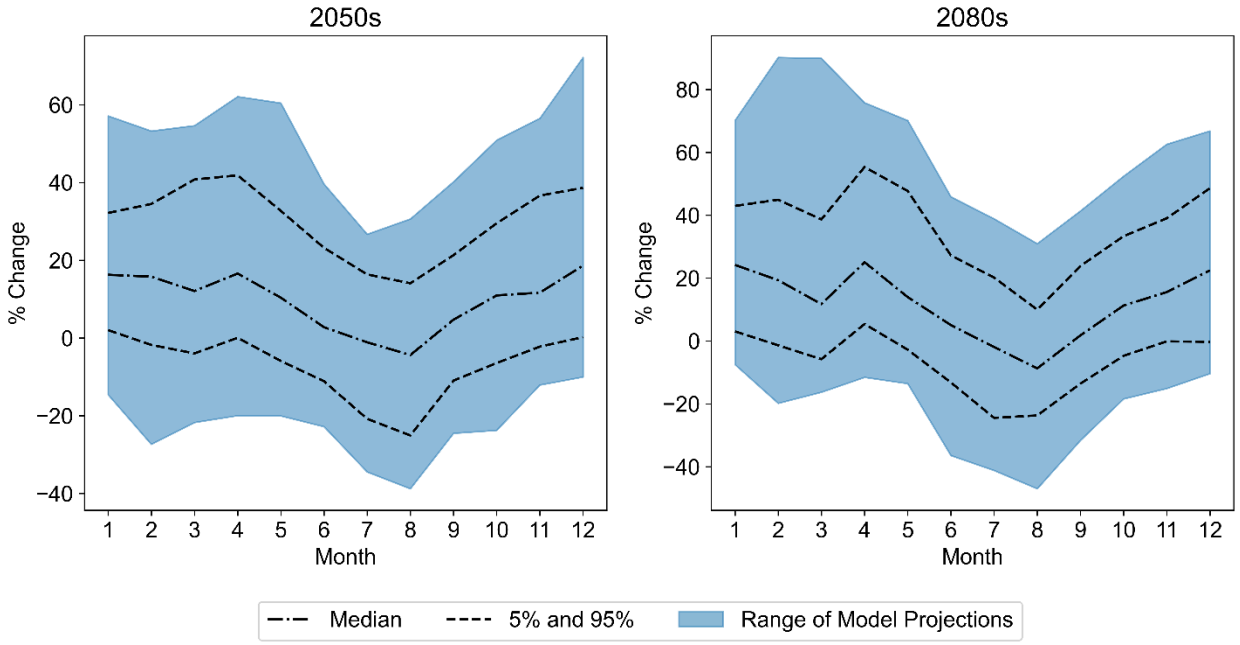

Figure 9: Range of Projected Changes in Monthly Total Precipitation for the Multi-Model Ensemble.

The seasonal variation provided in this report (increasing total precipitation in winter and decreasing in summer) is supported by Bush and Lemmen (2019). The values provided in Bush and Lemmen (2019) are based on coarse resolution global climate models; however, it is shown that in the winter months for the 2031 to 2050 period, Bush and Lemmen (2019) show projected changes in precipitation ranging from 0 to 20%, while in the summer months the ensemble projections range from -10% to 10% for the Ignace study area. Bush and Lemmen (2019) also show that for the 2081 to 2100 period, a projected increase of 0 to 30% is shown for the winter months, while the summer months the changes in precipitation range from -10% to 10%.

The range of total monthly precipitation changes is larger in the 2080s, corresponding to -47% in August and 90.2% in February (Table 45). The 50th percentile may be used as a screening value for total monthly precipitation; however, it should be noted that there is a large range of projections of total precipitation at the Ignace study area, indicating lack of agreement or uncertainty in the projections. In all months, the multi-model ensemble range covers both a projected increase and decrease in total precipitation.

Table 44: Projected Changes in Monthly Total Precipitation for the 2050s (%)

Statistic	Jan	Feb	Mar	Apr	May	Jun	Jul	Aug	Sep	Oct	Nov	Dec	Annual
Minimum	-14.6%	-27.4%	-21.7%	-20.0%	-20.0%	-22.8%	-34.5%	-38.8%	-24.5%	-23.8%	-12.1%	-10.0%	-5.4%
10%	2.0%	-1.8%	-4.0%	0.0%	-5.9%	-11.1%	-20.8%	-25.1%	-11.0%	-6.4%	-2.2%	0.2%	0.6%
25%	7.7%	6.0%	1.5%	7.4%	-0.2%	-6.3%	-10.4%	-13.3%	-5.5%	0.5%	3.8%	8.1%	3.5%
50%	16.3%	15.8%	12.1%	16.6%	10.4%	2.8%	-1.1%	-4.4%	4.7%	11.0%	11.7%	18.6%	6.8%
75%	24.2%	24.9%	26.2%	29.5%	20.1%	14.1%	9.2%	7.0%	14.0%	21.3%	23.7%	31.1%	11.8%
90%	32.2%	34.5%	40.8%	41.9%	32.7%	23.2%	16.4%	14.1%	21.3%	29.5%	36.7%	38.6%	17.3%
95%	36.0%	42.2%	45.4%	46.2%	36.1%	29.5%	19.6%	17.5%	25.1%	34.8%	39.6%	51.5%	19.3%
99%	46.9%	48.8%	50.5%	59.4%	50.8%	33.8%	25.1%	28.1%	34.0%	42.5%	48.0%	67.5%	22.8%
Maximum	57.2%	53.3%	54.6%	62.1%	60.5%	39.6%	26.7%	30.6%	40.2%	50.9%	56.5%	72.2%	24.3%
Mean	16.4%	15.6%	14.8%	19.0%	11.3%	4.3%	-1.1%	-4.0%	5.0%	11.1%	14.2%	20.3%	7.9%
Standard Deviation	12.3%	15.8%	17.0%	16.0%	15.1%	13.7%	13.9%	15.0%	12.5%	14.5%	14.6%	16.6%	6.4%

Table 45: Projected Changes in Monthly Total Precipitation for the 2080s (%)

Statistic	Jan	Feb	Mar	Apr	May	Jun	Jul	Aug	Sep	Oct	Nov	Dec	Annual
Minimum	-7.5%	-19.8%	-16.3%	-11.6%	-13.6%	-36.4%	-41.2%	-47.0%	-31.6%	-18.4%	-15.1%	-10.4%	-6.0%
10%	3.0%	-1.4%	-5.8%	5.4%	-2.8%	-13.2%	-24.5%	-23.7%	-13.6%	-4.7%	-0.1%	-0.3%	1.4%
25%	11.9%	10.8%	3.5%	14.1%	5.3%	-5.7%	-14.7%	-14.4%	-3.5%	1.8%	5.7%	8.5%	4.9%
50%	24.2%	19.3%	11.7%	25.1%	14.0%	5.0%	-1.9%	-8.7%	1.8%	11.3%	15.5%	22.4%	9.4%
75%	32.9%	34.9%	24.0%	37.8%	28.1%	15.0%	8.5%	3.6%	12.8%	22.1%	30.4%	37.4%	13.4%
90%	43.0%	44.9%	38.7%	55.3%	47.7%	27.2%	20.2%	10.0%	23.9%	33.3%	39.0%	48.6%	18.9%
95%	48.2%	51.7%	51.7%	67.9%	51.1%	31.9%	31.3%	14.2%	28.5%	38.1%	46.5%	62.1%	24.9%
99%	60.9%	75.6%	76.2%	74.8%	67.4%	37.9%	36.1%	24.4%	39.3%	50.7%	60.1%	65.9%	29.5%
Maximum	70.2%	90.2%	89.9%	75.8%	70.1%	45.9%	38.9%	31.0%	41.4%	52.4%	62.6%	66.8%	31.0%
Mean	23.4%	21.9%	15.2%	27.5%	18.3%	5.4%	-1.9%	-7.0%	3.8%	12.9%	17.5%	24.1%	9.9%
Standard Deviation	15.9%	19.1%	19.1%	19.6%	18.5%	15.5%	17.3%	14.4%	14.5%	14.9%	16.4%	19.1%	7.4%

Table 46: Projected Changes in Monthly Mean Temperature for the 2050s (°C)

Statistic	Jan	Feb	Mar	Apr	May	Jun	Jul	Aug	Sep	Oct	Nov	Dec	Annual
Minimum	1.2	0.6	0.8	0.5	0.2	0.4	0.6	0.9	0.7	1.0	0.8	1.6	1.2
10%	2.3	1.9	1.5	1.5	1.2	1.3	1.5	1.8	1.9	1.9	2.2	3.0	2.3
25%	3.3	2.5	2.2	2.1	1.8	2.1	2.4	2.4	2.4	2.4	2.7	3.4	3.3
50%	3.9	3.4	2.9	2.9	2.6	3.0	3.1	3.1	3.1	3.1	3.5	4.3	3.9
75%	5.1	4.2	3.8	3.5	3.4	3.7	4.2	4.1	3.8	3.8	4.4	5.4	5.1
90%	6.1	5.4	5.0	5.6	4.3	4.5	4.6	4.7	4.6	4.6	5.2	6.3	6.1
95%	6.8	6.0	7.5	8.2	4.6	5.1	5.2	5.2	5.3	5.1	5.7	7.2	6.8
99%	8.1	8.0	9.8	9.8	5.8	5.5	6.4	5.6	5.8	5.8	5.9	7.7	8.1
Maximum	8.5	8.6	10.9	9.9	6.1	6.1	7.1	6.1	6.0	5.9	6.2	7.8	8.5
Mean	4.2	3.5	3.2	3.2	2.7	3.0	3.2	3.3	3.2	3.1	3.6	4.5	4.2
Standard Deviation	1.5	1.5	1.8	2.0	1.2	1.2	1.2	1.1	1.1	1.1	1.1	1.4	1.5

Table 47: Projected Changes in Monthly Mean Temperature for the 2080s (°C)

Statistic	Jan	Feb	Mar	Apr	May	Jun	Jul	Aug	Sep	Oct	Nov	Dec	Annual
Minimum	1.2	-0.2	-0.2	-0.7	0.0	0.0	0.6	0.5	0.5	1.3	0.4	1.6	1.0
10%	2.9	2.3	1.5	1.8	1.5	1.7	2.0	2.1	1.8	2.1	2.6	3.1	2.1
25%	3.5	3.1	2.8	2.8	2.2	2.5	2.8	2.8	2.8	2.8	3.4	4.1	3.2
50%	5.4	4.5	4.2	3.9	3.5	3.9	4.1	3.8	4.3	4.1	4.5	5.7	4.4
75%	7.3	6.4	5.7	5.6	5.1	5.6	6.2	6.2	5.9	5.7	6.4	7.5	6.1
90%	9.3	7.9	7.3	6.7	6.4	6.6	7.3	7.6	7.6	7.0	7.7	9.1	7.4
95%	10.3	8.4	9.1	9.6	7.4	7.6	8.1	8.2	8.3	7.8	8.4	10.3	8.6
99%	12.2	12.4	14.9	12.6	8.7	9.1	9.5	9.9	10.1	9.2	9.0	10.7	9.7
Maximum	12.3	12.9	15.3	13.2	9.1	9.3	9.9	10.3	10.1	9.5	9.0	11.4	9.8
Mean	5.7	5.0	4.5	4.4	3.8	4.1	4.5	4.5	4.5	4.4	4.8	5.9	4.7
Standard Deviation	2.5	2.5	2.8	2.5	1.9	2.0	2.1	2.2	2.2	1.9	2.0	2.3	2.0

Annual average temperature is projected to change by 3.9°C in the 2050s and 4.4°C in the 2080s, indicating an increasing trend due to changing climate (Table 46 and Table 47). The projected changes for the mean monthly temperature are generally greatest for the winter months at the 50th percentile (Figure 10). In the 2050s, January and December are expected to be 3.9°C and 4.3°C warmer than the current climate baseline at the 50th percentile, while the month of May has the lowest projected temperature change of 2.6°C (Table 46). In the 2080s, January and December also have the highest projected changes in minimum temperature at 5.4°C and 5.7°C, with the month of May having the lowest projected change of 3.5°C at the 50th percentile (Table 47). Greater projected changes for the winter months is a common feature of climate change in higher latitudes, as the reductions in snow and ice lead to reductions in albedo and increased heat transport from southern latitudes (Bush and Lemmen 2019). For all months in both time periods, the mean projected change of the multi-model ensemble is greater than the median. This suggests that there are scenarios projecting significantly higher temperatures than the rest of the ensemble.

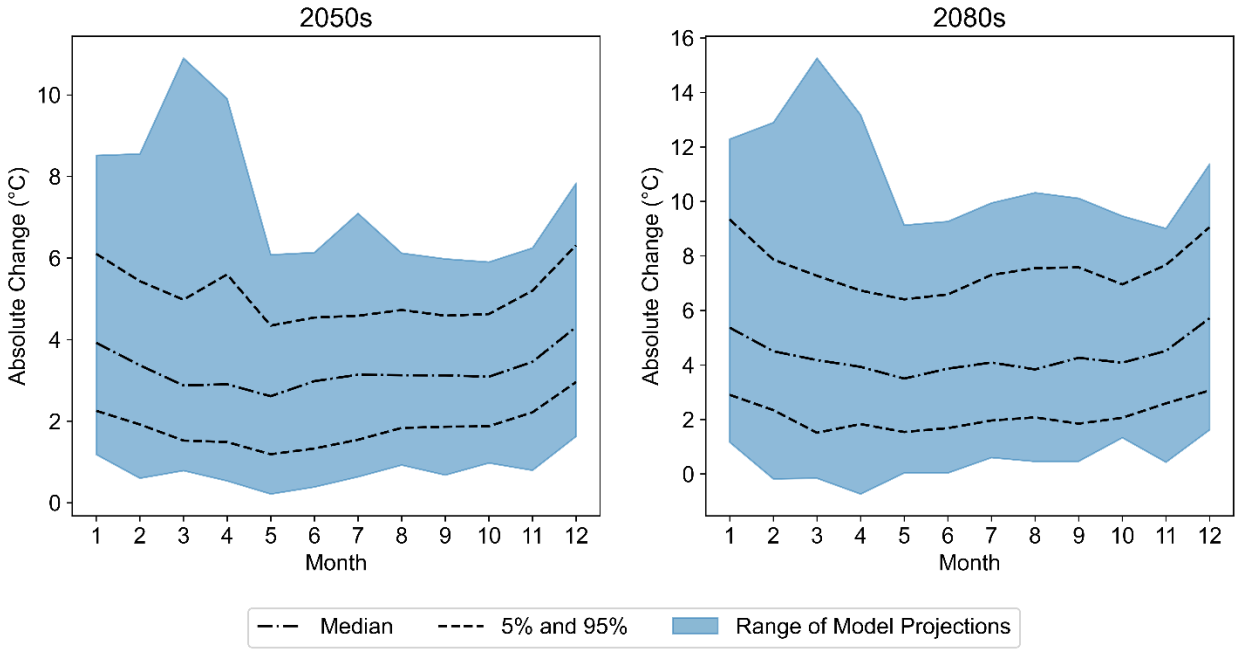

Figure 10: Range of Projected Changes in Monthly Mean Temperature for the Multi-Model Ensemble

Similarly, Bush and Lemmen (2019) show a median annual increase across Ontario of 1.5°C (1.1°C to 2.1°C, 25th and 75th percentile respectively) for RCP2.6 and 2.3°C (1.7°C to 2.9°C, 25th and 75th percentile respectively) for RCP8.5, for the period from 2031 to 2050. Again, these projections are in line with, but lower than, the projected increases for the Ignace study area but reflect differences in the regions covered and the future time periods considered. The period from 2081 to 2100 shows increases of 1.7°C (1.0°C and 2.1°C for the 25th and 75th percentiles) for RCP 2.6 and 6.3°C (5.3°C and 6.9°C for the 25th and 75th percentiles) for RCP8.5, which encompasses monthly median values in Table 46 and Table 47.

Seasonal variation results provided here are in agreement with that of Bush and Lemmen (2019)In Bush and Lemmen (2019), projected changes in temperature range from 1.5°C to 3°C in the winter months and 0.5°C to 3°C in the summer months for the 2031 to 2050 period. In the 2081 to 2100 period, projected changes range from 2°C to 9°C in the winter months and 0.5°C to 7°C in the summer months. Similarly, the values provided in this report show greater projected increases in temperature for the winter months than the summer months.

In addition to monthly projected changes in precipitation and temperature, a set of daily future time series are provided; continuous daily climate data series are often needed to drive climate change impact models such as water balance or hydrological models. Directly using climate model outputs is not recommended, as modelled precipitation typically suffers from the effect of drizzle (Werner and Cannon 2016). This means that there are more wet days with low amounts of precipitation and consequently, lower magnitudes of precipitation for extreme events. The more frequent occurrence of wet days would result in higher antecedent soil moisture conditions prior to rainfall events, while lower values of precipitation extremes may underestimate the magnitude and frequency of peak runoff.

The statistically downscaled climate projections used in the previous sections include bias correction methods to minimize the effect of drizzle present in global climate models and are sufficient for the relative comparisons completed above. However, these effects may still be present when developing daily time series. Furthermore, the historical data sources used in the statistically downscaled climate projections are either spatially interpolated or rely on reanalysis datasets that may not capture site climate conditions. The methodology in Appendix A.3.6.1 is used to overcome these limitations by incorporating the daily infilled dataset for Ignace (Section 3.1.2). Using this method, a corrected daily timeseries is provided for precipitation, rain, snow, and snow depth. Daily temperature variables as well as potential evapotranspiration are also included in the daily timeseries. All daily future timeseries for each member of the multi-model ensemble are included in Appendix C.

The correction of the distribution of daily precipitation values can be examined using a quantile-quantile plot, which compares the observed and modelled (both corrected and uncorrected) values across the same set of quantiles for the model baseline period of 1950 to 1993 (Figure 11). The observed values in Figure 11 are equivalent to a 1:1 line, while modelled values closer to the 1:1 indicate a distribution that is more statistically similar to what is observed. The shaded area represents the range of climate scenarios across the multi-model ensemble. The uncorrected downscaled climate model projections show slightly higher values for the lowest amounts of observed precipitation indicating the effect of drizzle, while observed precipitation greater than approximately 5 mm/day is typically underestimated. The range of bias corrected precipitation values are shown to overlap the observed precipitation values across the entire distribution. This indicates that the bias correction method used reduces the effect of drizzle and can better capture the magnitude and frequency of precipitation extremes. Even with bias correction, there is still the potential for underestimation of precipitation extremes, but there is significant improvement with bias correction.

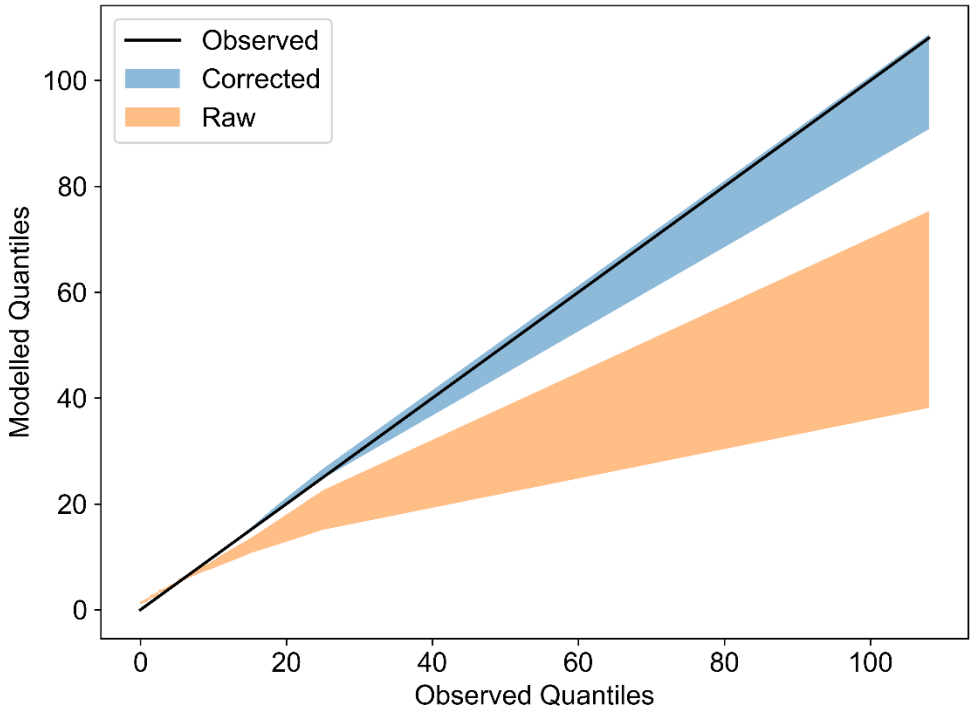

Figure 11: Quantile-Quantile Plot for Corrected and Uncorrected Climate Projections for Daily Precipitation over the Model Baseline Period

The wet and dry day frequencies for modelled precipitation both with and without bias correction compared to observations are shown in Figure 12 and Figure 13. Wet days correspond to days with precipitation greater than 1 mm while dry days correspond to days with precipitation less than or equal to 1 mm. The mean number of wet days per month is highly variable across the uncorrected climate models, indicated by a large range in the yellow shaded area (Figure 12). The shaded area does not overlap observations for all months except February, March, and September. In contrast, the bias corrected climate models have a smaller range in the mean number of wet days per month, and are much closer to the observations, even though there is no overlap with the observations for the months of August and October. For the mean number of dry days, the findings are similar (Figure 13). Overall, the range of modelled dry days is smaller and closer to the observations with bias correction.

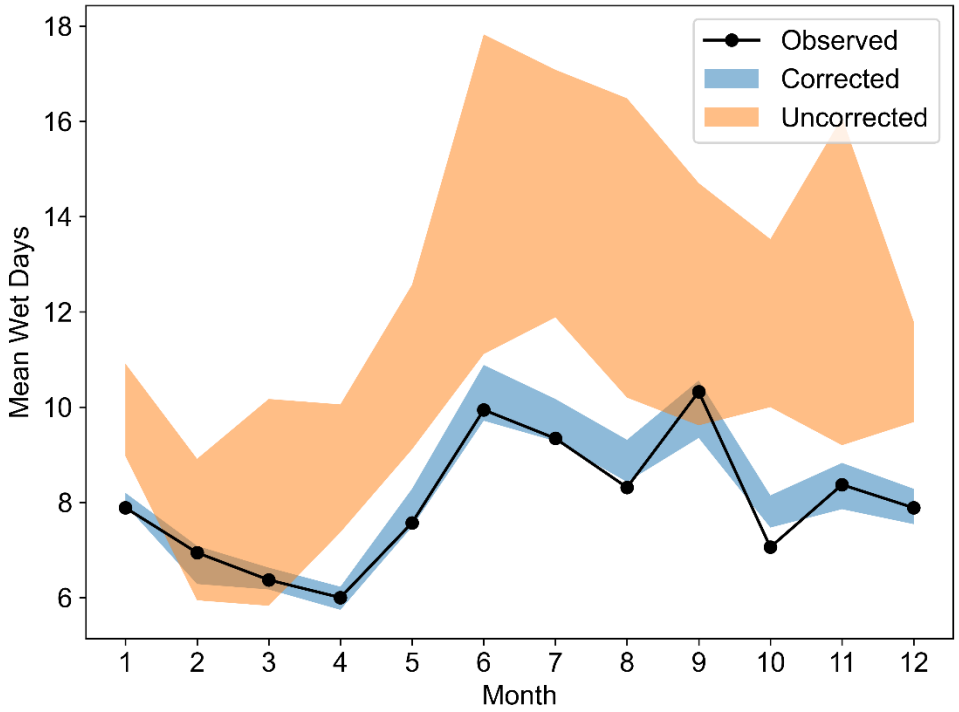

Figure 12: Mean Wet Days Across Calendar Months for Corrected and Uncorrected Modelled Precipitation Compared to Observations

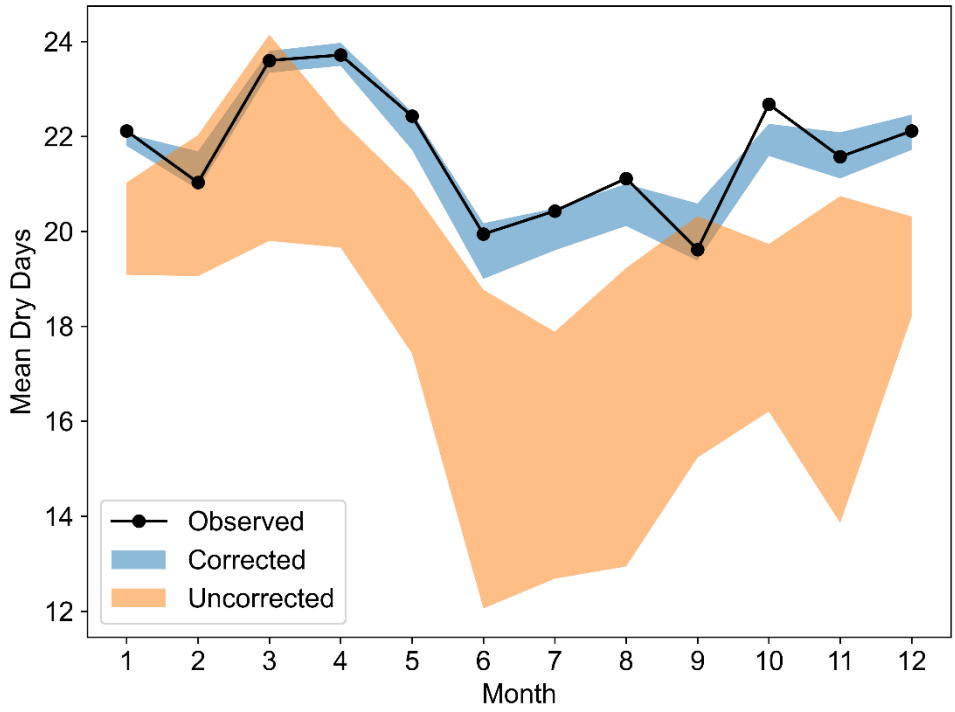

Figure 13: Mean Dry Days Across Calendar Months for Corrected and Uncorrected Modelled Precipitation Compared to Observations

The seasonal variation in precipitation is shown through a comparison of the total monthly precipitation for both corrected and uncorrected values compared to observations, along with derived rain, snow, and snow depth (Figure 14). The corrected and uncorrected values for monthly total precipitation and the derived variables have similar shaded areas. Both appear to capture seasonal variations compared to the observations and show some underestimation of mean snow and snow depth, as well as slight overestimation of mean total rain for October and November. These differences are likely due to small amounts of bias in the temperature projections data used to separate rain and snow and estimate snowmelt and snow depth accumulation. If a higher degree of accuracy is required for rain, snow, and snow depth, then an additional bias correction is recommended as additional work on the temperature variables. From June to September, the corrected mean total precipitation values appear to be higher than the uncorrected values. Although the correction methodology addresses the effect of drizzle, the underestimation of extremes is also corrected leading to greater total monthly values during these months.

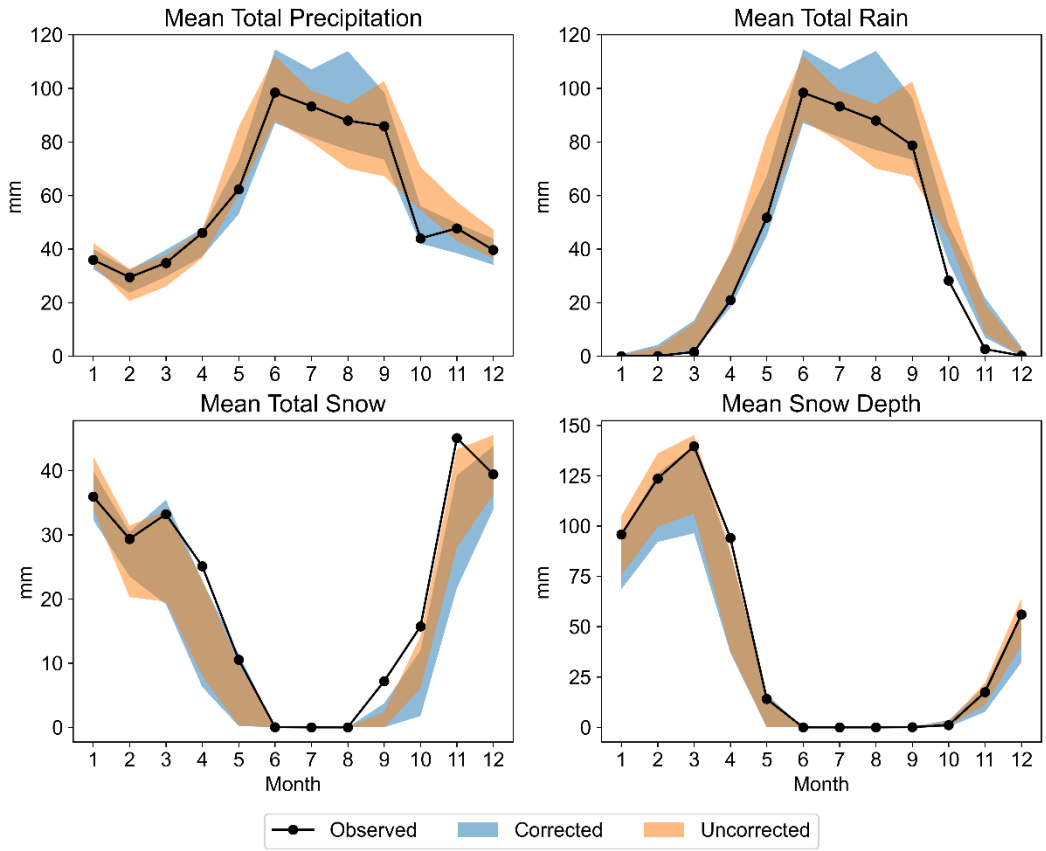

Figure 14: Range of Mean Total Monthly Precipitation Projections and Derived Variables Corrected and Uncorrected Compared to Observations

The application of bias correction to the statistically downscaled climate model outputs for the Ignace study area has led to improved estimation of precipitation across the distribution of daily values, including daily extremes. Both wet and dry day frequencies are now more like that of the observed precipitation values, while better capturing the seasonal variation in mean monthly precipitation totals. The assumption when applying bias correction to climate models is that the same bias between the model baseline and observations will carry forward into the future. This cannot be evaluated as future observations do not exist; however, the results of this bias correction can provide confidence that the daily timeseries of future projections will be more applicable to the site. The complete bias corrected precipitation timeseries from 1950 to 2100 for each of the 136 climate projections, along with the derived rain, snow, snow depth and potential evapotranspiration timeseries are provided in Appendix C.

4.5.2 WMO Climate Indices

The change in WMO climate indices from the model baseline to the 2050s and 2080s future time periods provide an indication on how climate extremes may change under future climate conditions. The distribution of changes to each of the 27 climate indices for the 2050s and 2080s are provided in Table 48 and Table 49 respectively. The projected changes are shown as absolute values to preserve the different units being used for the indices, as some are shown as days, mm, mm/day, and °C. The calculation of various WMO indices was performed considering different time periods within the year (e.g., growing season); therefore, monthly values cannot be provided as the focus is on the project change of the aggregated indices.
In the 2050s with regards to precipitation indices, the projected changes in WMO indices at the 50th percentile appear to indicate a future that is wetter with slightly more consecutive wet days and less consecutive dry days than the baseline period (Table 48). The annual amount of precipitation on wet days is projected to increase by 52.7 mm per year on average from 747.6 mm under current climate conditions (Table 29), with slightly more days above the 10 mm, 20 mm, and 30 mm thresholds corresponding to 2.1, 0.9, and 0.3 days on average, respectively. Maximum 1- and 5-day rainfall amounts are also projected to increase at the 50th percentile by 3 mm and 5.8 mm, respectively. In the 2080s the same patterns are present, however there is no change in the number of wet days, and the precipitation amounts and number of days above precipitation thresholds are slightly higher than the 2050s (Table 49).

Under current climate conditions, months of June to September typically have the greatest precipitation amounts (Section 3.5.1), while under future climate conditions, July and August are projected to have a small decrease in precipitation at the 50th percentile (Section 4.5.1). However, precipitation extremes are projected to increase. This indicates that in July and August, smaller precipitation events may become less frequent while larger precipitation events will be more frequent for there to be a projected decrease during these months. The trajectory of precipitation extremes including annual total wet-day precipitation, the number of heavy and very heavy precipitation days, very wet days, and maximum 1-day precipitation amounts, differs between the current future projected conditions. In the current climate baseline, the trends in the WMO indices showed decreasing trends in extreme precipitation (Table 30), while the change projected for the 2050s and 2080s (Table 48 and Table 49) shows increasing extreme precipitation. This indicates that a shift in rainfall pattern is projected for the Ignace study area.

Based on these results, future precipitation is expected to yield more frequent intense rainfall events, and greater precipitation amounts annually. As noted in Section 4.5.1 for the changes to monthly precipitation amounts, there is a considerable level of uncertainty in the projected changes to precipitation-based indices, as the range of projections across the multi-model ensemble indicate both an increase and decrease for each of the indices. The 50th percentile may be used for screening purpose; however, a different percentile should be considered for design purposes to better capture the desired risk level.

For the temperature-based indices, fewer cold spells and more warm spells are indicated for the 2050s at the 50th percentile (Table 48). Fewer freezing, and icing days are projected along with a longer growing season, more summer days, and greater extreme minimum and maximum daily temperatures. In the 2080s, there is further warming indicated by greater increases in growing season, summer days, and extreme minimum and maximum daily temperatures along with further reductions to the number of freezing and icing days at the 50th percentile (Table 49). The temperature-based current climate trends agree with the direction of change projected for future climate except for the number of summer days (average days above 25°C in the year). In the current climate, summer days have been shown to decrease (Table 30), while they are projected to increase in future climate. This indicates a shift in temperature patterns at the Ignace study in the summer months, which is confirmed by the projected increases shown in Section 4.5.1.

4.5.3 Potential Evapotranspiration

Changes to potential evapotranspiration rates are a key consideration for water balance assessments of climate change. This section summarizes the distribution of projected changes from the model baseline for each calendar month for the 2050s and 2080s future time periods (Table 50 and Table 51). The projected changes are provided as a percentage change from the model baseline.

Annual total potential evapotranspiration is projected to increase by 13.2% in the 2050s and 16.9% by the 2080s at the 50th percentile, compared to the model baseline. This indicates an increasing trend in potential evapotranspiration due to climate change. In the 2050s nearly all months indicate a projected increase in potential evapotranspiration across the multi-model ensemble, except for the minimum projection for April, May and June, with percentage changes ranging from 9.7% to 66% across calendar months at the 50th percentile (Table 50). The largest changes occur during months where there are typically low amounts of potential evapotranspiration (November through March) in Table 31, indicating that the large percentage changes correspond with small absolute changes. July was found to be the month with the highest evapotranspiration rates in the current climate baseline (see Section 3.5.3) and is projected to have a 10.3% increase for the 2050s future period at the 50th percentile. Overall, the distribution of projected changes across the climate model ensemble for each month is similar to that of the mean temperature (Section 4.5.1). This is due to the way that potential evapotranspiration is calculated using the Hargreaves equation. Other methods such as the Penman-Monteith equation would take into consideration changes in wind speed and relative humidity; however, these variables are not available for the downscaled multi-model ensemble.

In the 2080s, projected changes in potential evapotranspiration rates are greater for all months at the 50th percentile, ranging from 11.8% to 92.8% (Table 51). This is expected, as in the 2080s period, projected changes in monthly temperatures are greater at the 50th percentile. The projected changes in the 2080s follow the same pattern across month and climate model projections; however, there is a larger spread in projected changes from the model baseline, indicated by the higher standard deviation in projections for each month. Potential evapotranspiration extremes are likely to change in similar manner to the WMO indices due to the dependence on temperature (Section 4.5.2). Therefore, it can be assumed that based on the projections, more warm spells and summer days will result in more periods of elevated potential evapotranspiration rates.

Potential evapotranspiration was calculated on a daily time scale using the temperature projections from the multi model ensemble. The resulting daily data set is provided in Appendix C.

4.5.4 Drought Index

The drought index was estimated using the standard precipitation and evapotranspiration index (SPEI) of Vicente-Serrano et al. (2010), which is based on the standard precipitation index described in WMO (2012). This method illustrates the number of standard deviations that monthly net precipitation (precipitation less evapotranspiration) is from the median. By using net precipitation, both precipitation and temperature influence the drought index instead of only precipitation. The SPEI was calculated on a monthly timescale using a 12-month calculation interval which accounts for available water deficit in a 12-month rolling window (see Appendix A.3.6.4). Due to the method of calculation, aggregated annual values are not meaningful; therefore, the focus of the results was on the monthly distribution of SPEI. The distribution of SPEI for the multi-model ensemble is shown for the 2050s and 2080s future periods in Table 52 and Table 53.

At the 50th percentile, the months of March to September all have projected decreases in SPEI, indicating drier conditions, while November to February show projected increases for the 2050s (Table 52). The month of August shows the greatest projected decrease at -39.5%, while the largest increase corresponds to the month of December at 35.6%. The greatest potential decrease within the multi-model set occurs in December at -163.3% while the month of December holds the greatest potential increase at 146.6%. For the 2080s at the 50th percentile, months projected to become drier correspond to March to October, while November to February are projected to become wetter (Table 53). The range of projected changes to SPEI is similar in the 2080s compared to the 2050s with -49.2% in August and 26.8% in December at the 50th percentile. The spread across the multi-model ensemble is higher as shown by the higher standard deviation. Under current climate conditions, the summer months are projected to be drier than the winter months. This indicates that the driest seasons will become drier and the wetter seasons more so. This finding agrees with the projected decrease in July and August precipitation, and increased summer potential evapotranspiration shown for the Ignace study area in Section 4.5.1 and Section 4.5.3 respectively.

Table 48: Distribution of Projected Changes in WMO Climate Indices for the 2050s

WMO Indices	Min	5%	10%	50%	75%	90%	95%	99%	Max	Mean	Std. Dev.
Consecutive dry days (days)	-3.7	-2.8	-2.4	-0.6	0.4	1.3	2.1	3.4	4.2	-0.5	1.5
Cold spell duration indicator (days)	-6.8	-5.9	-4.7	-2.3	-1.6	-1.3	-1.1	-0.7	-0.6	-2.7	1.5
Consecutive wet days (days)	-1.9	-1.0	-0.9	0.1	0.4	0.9	1.1	2.1	3.0	0.0	0.7
Diurnal temperature range (°C)	-1.5	-0.9	-0.7	-0.2	0.0	0.1	0.2	0.5	0.5	-0.3	0.3
Frost days (days)	-64.0	-50.4	-42.9	-26.1	-20.9	-16.8	-14.6	-11.4	-10.6	-28.7	10.9
Growing season length (days)	5.5	11.4	14.3	24.3	31.1	37.9	44.3	56.4	56.5	25.5	10.4
Ice days (days)	-58.4	-39.2	-35.6	-19.3	-14.3	-10.8	-10.2	-7.9	-6.6	-21.8	10.1
Annual total wet-day precipitation (mm)	-38.9	-23.1	5.1	52.7	88.2	125.0	137.6	161.0	172.3	57.7	45.9
Heavy precipitation days (days)	-2.6	0.0	0.6	2.1	3.8	5.1	6.2	7.1	7.6	2.6	2.0
Very heavy precipitation days (days)	-1.4	-0.3	0.0	0.9	1.3	1.9	2.2	2.5	3.0	0.9	0.8
Very wet days (mm)	-23.4	-4.3	4.6	35.3	57.6	82.8	91.1	101.3	104.1	39.0	28.9
Extremely wet days (mm)	-25.2	-3.1	-0.2	17.9	32.4	46.9	55.9	59.8	79.3	21.0	18.0
Days above 25 mm (days)	-0.6	-0.1	0.0	0.3	0.5	0.9	1.1	1.4	1.4	0.3	0.4
Max 1-day precipitation (mm)	-5.5	-1.0	-0.4	3.0	5.1	7.1	9.2	10.6	11.0	3.3	3.0
Max 5-day precipitation (mm)	-8.6	-3.4	-1.0	5.8	9.7	13.3	16.0	20.1	23.2	6.2	5.8
Simple daily intensity index (mm/day)	-0.1	0.1	0.1	0.3	0.5	0.7	0.8	0.8	0.9	0.3	0.2
Summer days (days)	7.2	10.8	15.7	32.3	42.3	46.9	51.2	55.9	59.5	32.0	12.2
Cool nights (% of days)	-9.9	-9.6	-9.3	-8.0	-6.9	-6.2	-5.7	-5.2	-3.9	-7.8	1.2
Warm nights (% of days)	5.4	7.4	8.8	15.2	20.5	25.2	28.2	37.4	38.6	16.5	6.9
Min Tmin (°C)	1.5	2.6	3.1	5.1	6.6	7.6	8.6	9.3	9.7	5.3	1.8
Max Tmin (°C)	0.6	1.2	1.5	3.0	3.8	4.5	5.1	5.9	6.3	3.0	1.2
Tropical nights (days)	0.0	0.8	1.2	4.0	6.6	10.3	12.8	20.7	23.4	5.1	4.2
Cool days (% of days)	-9.9	-9.5	-9.1	-7.8	-6.6	-5.8	-5.3	-4.3	-3.7	-7.6	1.3
Warm days (% of days)	3.2	5.2	7.4	15.1	20.0	24.7	26.8	33.2	36.8	15.5	6.7
Min Tmax (°C)	1.5	2.6	3.2	4.9	6.3	7.4	8.0	9.1	9.4	5.1	1.7
Max Tmax (°C)	0.5	1.4	1.8	3.5	4.3	5.3	5.8	6.8	7.0	3.5	1.4
Warm spell duration indicator (days)	5.8	9.8	14.5	29.4	43.0	58.8	71.6	90.6	111.4	33.4	19.3

Table 49: Distribution of Projected Changes in WMO Climate Indices for the 2080s

WMO Indices	Min	5%	10%	50%	75%	90%	95%	99%	Max	Mean	Std. Dev.
Consecutive dry days (days)	-3.7	-3.3	-2.7	-0.9	0.5	1.2	2.0	3.0	4.5	-0.7	1.6
Cold spell duration indicator (days)	-6.8	-6.1	-4.9	-2.3	-1.7	-1.3	-1.0	-0.6	-0.6	-2.8	1.5
Consecutive wet days (days)	-1.7	-1.1	-0.9	0.0	0.3	0.7	0.8	1.5	1.9	-0.1	0.6
Diurnal temperature range (°C)	-1.8	-1.2	-0.9	-0.3	0.0	0.2	0.2	0.5	0.5	-0.4	0.5
Frost days (days)	-87.2	-67.5	-60.1	-38.6	-24.8	-18.0	-15.9	-14.3	-13.3	-39.0	16.9
Growing season length (days)	7.2	12.9	14.7	33.5	43.9	56.4	59.1	79.3	82.6	34.8	15.9
Ice days (days)	-79.5	-57.9	-51.2	-28.2	-19.0	-12.5	-9.9	-6.7	-6.3	-30.8	16.1
Annual total wet-day precipitation (mm)	-41.6	-0.1	7.9	68.6	103.5	139.3	174.4	212.2	220.8	73.3	53.8
Heavy precipitation days (days)	-1.4	0.1	0.7	2.9	4.3	6.2	7.5	10.0	11.1	3.3	2.3
Very heavy precipitation days (days)	-1.2	-0.1	0.2	1.0	1.7	2.5	2.8	3.5	3.7	1.2	0.9
Very wet days (mm)	-37.4	-1.9	13.5	45.6	64.2	103.2	118.1	154.2	187.9	51.4	37.3
Extremely wet days (mm)	-12.5	-1.7	6.1	25.5	38.6	62.4	69.5	94.3	102.0	28.8	21.4
Days above 25 mm (days)	-0.5	-0.1	0.0	0.4	0.6	1.0	1.3	1.7	2.3	0.4	0.4
Max 1-day precipitation (mm)	-2.0	-1.0	0.4	4.1	6.9	8.6	10.3	12.4	15.3	4.6	3.4
Max 5-day precipitation (mm)	-2.7	0.3	0.7	8.2	12.2	17.9	19.1	21.8	22.2	8.6	6.0
Simple daily intensity index (mm/day)	-0.1	0.1	0.2	0.4	0.5	0.8	1.1	1.2	1.3	0.4	0.3
Summer days (days)	2.5	14.1	17.8	42.8	59.5	73.3	78.8	91.3	95.8	44.5	21.0
Cool nights (% of days)	-10.3	-10.2	-10.1	-9.1	-7.8	-6.3	-5.8	-4.8	-3.0	-8.6	1.5
Warm nights (% of days)	4.3	7.9	9.0	22.1	34.7	41.4	49.3	62.6	63.4	25.0	13.7
Min Tmin (°C)	0.6	3.0	3.5	7.3	10.4	12.5	14.2	15.7	17.1	7.6	3.5
Max Tmin (°C)	0.4	1.3	1.7	3.9	5.6	7.0	8.2	9.1	9.4	4.2	2.1
Tropical nights (days)	0.2	1.0	1.3	7.3	16.8	29.0	35.3	53.3	61.1	11.9	12.2
Cool days (% of days)	-10.3	-10.2	-10.0	-8.9	-7.6	-6.2	-5.5	-3.8	-3.2	-8.4	1.6
Warm days (% of days)	3.7	6.5	8.1	20.9	32.2	41.6	45.4	58.0	59.4	23.3	12.9
Min Tmax (°C)	1.7	2.5	3.2	6.9	8.9	12.5	13.5	15.2	15.5	7.2	3.3
Max Tmax (°C)	0.2	1.6	2.0	4.3	6.8	8.3	9.2	10.1	10.2	4.8	2.4
Warm spell duration indicator (days)	6.5	11.5	13.7	46.1	83.1	122.5	142.9	199.7	210.4	59.8	45.0

Table 50: Projected Changes in Monthly Total Potential Evapotranspiration for the 2050s (%)

Statistic	Jan	Feb	Mar	Apr	May	Jun	Jul	Aug	Sep	Oct	Nov	Dec	Annual
Minimum	10.8%	3.7%	1.7%	-3.7%	-10.1%	-2.7%	0.4%	0.6%	1.8%	3.2%	9.0%	13.6%	1.5%
10%	30.9%	18.6%	13.3%	4.8%	2.4%	3.5%	3.7%	5.3%	6.5%	7.5%	13.7%	31.7%	5.2%
25%	46.9%	27.3%	16.7%	10.3%	6.4%	6.3%	6.6%	7.6%	9.2%	11.7%	17.8%	38.5%	8.9%
50%	66.0%	41.0%	23.3%	15.4%	10.2%	9.7%	10.3%	11.1%	12.9%	14.9%	23.7%	48.9%	13.2%
75%	91.5%	54.4%	33.5%	19.3%	13.1%	12.9%	13.7%	14.8%	16.9%	17.9%	30.1%	63.9%	16.5%
90%	118.2%	73.8%	44.8%	34.7%	17.5%	15.2%	16.6%	17.5%	19.9%	23.6%	40.5%	85.1%	19.1%
95%	129.0%	87.7%	84.6%	55.9%	18.6%	15.8%	17.5%	18.6%	21.2%	26.7%	44.0%	94.2%	21.4%
99%	169.7%	124.2%	109.8%	69.6%	22.7%	19.6%	18.9%	22.5%	25.3%	29.5%	52.3%	113.1%	23.9%
Maximum	203.0%	141.0%	128.0%	72.2%	23.5%	21.9%	19.7%	22.9%	26.1%	31.7%	59.9%	123.5%	24.5%
Mean	71.0%	44.0%	29.3%	18.1%	9.7%	9.5%	10.2%	11.3%	13.2%	15.2%	25.2%	53.6%	12.9%
Standard Deviation	34.7%	24.3%	21.2%	14.8%	5.8%	4.8%	4.7%	4.8%	5.1%	5.9%	10.2%	21.3%	5.2%

Table 51: Projected Changes in Monthly Total Potential Evapotranspiration for the 2080s (%)

Statistic	Jan	Feb	Mar	Apr	May	Jun	Jul	Aug	Sep	Oct	Nov	Dec	Annual
Minimum	9.7%	-0.5%	-1.2%	-5.3%	-12.2%	-4.0%	-1.3%	-1.2%	1.3%	3.2%	4.3%	12.7%	1.6%
10%	37.2%	27.0%	12.0%	7.0%	3.1%	3.4%	4.6%	5.9%	7.0%	8.4%	16.8%	30.6%	7.0%
25%	54.9%	34.4%	21.8%	13.6%	7.2%	7.2%	8.7%	9.6%	11.8%	13.0%	23.5%	47.0%	10.7%
50%	92.8%	53.9%	36.0%	19.3%	13.0%	12.0%	11.8%	13.6%	17.3%	20.0%	31.5%	65.9%	16.9%
75%	129.9%	84.5%	51.5%	29.2%	19.6%	18.6%	19.6%	22.1%	24.3%	26.8%	44.6%	96.3%	23.2%
90%	180.2%	110.6%	66.3%	43.2%	23.9%	24.3%	25.4%	27.5%	30.9%	34.9%	56.7%	118.0%	30.8%
95%	213.2%	129.7%	93.6%	63.8%	27.9%	26.4%	27.1%	30.3%	35.5%	40.0%	62.5%	131.6%	33.6%
99%	271.5%	212.9%	173.4%	77.9%	31.5%	28.5%	30.2%	32.6%	41.9%	44.5%	73.6%	172.8%	38.2%
Maximum	305.9%	223.6%	188.2%	87.7%	35.3%	30.4%	31.0%	34.8%	44.6%	45.3%	85.2%	176.8%	39.0%
Mean	100.7%	64.7%	40.9%	23.8%	13.2%	13.0%	13.9%	15.5%	18.4%	20.7%	34.7%	73.4%	17.7%
Standard Deviation	59.4%	41.4%	31.5%	17.0%	8.6%	7.7%	7.6%	8.2%	9.6%	9.9%	15.7%	35.2%	9.0%

Table 52: Projected Changes in SPEI for the 2050s at the Ignace Study Area (%)

Month	Min	10%	25%	50%	75%	90%	Max	Mean	Std. Dev.
January	-32.8%	-5.1%	9.1%	26.2%	41.8%	56.6%	98.2%	26.4%	24.8%
February	-90.7%	-30.5%	-9.1%	8.4%	28.5%	51.7%	84.5%	8.2%	33.7%
March	-126.8%	-58.7%	-35.5%	-13.9%	14.2%	37.6%	68.4%	-12.2%	39.8%
April	-149.7%	-62.7%	-30.6%	-7.8%	15.1%	33.0%	75.9%	-12.2%	43.1%
May	-90.6%	-54.2%	-28.8%	-11.9%	9.7%	34.7%	85.2%	-9.5%	33.5%
June	-117.5%	-66.7%	-46.2%	-23.2%	11.1%	34.4%	60.0%	-20.0%	39.4%
July	-163.3%	-104.2%	-72.7%	-36.8%	-8.0%	14.1%	46.5%	-41.9%	44.5%
August	-159.1%	-100.0%	-69.0%	-39.5%	-11.4%	6.9%	51.7%	-41.9%	42.1%
September	-84.2%	-54.5%	-37.0%	-10.0%	9.8%	24.4%	55.5%	-12.4%	29.5%
October	-66.2%	-33.2%	-16.9%	3.4%	28.1%	50.8%	100.7%	5.8%	32.3%
November	-62.9%	-17.2%	-5.0%	13.2%	47.4%	72.4%	106.3%	20.1%	34.4%
December	-43.5%	-13.4%	11.3%	35.6%	60.2%	79.3%	146.6%	36.8%	38.6%

Table 53: Projected Changes in SPEI for the 2080s at the Ignace Study Area (%)

Month	Min	10%	25%	50%	75%	90%	Max	Mean	Std. Dev.
January	-44.8%	-14.9%	3.2%	26.8%	49.3%	66.3%	100.7%	27.3%	31.4%
February	-88.8%	-42.2%	-21.9%	-4.0%	11.2%	39.0%	115.7%	-3.4%	34.3%
March	-203.0%	-69.2%	-48.5%	-23.2%	1.3%	14.3%	49.2%	-29.1%	43.2%
April	-103.7%	-69.4%	-34.2%	-6.5%	11.5%	34.8%	133.0%	-10.8%	40.3%
May	-97.2%	-53.1%	-35.8%	-4.6%	19.7%	33.3%	100.7%	-6.9%	37.3%
June	-153.6%	-80.5%	-53.1%	-18.5%	11.0%	35.8%	63.0%	-23.3%	46.3%
July	-204.4%	-143.4%	-94.2%	-43.1%	-4.9%	19.4%	69.8%	-52.4%	62.4%
August	-170.8%	-135.9%	-82.3%	-49.2%	-18.4%	3.8%	37.5%	-55.6%	49.7%
September	-138.4%	-80.4%	-49.5%	-23.7%	2.7%	24.0%	84.0%	-24.9%	41.1%
October	-72.5%	-41.1%	-22.2%	-3.8%	16.5%	40.2%	77.7%	-2.8%	31.4%
November	-77.2%	-41.5%	-12.3%	9.7%	29.7%	56.3%	113.7%	8.7%	36.7%
December	-41.3%	-17.0%	5.1%	26.2%	51.7%	75.8%	115.2%	28.0%	34.2%

Previous studies have analyzed the projected changes in SPEI index across Canada using an ensemble mean of Coupled Model Intercomparison 5 (CMIP5) global climate models. In the region of the Ignace study area, the SPEI index has been projected to decrease during summer and fall and increase during the winter and spring (Tam et al. 2019). The results shown here for the mean projected changes indicate a decrease in SPEI from spring to early fall (drier conditions), and an increase in SPEI from late fall through the winter months (wetter conditions). The projections for drier summer months agree between the two studies, thereby increasing confidence in the projections. Differences between result provided here and Tam et al. (2019) for the spring months may be due to the use of global climate models from the CMIP5 in Tam et al. (2019), which have a coarser resolution and no bias correction compared to downscaled climate models in this work. The downscaled climate models more accurately capture site conditions for temperature and potential evapotranspiration; therefore, the values provided here are more relevant for the Ignace study area.

4.5.5 Wind Speed and Relative Humidity

Projected changes in wind speed were obtained from ECCC for an ensemble of 29 GCMs from the CMIP5 (ECCC 2018). The ECCC has provided annual summaries of mean daily wind speed, with each year summarized by the 5th, 25th, 50th, 75th, and 95th percentile. The result of which is shown in Table 54. The projected changes in wind speeds in the 2050s and 2080s range from -5.1% to 2.4% and -8.1% to 1.5%, respectively. The lowest daily mean winds speeds (5th percentile) are projected to have the greatest potential decrease ranging from -8.1% to 1.7%, while the highest wind speeds (95th percentile) have projected changes that are mostly all positive ranging from -0.6% to 1.5%. The projected overall decrease in future wind speeds for the Ignace study area agrees with the current climate trends mentioned in Section 3.5.5.

Table 54: Projected Changes in Wind Speed (%)

Time Period	Scenario	5%	25%	50%	75%	95%
2050s	RCP2.6	-4.8%	-4.7%	-0.7%	0.2%	0.7%
	RCP4.5	1.7%	-5.1%	2.4%	-1.5%	-0.6%
	RCP8.5	-2.2%	-5.1%	-0.4%	0.3%	0.2%
2080s	RCP2.6	-2.6%	-4.3%	-1.2%	-1.1%	1.1%
	RCP4.5	1.1%	-4.8%	0.7%	-1.5%	0.2%
	RCP8.5	-8.1%	-5.7%	-0.8%	0.6%	1.5%

Jeong and Sushama (2019) projected changes to both mean and extreme wind speeds across Canada under RCP4.5 and RCP8.5 emission scenarios using a regional climate model. From this study it was estimated that the 50-year annual maximum daily wind speed would change between -4% to 8% for the 2071-2100 future period relative to the 1981 to 2010 baseline. For the same time periods, the mean daily wind speed was projected to change between -4% to 4%. This range of projected changes is slightly smaller but comparable to that from the ECCC global climate model ensemble; however, only one global climate model was used to drive the regional climate model in Jeong and Sushama (2019).

Climate change is expected to increase levels of atmospheric humidity due to elevated temperatures which the atmospheric moisture capacity at a theoretical rate of 7% per °C, according to the Clausius-Clapeyron relationship (CSA 2019). Observations have shown that it is very likely global specific humidity has increased by the 1970s, consistent with observed temperature increase (Hartmann et al. 2013). Increased atmospheric moisture content due to global warming can lead to more intense precipitation events (Bush and Lemmen 2019). Projections of relative humidity in the literature are not available for the Ignace study area. To provide an estimate of how relative humidity may change in the future, the changes are calculated using the approximations of Alduchov et al. (1996) for the multi-model ensemble of climate projections.

Annual and monthly percentage changes in relative humidity from the model baseline to the future periods were calculated for the 2050s and 2080s future time periods and are presented in Table 55 and Table 56, respectively. Annual average relative humidity is projected to increase by 2.1% in the 2050s and 2.7% in the 2080s at the 50th percentile, indicating an overall upward trajectory. This annual increase is relatively low; however, seasonal variation can be analysed in the form of monthly projected changes to provide more detail.

In both the 2050s and 2080s, the months of April to September show changes of less than 1%, while from October to March, projected changes range from 3% to 6.7% in the 2050s and 3.4% to 8.4% in the 2080s at the 50th percentile. The months with the greatest changes in relative humidity are consistent with the greatest projected changes in precipitation (Table 44 and Table 45). This is expected, as more atmospheric moisture would likely lead to greatest precipitation amounts. It is noted that the mean projected changes in relative humidity are significantly greater than the 50th percentile of the multi-model ensemble, indicating the presence of outliers on the high-end of the projected changes.

Even though there will likely be more moisture in the atmosphere (Kunkel et al. 2013), the saturation vapor pressure will also increase due to rising temperatures, which can reduce the relative humidity. This is confirmed in the literature, as decreasing relative humidity trends have been found in the mid latitudes despite increases in specific humidity (Byrne and Gorman 2018). However, in the case of the Ignace study area, increasing atmospheric moisture will likely dominate over the effect of increasing saturation vapor pressure.

Under current climate conditions, relative humidity in the afternoon (3 pm) is highest during the fall and winter months (Table 33 and Table 34), which also coincides with the greatest projected change in relative humidity result. This indicates that seasonal variation in relative humidity will be greater in the future, with greater contrast between seasons.

Table 55: Projected Changes in Relative Humidity for the 2050s (%)

Month	Min	10%	25%	50%	75%	90%	Max	Mean	Std. Dev.
January	-0.4%	3.0%	4.5%	6.1%	8.0%	9.9%	11.1%	12.8%	13.9%
February	-0.1%	2.1%	3.5%	5.5%	7.6%	9.7%	10.9%	14.1%	16.9%
March	-2.4%	0.1%	2.3%	3.6%	5.4%	7.8%	9.0%	11.6%	12.1%
April	-7.9%	-4.2%	-1.1%	0.8%	1.9%	3.6%	4.5%	9.3%	12.0%
May	-3.3%	-1.7%	-0.5%	0.6%	1.8%	4.1%	5.2%	11.2%	11.6%
June	-2.7%	-1.8%	-0.9%	0.6%	1.7%	2.8%	3.4%	8.2%	9.1%
July	-3.3%	-2.2%	-1.0%	0.4%	1.1%	2.0%	2.8%	5.4%	7.0%
August	-4.1%	-2.2%	-1.2%	-0.3%	0.8%	1.7%	2.2%	4.5%	6.0%
September	-3.4%	-2.3%	-1.4%	-0.1%	0.7%	1.5%	2.1%	4.0%	5.7%
October	-3.2%	-1.8%	-1.0%	0.1%	1.2%	2.8%	3.6%	5.1%	5.4%
November	-2.9%	0.2%	1.4%	3.0%	4.3%	5.8%	6.9%	7.5%	7.5%
December	1.2%	2.8%	4.2%	6.7%	8.2%	9.9%	11.0%	13.2%	14.3%
Annual	-0.9%	0.8%	1.4%	2.1%	3.0%	3.5%	4.5%	6.0%	6.3%

Table 56: Projected Changes in Relative Humidity for the 2080s (%)

Month	Min	10%	25%	50%	75%	90%	Max	Mean	Std. Dev.
January	-1.3%	2.9%	5.3%	8.4%	12.2%	16.2%	20.2%	8.9%	4.9%
February	-0.2%	3.3%	4.9%	7.7%	11.4%	16.1%	23.2%	8.6%	4.9%
March	-3.2%	0.8%	2.5%	4.7%	7.6%	11.0%	16.2%	5.2%	4.0%
April	-8.5%	-3.5%	-0.5%	0.8%	2.2%	3.7%	12.2%	0.8%	3.4%
May	-4.2%	-1.9%	-0.2%	1.0%	2.8%	5.5%	16.1%	1.6%	3.2%
June	-3.2%	-2.2%	-1.0%	0.9%	2.4%	3.6%	9.1%	0.8%	2.4%
July	-4.2%	-2.7%	-1.2%	0.4%	1.6%	2.9%	6.0%	0.3%	2.1%
August	-4.3%	-2.7%	-1.2%	-0.4%	1.0%	1.8%	6.4%	-0.2%	1.8%
September	-4.1%	-3.0%	-1.7%	-0.5%	0.9%	1.9%	5.1%	-0.4%	1.9%
October	-5.9%	-1.7%	-0.7%	0.4%	1.6%	3.0%	7.1%	0.6%	2.0%
November	-2.4%	-0.1%	1.4%	3.4%	5.2%	6.7%	10.9%	3.5%	2.7%
December	1.0%	3.4%	5.9%	7.7%	11.5%	14.4%	17.8%	8.6%	4.0%
Annual	-1.1%	0.8%	1.6%	2.7%	4.3%	5.8%	8.0%	3.0%	1.9%

5. QUALITATIVE CLIMATE ASSESSMENT BEYOND THE YEAR 2100

The daily future climate projections used in this report are only available to the year 2100. Future climate assessments beyond 2100 can only be made qualitatively based on the best available information from literature and an understanding of climate change trends up to 2100. Extended concentration pathways (ECPs) provide qualitative estimates of future temperature on a global scale up to the year 2500. It is generally accepted that with increased temperature (through increased radiative forcing), mean global precipitation will also increase by an estimated 1-3% per degree Celsius increase in temperature (IPCC 2013). With this information, the ECP projections can be used to qualitatively inform precipitation trends in the far future for the site.

The ECP global projections indicate that beyond 2100, the radiative forcing driven by greenhouse gas emissions will gradually slow down and stabilize (Figure 15). The ECP 8.5 scenario results in increasing radiative forcing which slows down and stabilizes by the year 2250. The ECP 4.5 scenario results in stabilized (no change) radiative forcing, while the ECP 3-PD shows gradually decreasing radiative forcing levels. As a conservative measure, projections are provided based on the ECP 8.5 scenario.

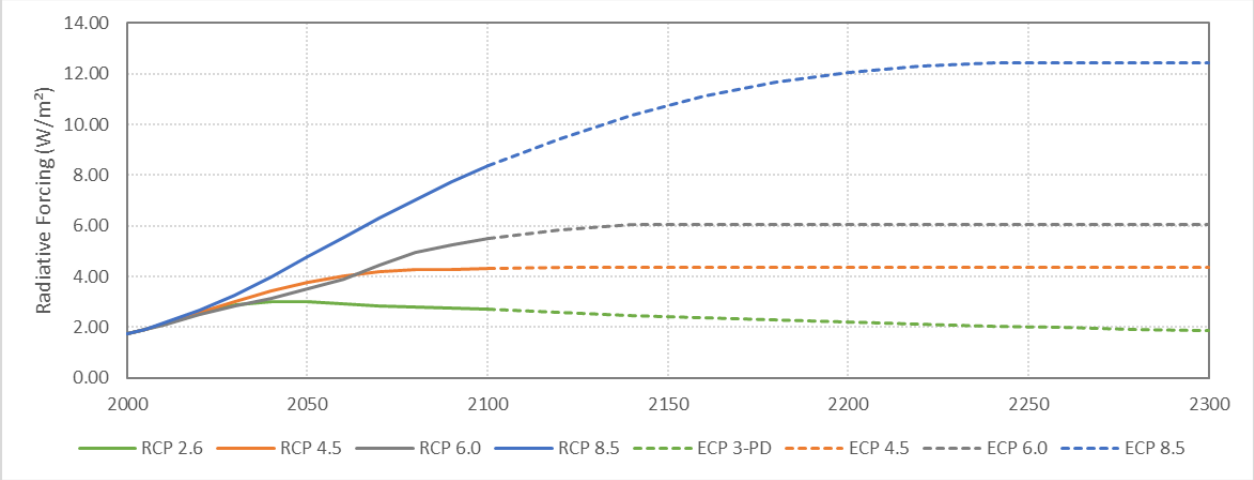

Figure 15: Illustration of RCP and ECP Scenario Radiative Forcing from 2000 to 2300

Two future climate periods (2050s and 2080s) have been used in this report, which allows for the trajectory of the projected changes to be estimated beyond these periods. Comparison of the differences between the percentage changes from the model baseline for the 2050s and 2080s time periods shows that on average across durations and return periods:

- Sub-daily IDF curves are projected to increase by 2.1%
- Daily and multi-day IDF curves are projected to increase by 2.4%
- PMP is projected to increase by 11.28%
- Rainfall on snow is projected to decrease by 5.6% (change of -5.6%)
- Peak snowpack accumulation is projected to decrease by 2.5% (change of -2.5%)

This indicates that the overall direction of change for extreme rainfall events is increasing and snowpack and combined rainfall and snowmelt are decreasing between the 2050s and 2080s time periods. Based on the ECP 8.5 scenario and the relationship between radiative forcing, temperature and precipitation, these changes may continue well into the future but may slow down and stabilize. There is a delay in the response of global temperatures to radiative forcing; therefore, changes in temperature and precipitation may continue past 2250 when the radiative forcing stabilizes.

By considering the trends in temperature and precipitation beyond 2100 and comparing the estimates for the 2050s and 2080s, it is likely that monthly precipitation and temperature values may be increased beyond 2100. As a result, greater temperature and precipitation extremes are expected, based on the trajectory of the WMO indices from the 2050s to 2080s time periods. Potential evapotranspiration is expected to continue to increase due to rising temperatures. A combination of increasing monthly precipitation and evapotranspiration results in mixed estimates for drought across calendar months, as both precipitation and evapotranspiration are used for the calculation. Most months show a decrease in the drought index (more severe drought) when comparing the difference between the 2050s and 2080s projected changes. Relative humidity should be expected to decrease with increasing temperatures as mentioned previously in Section 4.5.5. The highest daily mean wind speeds (95^{th} percentile) are increasing while the lowest daily mean wind speeds (5^{th} percentile) are decreasing. Overall, the future may be expected to become warmer, wetter, and more extreme at the Ignace study area.

Due to the large range of radiative forcing in the ECP scenarios, there exists a large amount of uncertainty on how climate will change globally beyond the year 2100, and even more so at the scale of the study site. Updated climate assessments should be made throughout the project lifecycle to account for updated climate models and scenarios.

6. UNCERTAINTY OF CLIMATE CHANGE PROJECTIONS FOR PMP, IDF, AND ADDITIONAL CLIMATE VARIABLES

This assessment is based on the current available climate science. The nature of the work undertaken is stochastic with substantial inherent uncertainty around any given data points. The uncertainty associated with any projections or forecasts is increased with a longer time horizon into the future for the projected period. The projections are subject to change with future developments; therefore, this study should be updated, as new climate science is developed and after the release of the latest assessment report by the IPCC. The approach to reduce levels of uncertainty with the future climate projections for this study is based on using multiple projections from multiple models and scenarios (multi-model ensemble approach), as recommended by the IPCC (IPCC 2013), and discussed in Section 4.1. Overall, there is less variability and uncertainty (measured as the agreement within the ensemble or range of projected anomalies) during the 2050s, with variability/uncertainty increasing during the 2080s. In addition, precipitation projections typically have larger uncertainty than temperature projections due to the challenge of capturing precipitation in the climate models (temperature is well understood). Therefore, the level of uncertainty in this assessment, focused on PMP and IDF estimates, precipitation based WMO climate indices and drought are generally higher than climate change studies focused on temperature.

The estimation of PMP (current and future projected) require moisture content and other variables, which were not readily available from the climate datasets. In order to calculate the moisture content for the model result datasets that do not provide these variables, Golder used the daily minimum temperature projections as a proxy for the dew point temperature and the surface specific humidity as a proxy for the precipitable water. Similar proxies were used to describe additional variables where they were not available from the climate datasets. The selection of proxy data to fill gaps in the climatic datasets added uncertainty around the estimation of PMP.

The assessment of additional climate variables carries the same uncertainty inherited from the climate projections; however, there are also additional uncertainties to consider. The Hargreaves method used to estimate potential evapotranspiration is one of many that are available; however, it was selected partly because it is only dependent on readily available temperature variables as opposed to wind speed and relative humidity. However, in this report it was shown that relative humidity and wind speed may also change in the future. Therefore, this method does not capture the effects of these changes and adds a level of uncertainty in the future potential evapotranspiration estimates. This uncertainty should also be noted for the drought index, as potential evapotranspiration is used in its calculation. The qualitative analyses for relative humidity and wind speed also carry additional uncertainty, as the available data is either taken from the literature, or from data sources that may not be as applicable to the site compared to the downscaled multi-model ensemble used for precipitation and temperature variables.

7. USING THE RESULTS OF THIS ASSESSMENT IN DECISION MAKING

To better describe the uncertainty around future projections, the estimated percent changes to precipitation (PMP and IDF curves) are described in terms of percentiles, allowing for different levels of acceptable risk. The projections at 50th percentile represent the ensemble median.

When considering the impact of future projected climate on current design parameters, the level of acceptable risk can be selected by using the desired percentile. Selection of future projections for climate change risk assessment should be based on the balance between the extra investment and consequential risks.

Therefore, it is recommended the results in this report be used as follows:

- For the ensemble mean projections, the projections at 50th percentile should be selected as the starting point, which NWMO should consider regarding risk assessment and undertaking planning and engineering design applications of infrastructure in the future.
- To relate the Project phases to the climate assessment periods, the distribution of the projections should be considered by examining the percentiles from the multi-model ensemble. For screening purposes, the 50th percentile may be used from the mid-century climate period for the site characterization, preparation, and construction phase, and the end of century climate period for the operational project phase. For Project phases beyond 2100, a high percentile may be used from the end-of-century climate assessment period as a screening value. Other percentiles may be used to relate to the Project phases. For example, if conservatism is not required, then a lower percentile from the mid-century climate period could be used for the site characterization, preparation, and construction phase.
- For critical infrastructure, selection of future projections at higher percentile and higher return periods should be considered. For example, for critical infrastructure whose failure is considered unacceptable, a 95th percentile could be considered over the typical 50th percentile. With regards to the return period, the storm associated with a return period sufficiently larger than the planning horizon for the infrastructure should be used. In the case of the Project, the decommissioning phase is planned to conclude in 2180, which is approximately 160 years from the publication of this report. Therefore, a return period that is at least larger than 160 years should be used for future extreme rainfall projections. For critical infrastructure it may be more appropriate to select the 1000 or 2000- year return period.
- Projected changes in the future climate assessments (Section 4) may be applied to the corresponding current climate baseline assessments (Section 3). Percentage changes should be multiplied by the corresponding current climate baseline values, while absolute changes may be added to the current climate baseline values. Applying the projected changes in this way help to reduce potential bias in the future climate projections of the multi-model ensemble.
- Where several results overlap specific parameter based on different methods (for instance, the PMP estimates under current climate conditions using the Transposition and Hershfield methods), this report recommends that the most conservative method (i.e., the one that generates the largest future rainfall depth) be used.

- The daily future timeseries provided in Appendix C may be used for additional studies at the Ignace study area. Bias correction of precipitation using the current climate baseline dataset for the area provides future projections that may be used in climate change impact models. A total of 136 projections (one for each member of the multi-model ensemble) are provided for each climate variable. It is recommended all members of the multi-model ensemble be used. If this is not possible a subset of scenarios should be selected to cover the range of uncertainty in the climate change impact model (see Appendix C for details).
- The qualitative values provided for wind speed and relative humidity should be used with caution, as they have a higher degree of uncertainty due to lack of data availability and the need for alternative sources to represent the Ignace study area.
- If a risk is identified for an infrastructure component for the area, then a more refined analysis should be performed to further define the risks using the projections at different percentile levels.

8. CONCLUSIONS AND RECOMMENDATIONS

The baseline assessment of the Ignace study area was completed using publicly available data in the region from ECCC. The 24-hours 100-year return period precipitation was estimated at 125.5 mm and the 500-year return period at 167.9 mm from the interpolated IDF curve at the Ignace study area (Table 13). The PMP calculation yielded a 1-day value of 364.3 mm, 411.7 mm for 24-hours, 482.2 mm for 2-day, and 510.1 mm for 3-day with the Hershfield method (Table 17). With the DAD curves in the Transposition method for 1,000 km^2 watershed area, the estimates were slightly higher being 374.0 mm for 1-day and 422.6 mm for 24-hours, and slightly lower being 473.6 mm for 2-day, and 477.8 mm for 3-day (Table 20). The values of IDF and PMP estimates were compared with literature sources and found in agreement with previous studies.

The current climate analyses for the additional climate variables indicate that the warmest temperatures occur in the month of July, which also has the highest potential evapotranspiration rates, while the months of June to September are the wettest months of the year on average. Analysis of the WMO climate indices shows that the number of wet days were found to be increasing over the current climate baseline; however, the number of days with heavy precipitation and the 1- and 5- day maximum precipitation amounts are shown to be decreasing. Temperature related indices show significant upward trends in daily minimum temperatures and the number of warm nights per year. A comparison of the annual average total precipitation to the annual average total potential evapotranspiration indicates that a small surplus in net precipitation is expected for the Ignace study area on average. The SPEI drought index shows that the most severe drought periods have occurred in April and May, while the greatest wet periods have occurred in January, November and December. Wind speed and relative humidity were characterized for the Ignace study area using two climate stations in the region which had climate normals available for these climate variables. The values provided should be interpreted qualitatively as the climate stations that represent the best available observations for wind speed and relative humidity are located approximately 75 km away from the study area.

Future projected climate results are presented for the range of models within the “ensemble” and expressed in terms of percentiles. When considering the impact of future projected climate on current design parameters, the level of acceptable risk can be selected by using the desired percentile.

The trends in future climate extremes follow a pathway that is consistent with the trends in climate normals for both the current and future climate projections. From the median (50^{th} percentile) values for the 2050s and 2080s, the projected future climate extremes are indicating a future that is likely to be wetter. The 1-day PMP values are projected to increase between approximately 18.7% and 25.4% in the 2050s and in the 2080s, respectively, at the 50^{th} percentile (Table 39 and Table 40), relative to the model baseline from the GCM ensemble. The 1-day rainfall events are projected to increase by 9.5% to 16.8% in the 2050s (Table 37) and 11.8% to 18.1% in the 2080s (Table 38) at the 50^{th} percentile, relative to the model baseline from the GCM ensemble.

Analysis of future projections on the additional climate variables shows that annual total precipitation and mean temperature are expected to follow and upward trajectory from the baseline period to the 2080s at the 50th percentile. Monthly total precipitation is projected to increase for all calendar months except July and August, with the greatest change estimated for December at 18.6% at the 50th percentile for the 2050s (Table 44). The range of projected changes in monthly total precipitation was found to be larger in the 2080s (Table 45) than in the 2050s, indicating continued increase. At the 50th percentile, changes in monthly mean temperatures were found to range from 2.6°C to 4.3°C in the 2050s (Table 46), and 3.5°C to 5.7°C (Table 47) in the 2080s, with the greatest change projected for the coldest months of the year.

Projected changes in the WMO indices (Table 48 and Table 49) show that in general, there are more dry days expected with greater precipitation amounts on wet days. Shorter cold spells are expected with longer warm spells, longer growing season, more summer days, and increasing extreme temperatures.

Changes to potential evapotranspiration ranged from 9.7% to 66% in the 2050s (Table 49) and 11.8% to 92.8% in the 2080s (Table 51) across calendar months at the 50th percentile. The annual projected changes in potential evapotranspiration indicate an upward trajectory, with increases of 13.2% in the 2050s and 16.9% in the 2080s. The changes to the SPEI drought index revealed that summer months are projected to become drier with the greatest changes occurring in the month of August at -39.5% in the 2050s (Table 52) and -55% in the 2080s (Table 53) at the 50th percentile. Mean daily wind speed projections generally show decreasing wind speed in the future, particularly for the lower percentiles of wind speed with small increases to extreme mean daily wind speed (Table 54). Overall, relative humidity is projected to increase for both the 2050s and 2080s future periods, primarily for the late fall to early spring months (Table 55 and Table 56). This indicates that higher temperatures will lead to greater atmospheric moisture, which coincides with increased monthly precipitation amounts during this period. Precipitation bias correction for the development of daily future timeseries at the Ignace study area shows improved estimation of extreme precipitation events, wet and dry day frequencies and seasonal variation. Temperature projections were not corrected as they are generally captured well by the statistically downscaled climate models.

Qualitative assessment of climate change beyond the year 2100 was made using the projections for the 2050s and 2080s time periods and the global ECP scenarios. Overall, extreme precipitation statistics (IDF and PMP) are likely to increase beyond the year 2100 based on the comparison of projections between the 2050s and 2080s time periods. These changes may continue well into the future, as the ECP 8.5 scenario shows increased radiative forcing until the year 2250. It is recommended additional climate assessments be made throughout the project life cycle, so that updated climate projections and scenarios are used to reduce uncertainty associated with projections made far into the future.

The nature of the study has substantial level of inherent uncertainty. The approach to address levels of uncertainty around future climate projections in this study relies on the multi-model ensemble approach recommended by IPCC. Furthermore, the uncertainty associated with any projections is increased with the far future of the projected period, resulting into less variability and uncertainty during the 2050s, when compared to the 2080s. To acknowledge the uncertainty around future projections, the estimate percent changes to precipitation (PMP and IDF curves) is described in terms of percentiles, allowing for different levels of acceptable risk. When considering the impact of future projected climate on current design parameters, the level of acceptable risk can be selected by using the desired percentile. Selection of future projections for climate change risk assessment should be based on the balance between the extra investment and consequential risks.

Based on Golder's experience in climate change projections, the proposed approaches as described in this study are considered best guidance for the industry. The observations available at the Ignace study area are limited to 1993; therefore, it is recommended the meteorological station located in the study area (Ignace Station - 6033690) be reactivated or a new meteorological station be installed for continuous monitoring, should this study area be selected for the DGR location.

REFERENCES

Alduchov, O.A. and R.E. Eskridge. 1996. Improved Magnus' Form Approximation of saturation vapor pressure. Saturation Vapor Pressure. Journal of Applied Meteorology, 35, 601–609.

Anandhi, A., F. Allan, D.C. Pierson, E.M. Schneiderman, M.S. Zion, D. Lounsbury and A.H. Matonse. Examination of Change Factor Methodologies for climate change impact assessment. Climate Change Impact Assessment. Water Resources Research, 47(3). doi: 10.1029/2010WR009104.

AMEC. 2011. Maximum Flood Hazard Assessment. Nuclear Waste Management Organization Report DGR-TR-2011-35. Toronto, Canada. Available at https://archive.opg.com/pdf_archive/Deep%20Geologic%20Repository%20Documents/DGR%20Submission%20Documents/D175_26.Maximum-Flood-Hazard-Assessment.pdf.

Bush, E. and D.S. Lemmen, editors. 2019. Canada's Changing Climate Report. Government of Canada, Ottawa, ON. 444p. Available at https://www.nrcan.gc.ca/sites/www.nrcan.gc.ca/files/energy/Climate-change/pdf/CCCR_FULLREPORT-EN-FINAL.pdf.

Byrne, M.P. and P.A. Gorman. 2018. Trends in Continental Temperature and Humidity Directly Linked to ocean warming. Ocean Warming. Proceedings of the National Academy of Sciences, 115(19): 4863-4868. doi: 10.1073/pnas.1722312115.

Canadian Standards Association (CSA). 2012. Draft Standard Plus 4013-12 Technical Guide Development, Interpretation and Use of Rainfall Intensity-Duration-Frequency (IDF) Information: Guideline for Canadian Water Resources Practitioners. Toronto, Canada.

Canadian Standards Association (CSA). 2019. Draft Standard Plus 4013:19. Technical Guide Development, Interpretation and Use of Rainfall Intensity-Duration-Frequency (IDF) Information: Guideline for Canadian Water Resources Practitioners. Toronto, Canada.

Clavet-Gaumont, J., D. Huard, A. Frigon, K. Koenig, P. Slota, A. Rousseau, I. Klein, N. Thiémonge, F. Houdré, J. Perdikaris, R. Turcotte, J. Lafleur and B. Larouche. 2017. Probable Maximum Flood in a Changing Climate: An Overview for Canadian Basins. Journal of Hydrology: Regional Studies, 13, 11-25. doi:10.1016/j.ejrh.2017.07.003.

Climatedata. 2019. Statistically Downscaled Climate Scenarios - BCCAQv2. Available at https://climatedata.ca/.

Collins, M., R. Knutti, J. Arblaster, J.-L. Dufresne, T. Fichefet, P. Friedlingstein, X. Gao, W.J. Gutowski, T. Johns, G. Krinner, M. Shongwe, C. Tebaldi, A.J. Weaver and M. Wehner. (2013): Long-term Climate Change: Projections, Commitments and Irreversibility; in Climate Change 2013: The Physical Science Basis; Contribution of Working Group I to the Fifth Assessment Report of the Intergovernmental Panel on Climate Change, (ed.) T.F. Stocker, D. Qin, G.-K. Plattner, M. Tignor, S.K. Allen, J. Boschung, A. Nauels, Y. Xia, V. Bex and P.M. Midgley; Cambridge University Press, Cambridge, United Kingdom and New York, NY, USA; p. 1029–1136.

Environment and Climate Change Canada (ECCC). 2020. Canadian Climate Normals. Government of Canada. Available at: https://climate.weather.gc.ca/climate_normals/.

Environment and Climate Change Canada (ECCC). 2019. Historical Climate Data. Available at https://climate.weather.gc.ca/historical_data/search_historic_data_e.html. Accessed June 15, 2019.

Environment and Climate Change Canada (ECCC). 2018. Projected Surface Wind Speed Change Based on CMIP5 Multi-Model Ensembles. Government of Canada. Available at: https://open.canada.ca/data/en/dataset/e0c71149-db7a-4700-acfd-1c8f9d778354.

Environment and Climate Change Canada (ECCC). 2020. Canadian Climate Normals. Government of Canada. Available at: https://climate.weather.gc.ca/climate_normals/.

Hargreaves, G.H. and Z.A. Samani. 1985. Reference Crop Evapotranspiration from temperature. Temperature. Applied Engineering in Agriculture 1(2):96-99. DOI: 10.13031/2013.26773.

Hartmann, D.L., A.M.G. Klein Tank, M. Rusticucci, L.V. Alexander, S. Brönnimann, Y. Charabi, F.J. Dentener, E.J. Dlugokencky, D.R. Easterling, A. Kaplan, B.J. Soden, P.W. Thorne, M. Wild and P.M. Zhai. 2013. Observations: Atmosphere and Surface; in Climate Change 2013: The Physical Science Basis (Contribution of Working Group I to the Fifth Assessment Report of the Intergovernmental Panel on Climate Change), (ed.) T.F. Stocker, D. Qin, G.-K. Plattner, M. Tignor, S.K. Allen, J. Boschung, A. Nauels, Y. Xia, V. Bex and P.M. Midgley; Cambridge University Press, Cambridge, United Kingdom and New York, NY, USA, p. 159–254. doi:10.1017/CBO9781107415324.008

Hember, R.A., N.C. Coops and D.L. Spittlehouse. 2017. Spatial and Temporal Variability of Potential Evapotranspiration across North American Forests. Hydrology, 4(5). doi:10.3390/hydrology4010005.

Hosking, J.R.M. and J.R. Wallis. 1997. Regional Frequency Analysis. Cambridge University Press, Cambridge, U.K.

Jeong, D. and L. Sushama. 2019. Projected Changes to Mean and Extreme Surface Wind Speeds for North America Based on Regional Climate Model Simulations. Atmosphere, 10(9):497-516. doi: 10.3390/atmos10090497.

Intergovernmental Panel on Climate Change (IPCC). 2013. Climate Change 2013: The Physical Science Basis. Contribution of Working Group I to the Fifth Assessment Report of the Intergovernmental Panel on Climate Change. Retrieved on March 15, 2017 from https://www.ipcc.ch/report/ar5/wg1/.

IPCC. 2018. Global Warming of 1.5°C. An IPCC Special Report on the Impacts of Global Warming of 1.5°C above Pre-industrial Levels and Related Global Greenhouse Gas Emission Pathways, in the Context of Strengthening the Global Response to the Threat of Climate Change, Sustainable Development, and Efforts to Eradicate Poverty [Masson-Delmotte, V., P. Zhai, H.-O. Pörtner, D. Roberts, J. Skea, P.R. Shukla, A. Pirani, W. Moufouma-Okia, C. Péan, R. Pidcock, S. Connors, J.B.R. Matthews, Y. Chen, X. Zhou, M.I. Gomis, E. Lonnoy, T. Maycock, M. Tignor, and T. Waterfield (eds.)]. In Press.

Kunkel, K.E. 2013. Probable Maximum Precipitation and Climate Change. Geophysical Research Letters, Vol.40, Issue 7. March 2013.

Louie, P.Y.T. and W. D. Hogg. 1980. Extreme Value Estimates of Snowmelt. Proceedings of Canadian Hydrology Symposium 80 (Toronto, ON: 64-78 National Research Council Canada).

Ministry of Natural Resources and Forestry (MNRF). 2020. Ontario Flow Assessment Tool. Available at https://www.gisapplication.lrc.gov.on.ca/OFAT/Index.html?site=OFAT&viewer=OFAT&locale=en-US. Accessed March 2, 2020.

Murphy, B., P. Campbell, J. Cummine, R.P. Ford, B. Johnson, A. Thompson, P. Pilon and D. Brown. 2003. The 49th Parallel Severe Rainstorm, Flooding and High Water Events of June 2002. Meteorological Service of Canada, Environment Canada, Burlington, Ontario. 46 pp.

Ontario Climate Data Portal (OCDP). 2020. High Resolution Climate Change Projections for Ontario. Laboratory of Mathematical Parallel Systems, York University. Available at: http://lamps.math.yorku.ca/OntarioClimate/index_app_introduction.htm#/.

Ontario Ministry of Natural Resources (OMNR). 2006. PMP for Ontario. Prepared by IBI Group. December 2006.

Pierce, D. W., D. R. Cayan and B. L. Thrasher. Statistical Downscaling Using Localized Constructed Analogs (LOCA). Journal of Hydrometeorology, 15(6), 2558-2585.

Pysklywec, D.W., K.S. Davar and D.I. Bray. 1968. Snowmelt at an Index Plot. Water Resource. 4(5), 937-946.

Reclamation. 2013. Downscaled CMIP3 and CMIP5 Climate Projections: Release of Downscaled CMIP5 Climate Projections, Comparison with Preceding Information, and Summary of User Needs. U.S. Department of the Interior, Bureau of Reclamation, Technical Service Center, Denver, Colorado, 116 p. Available at: http://gdo-dcp.ucllnl.org/downscaled_cmip_projections/techmemo/downscaled_climate.pdf.

Tam, B.Y., K. Szeto, B. Bonsal, G. Flato, A.J. Cannon and R, Robin. 2019. CMIP5 Drought Projections in Canada Based on the Standardized Precipitation Evapotranspiration Index. Canadian Water Resources Journal, 44(1): 90-107. doi: 10.1080/07011784.2018.1537812.

Vicente-Serrano, S.M., S. Begueria and J.I. Lopez-Moreno. 2010. A Multiscalar Drought Index Sensitive to Global Warming: The Standardized Precipitation Evapotranspiration Index. Journal of Climate, 23(7):1696-1718. doi: 10.1175/2009JCLI2909.1.

Yan, H., N. Sun, M. Wigmosta, R. Skaggs, Z. Hou and R. Leung. 2018. Next-generation Intensity-Duration-Frequency Curves for Hydrologic Design in Snow-Dominated Environments. Water Resources Research, 54, 1093-1108. doi: 10.1002/2017WR021290.

Wan, H., X.L. Wang and V.R. Swail. 2010. Homogenization and Trend Analysis of Near-Surface Wind Speeds. Journal of Climate, 23(5):1209-1225. doi: 10.1175/2009JCLI3200.1.

Werner, A.T. and A.J. Cannon. 2016. Hydrologic Extremes – an Intercomparison of Multiple Gridded Statistical Downscaling Methods. Hydrology and Earth System Sciences, 20:1486-1508. doi: 10.5194/hess-20-1483-2016.

Wood. 2019. Climate Change Impacts Review and Method Development. NWMO-TR-2019-05. Toronto, Canada. Retrieved from http://rms.nwmo.ca/Sites/APM/Reports/NWMO-TR-2019-05.pdf.

World Meteorological Organization (WMO). 2009a. Manual on Estimation of Probable Maximum Precipitation (PMP). World Meteorological Organization (WMO). WMO-No. 1045. Geneva, Switzerland.

World Meteorological Organization (WMO). 2009b. Guidelines on Analysis of Extremes in a Changing Climate in Support of Informed Decisions for Adaptation. World Meteorological Organization (WMO). Climate Data and Monitoring WCDMP-No. 72. Geneva, Switzerland.

World Meteorological Organization. 2012. Standardized Precipitation Index: User Guide. Washington, DC: World Meteorological Organization. Technical report: WMO No. 1090. Geneva, Switzerland.

APPENDIX A: DETAILED METHODOLOGY

CONTENTS

Page

LIST OF TABLES

Page

LIST OF FIGURES

Page

A.1 INTRODUCTION

This appendix outlines in detail the PMP and IDF analyses approach and methodology applied to the Ignace study area and follows *Climate Change Impacts Review and Method Development* (NWMO-TR-2019-05 from Wood 2019) for PMP analyses. To provide additional context to the changes in PMP and IDF, additional climate variables were analyzed for the Ignace study area. These include annual and monthly temperature and precipitation statistics from which seasonal variation can be inferred. Derived climate variables are also provided, including WMO indices, rain and snow, snow depth, potential evapotranspiration, drought index, and qualitative information for wind speed and relative humidity. This stepwise approach combines information about the current climate conditions and publicly available projections of how the climate may change under future climate conditions to describe a range of future projections at the site of interest and represents the most recent best guidance found in literature.

Section A.2 provides the detailed methodology followed to develop a current climate observed baseline for PMPs, IDFs and additional climate variables (Section 3), while Section A.3 outlines the methods based on GCM ensemble to develop the projected changes in PMP, IDF, and additional climate variables in the future (Section 4).

A.2 CURRENT CLIMATE OBSERVED BASELINE DEVELOPMENT

Understanding the current climate and current climate trends is important when evaluating current design parameters and developing the percentile levels using the future climate projections. The process to develop the observed baselines for PMP, IDF, and additional climate variables is outlined in Figure A.1. Where available, the climate baseline is grounded in observations from local climate stations. Publicly available observations are used to establish the baseline infilled with reanalysis data (to meet data completeness requirements including only considering months and years where at least 90% of the data is available).

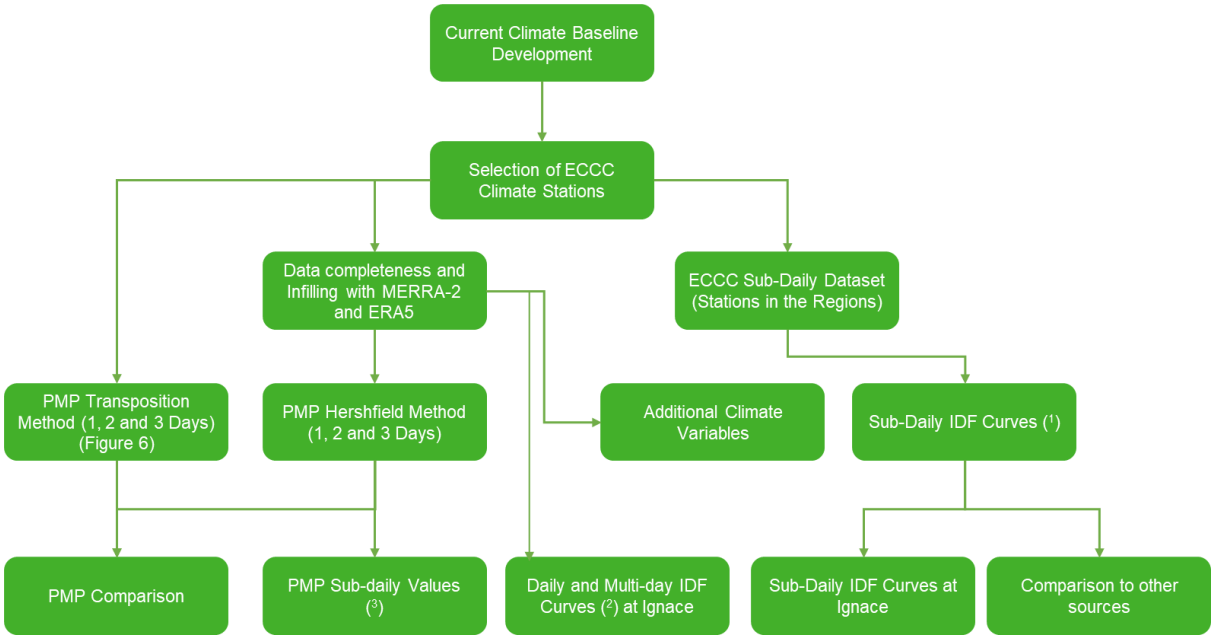

Notes:
1) IDF curves were developed for the following durations: 5, 10, 15, 30 minutes, 1, 2, 6 and 12 hours, and 2, 5, 20, 50, 100, 200, 500, 1000 and 2000 years return period.
2) IDF curves were developed for the following durations: 1, 2, 3, 4, 5, 6, 7, 10, 20, 30, 50, 75, 90, 120 days, and 2, 5, 20, 50, 100, 200, 500, 1000 and 2000 years return period.
3) Sub-daily PMP values were calculated for the following durations: 5, 10, 15, 30 minutes, 1, 2, 6, 12 and 24 hours.

Figure A.1: PMP, IDF, and Additional Climate Variables Baseline Analyses Flowchart

Before infilling, the reanalysis data is compared and correlated to the available regional climate station. This step is carried out to create a current climate baseline time series and is used to evaluate PMP, IDF, and additional climate variables for the region of interest. Additional data stations from the region are screened for the study of the extreme events as well as series from the Engineering Dataset for the IDF curves (ECCC 2019). If available, the Adjusted and Homogenized Canadian Climate Data (AHCCD) are used to apply adjustments to the station observations (infilled if necessary) to account for non-climatic shifts in data, mainly due to the relocation of stations and wind undercatch correction (ECCC 2019). Wind undercatch describes the effects of wind on rain gauges that can cause underestimation of rainfall which contributes to inconsistencies in the rainfall dataset (Guo et al. 2001).

The climate station selection is based on the following selection factors to identify the station which best represents the Ignace study area, meteorologically:

- the length of record (minimum 30 years of data);
- availability of a continuous record;
- proximity to the area of interest;
- age of observations compared to the currently accepted normal period;
- latitude;
- elevation of station;
- geographic siting; and
- monthly data availability threshold of 90% for all years.

The available climate data from each station must be compared to, and pass, the selection criteria outlined above. Data from most climate stations are constrained by low numbers of observations or a limited life span for the station (data quantity), and varying data quality. Therefore, the station which matches the most selection criteria, with the first three criteria bearing the most weight, is selected. Meeting the monthly data availability is often a challenge over the desired, long observation period. When available climate observations are representative of a site but fail to meet the required data completeness, reanalysis data from the National Aeronautics and Space Administration's (NASA's) Modern-Era Retrospective analysis for Research and Applications, Version 2 (MERRA-2) is used to represent current climate or to infill the missing data.

After the station observations have been reviewed for data completeness, infilling, and any available adjustments, the PMP, IDF, and additional climate variables are calculated. The current climate observed baseline is discussed in Section 3.

A.2.1 DATA SOURCES FOR CURRENT CLIMATE AND REANALYSIS

The current climate is based on available long term daily meteorological observations from climate stations near the Ignace study area. For the Ignace study area, the selected current climate baseline period is from 1889 through 1993. Meeting the monthly data availability is often a challenge over the desired, long observation period. The data availability is necessary to properly capture the different cycles impacting the observations (e.g., diurnal, seasonal) and avoid potential biases in the analysis of the observations (e.g., consistently missing observations during the nighttime or winter). When available climate observations are representative of a site but fail to meet the required data completeness, reanalysis data from the National Aeronautics and Space Administration's (NASA's) Modern-Era Retrospective analysis for Research and Applications, Version 2 (MERRA-2) are used to represent current climate or to infill the missing data. MERRA-2 is a NASA's atmospheric reanalysis using the Goddard Earth Observing System Model, along with its atmospheric data assimilation system that simulates temperature and precipitation on an hourly basis (NASA 2019). Additionally, data from the European Centre for Medium-Range Weather Forecasts (ECMWF) Re-Analysis (ERA5) are used to represent current climate or to infill the missing data from observations. The R-squared (R^2) statistics is used to select between MERRA-2 and ERA5 and complete missing historical observed dataset.

Infilling the missing data is a two-step process: the first step is to perform a correlation analysis for the concurrent period between the non-missing observations and MERRA-2 data, and the second step is to scale the reanalysis data using a linear relationship based on the correlation. Environment and Climate Change Canada (ECCC) has provided the AHCCD dataset that has adjusted measurements to account for non-climatic measurement issues (i.e., wind undercatch) and has combined observations from nearby stations to create longer time series that are useful for trend studies (Mekis and Vincent 2011). The AHCCD dataset includes daily observations for minimum, maximum and mean temperatures and total precipitation. The AHCCD dataset does not always include the most recent observations and as a result, a trending analysis is used to adjust the AHCCD dataset to match the infilled observations to account for any missing observations/years. This adjustment uses monthly factors based on the difference between the two datasets for the concurrent period. A sensitivity analysis is then conducted comparing the datasets to verify that the adjustments are consistent with the infilled dataset.

A.2.2 CALCULATION OF OBSERVED BASELINE IDF CURVES AND RAINFALL STATISTICS

This subsection describes the methodology to calculate the IDF curves for the baseline, divided into different durations (i.e., 1-day, 2-day, and 3-day for the meteorological stations and sub-daily for the stations where sub-daily data is available). The methodology requires fitting curves for several statistical distributions whose parameters are estimated using standard statistical methods. The preferred statistical distribution is then selected based on the results of the goodness-of-fit tests. This section supports the results and summary presented in Section 3.2.

To estimate the IDF values under historical climate conditions, the statistical distribution based on 'goodness-of-fit' criteria are used. For this step, three different distributions are assessed, namely: Gumbel, GEV (Generalized Extreme Value) and Log-Pearson type 3, and based on three goodness-of-fit criteria: Anderson-Darling, Kolmogorov-Smirnov and Chi-Squared tests described on the following sub-sections.

A.2.2.1 Sub-Daily and Daily Precipitation

Sub-daily IDF curves apply only to stations with sub-daily observation records. The sub-daily rainfall data was obtained from the ECCC database.

Consistent with all future projections, the GCM ensemble approach are used. The 1-day rainfall amounts for return periods of 2, 5, 20, 10, 50, 100, 200, 500, 1,000, and 2,000 years in the future periods at different percentile levels are presented.

A.2.2.2 Multi-Day Precipitation

Consistent with all future projections, the GCM ensemble approach is used. The 1-day, 2-day, 3-day, 4-day, 5-day, 10-day, 20-day, 30-day, 50-day, 75-day, 90-day and 120-day consecutive rainfall amounts for return periods of 2, 5, 20, 10, 50, 100, 200, 500, 1,000 and 2,000 years in the future periods at different percentile levels are presented.

A.2.2.3 Statistical Distributions

This subsection describes in detail the three candidate statistical distributions used to produce the IDF curve results. The distributions are Gumbel, Generalized Extreme Value (GEV) and Pearson or Log Pearson Type 3.

A.2.2.3.1 Gumbel Distribution (EV1)

The EV1 distribution has been widely recommended and adopted as the standard distribution by Environment and Climate Change Canada for all the Precipitation Frequency Analyses in Canada. The EV1 distribution for annual extremes can be expressed as:

$$Q(T) = \mu + k_T.\sigma \qquad \textbf{Equation 1}$$

$$k_T = -\frac{\sqrt{6}}{\pi}\left[0.5772 + ln\left(ln\left(\frac{T}{T-1}\right)\right)\right] \qquad \textbf{Equation 2}$$

where *Q(T)* is the exceedance value, μ and σ are the population mean and standard deviation of the annual extremes; T is return period in years.

A.2.2.3.2 Generalized Extreme Value (GEV) Distribution

The GEV distribution is a family of continuous probability distributions that combines the three asymptotic extreme value distributions into a single one: Gumbel (EV1), Fréchet (EV2) and Weibull (EV3) types. GEV uses three parameters: location, scale and shape. The location parameter describes the shift of a distribution in each direction on the horizontal axis. The scale parameter describes how spread out the distribution is and defines where the bulk of the distribution lies. As the scale parameter increases, the distribution becomes more spread out. The shape parameter affects the shape of the distribution and governs the tail of each distribution. The shape parameter is derived from skewness, as it represents where most of the data lies, which creates the tail(s) of the distribution. The value of shape parameter k = 0, indicates the EV1 distribution. Value of k > 0, indicates EV2 (Fréchet), and k < 0 the EV3 (Weibull). The Fréchet type has a longer upper tail than the Gumbel distribution and the Weibull type has a shorter tail (Overeem et al. 2007 and Millington et al. 2011).

The GEV cumulative distribution function *F(x)* is given by Equation 3 for *k* = 0 (EV1).

$$F(x) = \exp\left\{ -\left[1 - \frac{k}{\alpha}(x-\mu)\right]^{1/k}\right\} \quad \text{for k} \neq 0 \qquad \textbf{Equation 3}$$

$$F(x) = \exp\left\{ -exp\left[-\frac{1}{\alpha}(x-\mu)\right]\right\} \quad \text{for k} = 0 \qquad \textbf{Equation 4}$$

where μ is the location, α is the scale and *k* is the shape parameter of the distribution, and y is the GEV reduced variate, $y = -\ln(-\ln F)$.

The inverse distribution function or quantile function is given by Equation 5 for k ≠ 0 and Equation 6 for k = 0.

$$Q(x) = \mu + \alpha\{\ 1 - (-lnF)^k\}/k \quad \text{for k} \neq 0 \qquad \textbf{Equation 5}$$

$$Q(x) = \mu - \alpha\left\{\ -exp\left[-\frac{1}{\alpha}(F-\mu)\right]\right\} \quad \text{for k} = 0 \qquad \textbf{Equation 6}$$

A.2.2.3.3 Pearson and Log Pearson Type 3

The Pearson Type 3 (PE3) distribution is a member of the family of Pearson Type 3 distributions and is also referred to as the Gamma distribution. The PE3 is required for all Precipitation Frequency Analysis in the United States. Like GEV, the PE3 has three parameters, location (μ), scale (σ) and shape (γ). A problem arises with PE3 as it tends to give low upper bounds of the precipitation magnitudes, which is undesirable (Cunnane 1989). The CDF (Cumulative Density Function – *F*) and PDF (Probability Density Function – *f*) are defined in (Hosking and Wallis 1997) as:

$$\text{If } \gamma \neq 0, \text{ let } \alpha = 4/\gamma^2 \text{ and } \xi = \mu - 2\sigma/\gamma \qquad \textbf{Equation 7}$$

If $\gamma > 0$ then:

$$F(x) = G\left(\alpha, \frac{x-\xi}{\beta}\right)/\Gamma(\alpha) \qquad \textbf{Equation 8}$$

$$f(x) = \frac{(x-\xi)^{\alpha-1}e^{-(x-\xi)/\beta}}{\beta.\Gamma(\alpha)} \qquad \textbf{Equation 9}$$

If $\gamma < 0$ then:

$$F(x) = 1 - G\left(\alpha, \frac{\xi-x}{\beta}\right)/\Gamma(\alpha) \qquad \textbf{Equation 10}$$

$$f(x) = \frac{(\xi - x)^{\alpha-1} e^{-(\xi-x)/\beta}}{\beta.\Gamma(\alpha)}$$ **Equation 11**

If $\gamma = 0$ then Pearson type 3 follows the Normal distribution:

$$F(x) = \Phi\left(\frac{x-\mu}{\sigma}\right)$$ **Equation 12**

$$f(x) = \phi\left(\frac{x-\mu}{\sigma}\right)$$ **Equation 13**

Where *G* is the incomplete Gamma function and Φ the CDF and ϕ PDF of the Normal distribution.

A.2.2.4 Parameter estimation methods

A common statistical procedure for estimating distribution parameters is the use of a maximum likelihood estimator or the method of moments. ECCC uses and recommends the use of the method of moments technique to estimate the parameters for EV1. Golder uses the method of moments to calculate the parameters of the Gumbel distribution. Golder uses L-moments to calculate parameters of the GEV distribution. The following sections describe the method of moments procedure for calculating the parameters of the Gumbel distribution and L-moments method for calculating parameters of the GEV distribution.

A.2.2.4.1 Method of Moments

The most popular method for estimating the parameters of the Gumbel distribution is method of moments (Hogg et al. 1989). In the case of the Gumbel distribution, the number of unknown parameters is equal to the mean and standard deviation of the sample mean. The first two moments of the sample data are sufficient to derive the parameters of the Gumbel distribution in Equation 14 and Equation 15. These are defined as:

$$\mu = \frac{1}{N}\sum_{i=1}^{N} Q_i$$ **Equation 14**

$$\sigma = \sqrt{\frac{1}{N-1}\sum_{i=1}^{N}(Q_i - \bar{Q})}$$ **Equation 15**

Where μ is the mean, σ the value of standard deviation of the historical data, Q_i the maximum precipitation data for year *I*, and $\bar{Q}$ the mean of the precipitation data.

A.2.2.4.2 L-moments Method

The L-moments (Hosking and Wallis 1997) and maximum likelihood methods are commonly used to estimate the parameters of the GEV distribution and fit to annual maxima series. The L-moments are a modification of the probability-weighted moments (PWMs), as they use the PWMs to calculate parameters that are easier to interpret. The PWMs can be used in the calculation of parameters for statistical distributions (Millington et al. 2011). They provide an advantage, as they are easy to work with, and more reliable as they are less sensitive to outliers. L-moments are based on linear combinations of the order statistics of the annual maximum rainfall amounts (Hosking and Wallis 1997 and Overeem et al. 2007). The PWMs are estimated by:

$$b_0 = n^{-1}\sum_{j=1}^{n} x_j \quad \textbf{Equation 16}$$

$$b_1 = n^{-1}\sum_{j=2}^{n} \frac{j-1}{n-1} x_j \quad \textbf{Equation 17}$$

$$b_2 = n^{-1}\sum_{j=3}^{n} \frac{(j-1)(j-2)}{(n-1)(n-2)} x_j \quad \textbf{Equation 18}$$

Where x_j is the ordered sample of annual maximum series (AMS) and b_i are the first PWMs. The sample L-moments can them obtained as:

$$\ell_1 = b_0 \quad \textbf{Equation 19}$$

$$\ell_2 = 2b_1 - b_0 \quad \textbf{Equation 20}$$

$$\ell_3 = 6b_2 - 6b_1 + b_0 \quad \textbf{Equation 21}$$

A.2.2.4.3 L-Moments for the GEV parameters

The GEV parameters: location (μ), scale (α) and shape (k) are defined (Hosking and Wallis 1997) as:

$$k = 7.8590c + 2.9554c^2$$

where:

$$c = \frac{2}{3+\ell_3/\ell_2} - \frac{\ln(2)}{\ln(3)} \quad \textbf{Equation 22}$$

$$\alpha = \frac{\ell_2 k}{(1-2^{-k}).\Gamma(1+k)} \quad \textbf{Equation 23}$$

$$\mu = \ell_1 - \alpha\frac{1-\Gamma(1+k)}{k} \quad \textbf{Equation 24}$$

Where Γ is the gamma function,ℓ_1, ℓ_2 and ℓ_3 the L-moments, and μ the location, α the scale and k the shape parameters of the GEV distribution.

A.2.2.4.4 L-Moments for the Pearson Type 3 (PE3) and Log Pearson Type 3 (LP3)

The parameters location (μ), scale (σ) and shape (γ) are defined in (Hosking and Wallis 1997) for the Pearson Type 3 distribution are as follows:

$$\gamma = 2\alpha^{-0.5} + sign(\tau_3) \quad \textbf{Equation 25}$$

$$\sigma = \frac{\lambda_2 \pi^{0.5} \alpha^{0.5} \Gamma(\alpha)}{\Gamma(\alpha + 0.5)} \quad \textbf{Equation 26}$$

$$\mu = \lambda_1 \quad \textbf{Equation 27}$$

To estimate the value of α:

If $0 < |\tau_3| < \frac{1}{3}$, let $z = 3\pi\tau_3{}^2$ and use:

$$\alpha = \frac{1 + 0.2960.z}{z + 0.1880.z^2 + 0.0442.z^3} \quad \textbf{Equation 28}$$

If $\frac{1}{3} < |\tau_3| < 1$, let $z = 1 - |\tau_3|$ and use:

$$\alpha = \frac{0.3636.z - 0.59567.z^2 + 0.25361.z^3}{1 - 2.78861.z + 2.56096.z^2 - 0.77045.z^3} \quad \textbf{Equation 29}$$

A.2.2.5 Goodness-of-Fit tests

Goodness of fit tests can be reliably used in climate statistics to assist in selecting the best distribution to fit the given data. These tests are usually applied to reject candidate statistical distributions and provide a sense of how well a given distribution fits the data being tested. These tests describe the differences between the observed data points and the calculated values from the distribution. The performances the three statistical distribution considered are tested by using the following goodness-of-fit tests: Kolmogorov-Smirnov test, Anderson-Darling estimate and Chi-Squared test, described next.

A.2.2.5.1 Kolmogorov-Smirnov Test

The Kolmogorov-Smirnov (KS) test it is used to decide whether the sample being tested originates from a specific continuous statistical distribution. The KS statistic (*D*) is based on the largest vertical difference between the theoretical and the empirical CDFs (Cumulative Distribution Function) and is calculate as:

$$D = \max_{1 \le i \le n} \left(F(x_i) - \frac{i-1}{n}, \frac{i}{n} - F(x_i) \right) \quad \textbf{Equation 30}$$

Where, the samples x_i are assumed to be random, originating from some distribution with CDF of $F(x_i)$, *n* the sample size, and *i* the ith sample, calculated when the data is sorted in ascending order. The hypothesis for this distribution (test) is rejected if the test statistic is greater than the critical value at a chosen significance level. For the significance level of ***α=5%***, the critical value is selected is based on the sample size and tables are available. The value of the statistics *D* is used to rank the distributions.

A.2.2.5.2 Anderson-Darling Test

The Anderson-Darling (AD) test compares an observed CDF to an expected CDF. This method gives more weight to the tail of the distribution than KS test, which in turn leads to the AD test being stronger and having more weight than the KS test. The test rejects the hypothesis regarding the distribution level if the statistic obtained is greater than a critical value at a given significance level (*α*). The significance level most commonly used is *α* = 5%, producing a critical value of 2.5018. This number is then compared with the test distributions statistic to determine if it can be rejected or not. The AD test statistic is calculated as:

$$AD = -n - \frac{1}{n}\sum_{i=1}^{n}(2i-1)\ \left[ln\left(F(X_i)\right) + ln\left(1 - F(X_{n+1-i})\right)\right] \quad \textbf{Equation 31}$$

Where *n* the sample size, and *i* the i^{th} sample, calculated when the data is sorted in ascending order, $F(x_i)$ the CDF of the distribution being tested, and The samples x_i are assumed to be random, originating from some distribution with CDF of $F(x_i)$. The value of the *AD* test is used to rank the distributions.

A.2.2.5.3 Chi-Square Test

The Chi-Squared test is used to determine if a sample comes from a given distribution. The test is based on binned data, and the number of bins (k) is determined by:

$k = 1 + logN$ with N the sample size **Equation 32**

The test statistic (χ^2) is calculated as:

$$\chi^2 = \sum_{i=1}^{k}\frac{(O_i - E_i)^2}{E_i} \quad \textbf{Equation 33}$$

Where O_i is the observed frequency, $E_i = F(x2) - F(x1)$ with $x1$ and $x2$ as the limits of the i^{th} bin.

The statistics χ^2 is used to assist in ranking the distributions and the significance level, α = 0.05 produced a critical value of 12.592. For values above this threshold the distribution being tested is rejected.

A.2.3 CALCULATION OF BASELINE PROBABLE MAXIMUM PRECIPITATION (PMP)

This section describes the method of the calculation of the baseline values of the PMP using the Transposition method following the recommendation by Wood (2019) and corresponds to steps 1 through 5 from Figure A.2. The Transposition method is based on observed historical events and requires careful analysis and identification of major storms from the available records. The stations in the study area are screened for the largest storms in the observational record and are used to construct the DAD curves, which are then maximized by applying maximization and the transposition factors (described in Section A.2.3.2) to the area of study. These steps are described in the following subsections.

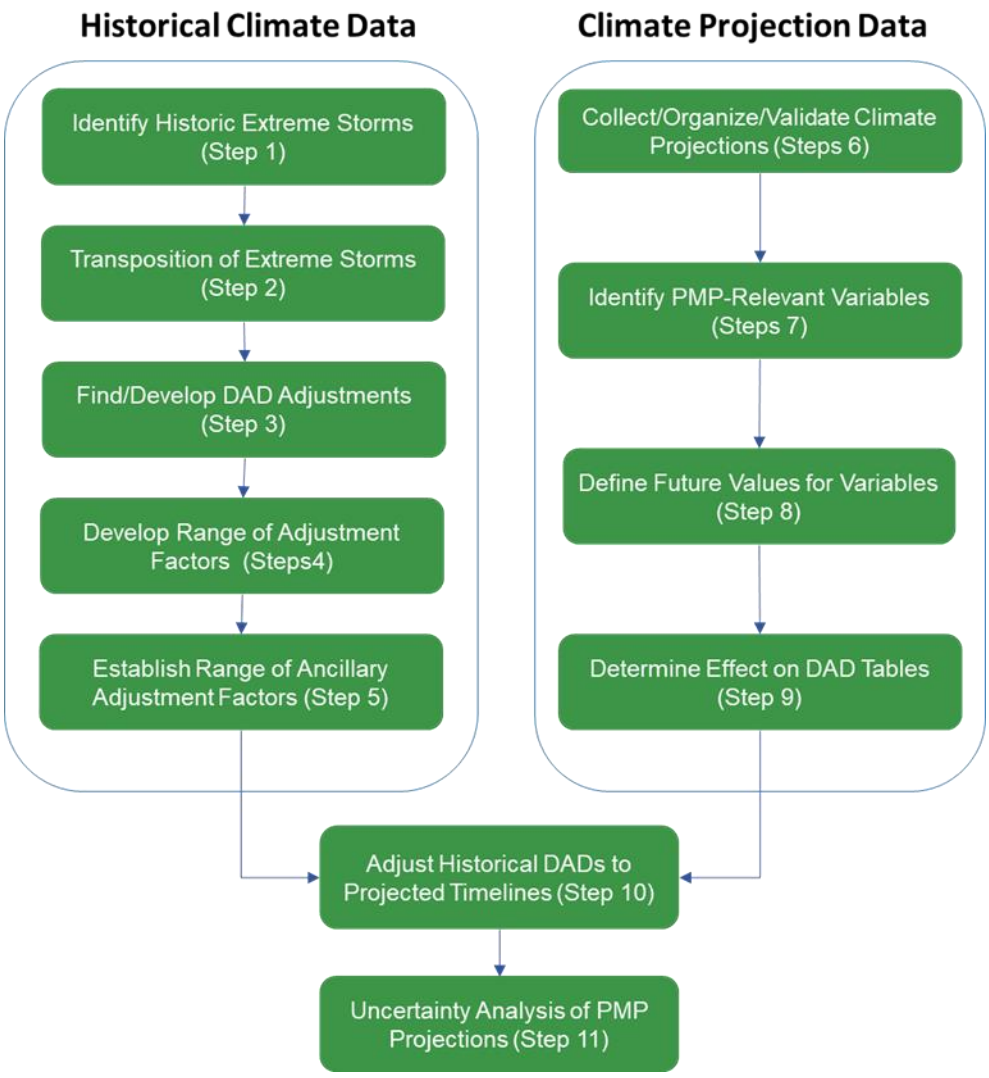

Figure A.2: Baseline and Future PMP Analyses Flowchart

A.2.3.1 Construction of the DAD Curves in the Hershfield Method

The methodology used in this study is based on the one described by WMO (2009a). The precipitation is weighted among stations according to their distance from other stations where the selected storms are recorded using a pairwise comparison. This step is equivalent to an averaged weighting of the precipitation. Averaged weighting is done pairwise with stations that have records for the selected storm, and the centre is defined at the station that recorded the highest precipitation for the selected event with additional meteorological information about the storm. From the centre of the storm, the area is defined using the distance to each station (also in a pairwise approach) defining the set of area/depth points used to develop the DAD curves (as in Section 3.3.3). This approach is a simplification of the methodology using isohyetal maps; however, given the very low density of stations utilized, it is expected to yield similar results to other methods. The depth-area-duration (DAD) curves are then constructed for 1-day, 2-day, and 3-day durations using envelopment (following WMO 2009a) of the area/depth points found as described above. The in-place storm maximization and storm transposition play a large role in the final value of the PMP calculated.

The WMO acknowledges that there is significant uncertainty regarding PMP calculations and recommends that a comparison of other method and reported values is conducted. A comparison with previous studies completed for the area and the Hershfield method is conducted to validate the result. The Hershfield method, described in WMO (2009a), is a robust statistical method to calculate the PMP values that relies on observations of annual maximum values of daily total precipitation. It is usually recommended for watersheds up to 1,000 km^2 (WMO 2009a). The PMP using the Hershfield method is calculated as follows:

$$PMP = X_n + KS_n \qquad \textbf{Equation 34}$$

Where X_n and S_n are the mean and standard deviation (respectively) of the annual maximum 1-day precipitation, and K is a frequency factor that is a function of X_n and rainfall intervals. Adjustments needed to be made to X_n and S_n to account for the length of record used and the maximum observed rainfall event. Multiplicative factors for X_n and S_n were found to be 1.005 and 1.035 respectively when accounting for the length of record used (Figure 4.4 of WMO 2009a). Multiplicative factors for X_n and S_n were found to be 0.997 and 0.971 respectively when accounting for the maximum observed rainfall event (Figure 4.2 of WMO 2009a). The values of K as a function of rainfall duration and mean of the annual maximum series are given in Figure 4.1 of WMO (2009a).

A.2.3.2 Storm Maximization and Transposition Method

One of the steps of the calculation of the PMP using DAD curves (Transposition method) is the storm maximization using precipitable water (PWC) content of the rainfall event and the transposition to the study area (WMO 2009a). For the storm maximization and transposition, the maximum PWC is estimated using the relationship between dew point temperature and the PWC as shown in Figure A.3. This relationship was determined by OMNR (2006) and is valid for the province of Ontario. The PWC values are based on the 12-hour persistent dewpoint maps (100-year return period with and adjusted statistical distribution as shown in Figure F3.2 from OMNR 2006), and the mean temperature as proxy for the dewpoint temperature, where dewpoint data is not available.

The in-place maximized storms are transposed to the Ignace area by evaluation of the precipitable water transposition factors. Based on the 100-year return period 12-hour persistent dew-point maps (Figure F3.2) from OMNR (2006), the in-place maximization ratio is calculated as follows:

$$r_{storm} = \frac{PWC_{100-year-A}}{PWC_{storm}} \qquad \textbf{Equation 35}$$

Where $PWC_{100-year-A}$ is the maximum precipitable water for 100-years return period of the 12-hour persistent dew point (using the maps provided by OMNR (2006)) and PWC_{storm} is the maximum precipitable water for the storm event both at the location of the storm center. The daily mean temperature is used as proxy for the dew point, since information on dew-point is not available, both at the location of the storm center and at the Ignace study area.

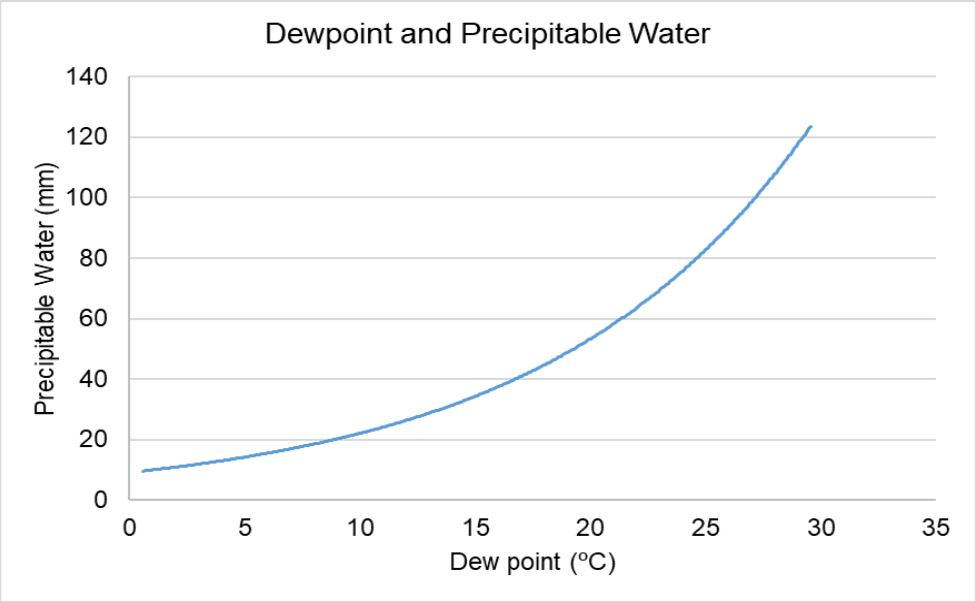

Figure A.3: Precipitable Water and Dew Point relationship (Adapted from: OMNR 2006)

The transposition ratio is calculated as follows:

$$r_{transp} = \frac{PWC_{100-year-B}}{PWC_{100-year-A}} \qquad \textbf{Equation 36}$$

Where $PWC_{100-year-B}$ is the maximum precipitable water for 100-years return period of the 12-hour persist dew point at the transposition location (using the maps provided by OMNR 2006).

The final storm maximization factor is calculated as

$$r = r_{storm} \times r_{transp} \qquad \textbf{Equation 37}$$

The maximization for the 2- and 3-Day PMP is calculated by adding the delta to the 2 and 3-day DAD from the 1-Day PMP maximization result.

This method is used to derive the final storm maximization factor in Section 3.3.3.

A.2.3.3 Converting Daily PMPs to Sub-Daily

The hourly precipitation data are not available from ECCC and therefore the sub-daily PMP is estimated using ratio factors calculated from the sub-daily IDF curves defined for the study area. The ratios are estimated by taking the 24-hour duration and 100-year return period as reference, and the other sub-daily durations (5, 10, 15, 30 minutes, 1, 2, 6, 12 hours) are scaled accordingly to calculate the sub-daily PMP values. The 100-year return period is selected since it provides a more realistic and reliable estimate among sub-daily durations than higher return period. It is important to note that this estimate has uncertainties and assumes that the PMP follows the same distribution as the IDF curves for 24-hours durations and 100-year return period.

A.2.4 RAIN ON SNOW PROCEDURE

The calculation of the rain on snow follows the methodology adopted by ECCC (Louie and Hogg 1980) to estimate runoff from snowmelt. The methodology uses a degree-day method to separate rainfall and snowfall from precipitation and model the processes of snow accumulation and melt. The following steps are used in the procedure:

1) The snowpack accumulation is estimated based on the daily mean temperature and the total rainfall. If temperature is > 0ºC, precipitation falls as rain and no snowpack is accumulated; if temperature is < 0ºC, precipitation falls as snow and is accumulated to the snowpack.
2) The snowmelt amount (SM) is estimated based on the model presented in Equation 38 for Eastern Canada Forested Basin (Pysklywec et al. 1968) and is depleted from the snowpack.

$$SM = 0.0397\ (Ta - 27.6)\ \ (\frac{inches}{day}) \qquad \textbf{Equation 38}$$

Where *Ta* is the mean daily air temperature in *ºF*.

3) The calculated snowmelt is added to the rainfall amount, if any (rain + snowmelt).
4) The process is repeated for all days in the data series are calculated.
5) Finally, the daily maximums of the combined rainfall and snowmelt for each year are calculated and a Gumbel distribution is fitted to estimate the several required return periods.

A.2.5 CALCULATION OF ADDITIONAL CLIMATE VARIABLES

Analysis of additional climate variables is important for providing context to climatic conditions on site and how they are projected to change in the future. This analysis may also provide useful information for further studies conducted at the site. The additional climate variables include monthly temperature and precipitation statistics along with derived climate variables including WMO climate indices, potential evapotranspiration, drought index, and qualitative information for wind speed and relative humidity. A daily future timeseries is also provided for the Ignace study area that includes bias correction of precipitation. The sections to follow provide detailed methodology for the analysis performed for each of the variables.

A.2.5.1 Monthly Mean, Minimum, and Maximum Temperature and Precipitation

Summary statistics for temperature and precipitation at a monthly time scale allow for seasonal variation in climate to be captured on site. The statistics are calculated in two steps:

1. Resampling – daily climate variables are resampled to a monthly timescale. This is done by taking the sum of daily precipitation and mean of the daily temperatures in each month.
2. Aggregation – each calendar month across all years is aggregated for the resampled monthly total precipitation and temperature variables. The mean, minimum, and maximum are taken to aggregate the monthly values across all years.

To ensure months with insufficient data were not included in these statistics, only months with greater than 90% data availability were considered.

Daily current climate timeseries are provided for total precipitation and mean temperature from the infilled dataset presented in Section 3.1.2 of the main report.

Derived variables including rain, snow, and snow depth are included using the ECCC methods discussed in Louie and Hogg (1980). The snow depth (same as snowpack) is estimated based on the daily mean temperature and the total rainfall. If temperature is > 0ºC, precipitation falls as rain and there is no snow depth. If temperature is < 0ºC, precipitation falls as snow and snow depth is accumulated.

A.2.5.2 WMO Climate Indices

The climate extremes are defined by the World Meteorological Organization's (WMO's) Expert Team on Climate Change Detection and Indices (ETCCDI; WMO 2009b) who recommend 27 indices (ClimDEX) as a means of summarizing daily temperature and precipitation statistics, focusing primarily on aspects of climate extremes. They have been developed to allow comparison of climate conditions on an international basis. Table A.1 provides a summary of these indices and their definitions.

The minimum, maximum, mean, and median of the annual values for each climate index are calculated, as well as trends to help provide a description of the current climate conditions. The trends are calculated using a Theil-Sen estimator, which estimates the slope of a linear trendline using the median of the slopes of all lines through pairs of points. The Mann-Kendall test is used to estimate the significance of the trends. Details on the implementation of these techniques can be found in (Salmi et. al. 2002).

Table A.1: List of WMO Recommended 27 Extreme Indices

ID	Indicator Name	Definitions [(1)]	Units
CDD	Consecutive dry days	Maximum number of consecutive days with daily precipitation amount less than 1 mm (RR<1 mm)	Days
CSDI	Cold spell duration indicator	Annual count of days with at least 6 consecutive days when daily minimum temperatures are less than the 10th percentile (TN<10th percentile)	Days
CWD	Consecutive wet days	Maximum number of consecutive days with daily precipitation amount greater than or equal to 1 mm (RR>=1 mm)	Days
DTR	Diurnal temperature range	Monthly mean difference between the daily minimum temperature (TX) and the daily maximum temperature (TN)	ºC
FD0	Frost days	Annual count when the daily minimum temperature is less than 0°C (TN<0ºC)	Days
GSL	Growing season length	Annual (1st Jan to 31st Dec in the northern hemisphere, 1st July to 30th June in the southern hemisphere) count between first span of at least 6 days with ground temperatures greater than 5°C (TG>5ºC) and first span after July 1 (January 1 in the southern hemisphere) of 6 days with ground temperatures less than 5°C (TG<5ºC)	Days
ID0	Ice days	Annual count when the daily maximum temperature is less than 0° (TX<0ºC)	Days
PRCPTOT	Annual total wet-day precipitation	Annual total precipitation (PRCP) in wet days where the daily precipitation is greater than or equal to 1 mm (RR>=1 mm)	mm
R10	Number of heavy precipitation days	Annual count of days when precipitation is greater than or equal to 10 mm) (PRCP>=10 mm)	Days
R20	Number of very heavy precipitation days	Annual count of days when precipitation is greater than or equal to 20 mm (PRCP>=20 mm)	Days
R95p	Very wet days	Annual total precipitation (PRCP) when the daily precipitation is greater than the 95th percentile (RR>95th percentile)	mm
R99p	Extremely wet days	Annual total precipitation (PRCP) when the daily precipitation is greater than the 99th percentile (RR>99th percentile)	mm
Rnn	Number of days above nn mm	Annual count of days when precipitation when precipitation is greater than or equal to a user defined threshold (PRCP>= “nn” mm, “nn” is user defined threshold)	Days
RX1day	Max 1-day precipitation amount	Monthly maximum 1-day precipitation	mm
Rx5day	Max 5-day precipitation amount	Monthly maximum consecutive 5-day precipitation	mm

ID	Indicator Name	Definitions [(1)]	Units
SDII	Simple daily intensity index	Annual total precipitation divided by the number of wet days (defined as PRCP>=1.0 mm) in the year	mm/day
SU25	Summer days	Annual count when the daily maximum temperature is greater than 25°C (TX>25ºC)	Days
TN10p	Cool nights	Percentage of days when the daily minimum temperature is less than the 10th percentile (TN<10th percentile	% of Days
TN90p	Warm nights	Percentage of days when the daily minimum temperature is greater than the 90th percentile (TN>90th percentile	% of Days
TNn	Min Tmin	Daily minimum value of daily minimum temp	ºC
TNx	Max Tmin	Daily maximum value of daily minimum temp	ºC
TR20	Tropical nights	Annual count when the daily minimum temperature is greater than 20°C (TN>20ºC)	Days
TX10p	Cool days	Percentage of days when the daily maximum temperature is less than the 10th percentile (TX<10th percentile)	% of Days
TX90p	Warm days	Percentage of days when the daily maximum temperature is greater than the 90th percentile (TX>90th percentile)	% of Days
TXn	Min Tmax	Daily minimum value of daily maximum temp	ºC
TXx	Max Tmax	Daily maximum value of daily maximum temp	ºC
WSDI	Warm spell duration indicator	Annual count of days with at least 6 consecutive days when the daily maximum temperature is greater than the 90th percentile (TX>90th percentile)	Days

Note:

(1) The abbreviations for the variables used in the definitions are as follows: SH is southern hemisphere; RR is the daily precipitation amount (mm); TX is the maximum temperature (°C); TN is the minimum temperature (°C); TG is the ground temperature (°C); PRCP is the precipitation amount (mm); RR – daily precipitation amount (mm).

A.2.5.3 Potential Evapotranspiration

Evapotranspiration is the combined process of evaporation and transpiration over a vegetated surface. The principal weather parameters affecting evapotranspiration are air temperature, extraterrestrial radiation, humidity and wind speed, and vegetation parameters. Potential evapotranspiration represents the maximum actual evapotranspiration expected from a given area with no moisture limitations. As only the observed minimum temperature, maximum temperature and total precipitation are available from the daily current climate dataset (no infilled observations of radiation, humidity, and wind speed are produced), an air temperature-based formula, namely the Hargreaves equation (Food and Agriculture Organization [FAO] 2006) will be used.

The Hargreaves equation was developed in 1982 as an alternative to the more complicated energy-balance approach of the Penman-Monteith equation (developed in 1948). The Penman-Monteith method required significant amounts of climate data including incoming solar radiation, wind speed, and humidity, which are often not available. By contrast, the Hargreaves equation requires only the daily minimum, maximum, and mean temperatures. The Hargreaves equation builds into a more complete model by making assumptions about the solar radiation (based on latitude), accounting for humidity (based on the difference between daily minimum and maximum temperatures), and assuming that the effect of wind is not significant. The FAO has noted that for potential evapotranspiration (ET_o):

> *"Temperatures methods remain empirical and require local calibration in order to achieve satisfactory results. A possible exception is the 1985 Hargreaves' method which has shown reasonable ET_o results with a global validity" (FAO 2006).*

The Hargreaves estimate of daily potential evapotranspiration is arrived at by the following formula:

$$E = 0.0023(T_{mean} + 17.8)(T_{max} - T_{min})^{0.5} R_a \qquad \textbf{Equation 39}$$

where T_{mean} is the average temperature, T_{max} and T_{min} are daily maximum and minimum temperatures (all in °C), and R_a is the extraterrestrial radiation (MJ/m^2/day). The R_a is calculated as:

$$R_a = \frac{24(60)}{\pi} G_{sc} d_r [w_s sin(\varphi) sin(\delta) + cos(\varphi) cos(\delta) sin(w_s)] \qquad \textbf{Equation 40}$$

where G_{sc} is the solar constant (0.0820 MJ/m^2/min);

d_r is the inverse relative distance Earth-Sun (dimensionless): $d_r = 1 + 0.033cos\left(\frac{2\pi}{365}J\right)$;

w_s is the sunset hour angle in radians: $w_s = arccos[-tan(\varphi)tan(\delta)]$;

φ is the latitude of the site in radians;

δ is the solar declination in radians: $\delta = 0.409sin\left(\frac{2\pi}{365}J - 1.39\right)$; and

J is the Julian day.

The daily potential evapotranspiration timeseries is derived from the infilled daily temperature dataset using the methods described above. It should be noted that with this method, potential evapotranspiration can occur during the winter months due to the inclusion of the diurnal temperature range (maximum temperature – minimum temperature) allowing for some potential evapotranspiration to occur in the winter months; however, ice/snow sublimation is not specifically accounted for. Due to the low temperatures and potential evapotranspiration rates during the winter months, it is anticipated that this simplification will not have a large impact on the final results.

A.2.5.4 Drought Index

The drought index is estimated using the standard precipitation and evapotranspiration index (SPEI) of Vincente-Serrano et al. (2010), which is based on the standard precipitation index described in WMO (2012). This method illustrates the number of standard deviations that net precipitation (precipitation less evapotranspiration) for a given month is from the median for all months. By using net precipitation, the effects of temperature variation for current climate is also able to impact the drought index instead of only precipitation.

The SPEI is calculated by first taking the difference between monthly total precipitation and evapotranspiration, D_i where i corresponds to a given month in the monthly baseline timeseries. Next, 1-dimensional convolution is performed on D_i according to the selected calculation interval, resulting in X_i. The calculation interval used is selected as 12 months, so that each monthly value contains the sum of the previous 12-months.The drought index is calculated using a running deficit/surplus of net precipitation; therefore, the calculation interval of 12 months is used to account for seasonal variability in net precipitation. The scale and shape parameters of a two-parameter gamma distribution is found for X_i. Using these parameters, the non-exceedance probabilities, P_i for each value in X_i is extracted from the cumulative distribution function of the gamma distribution. The SPEI values are then obtained by taking the quantiles of a normal distribution with mean of 0 and standard deviation of 1 that correspond to P_i. With this method, the mean and standard deviation of the SPEI will have values of 0 and 1 due to the normalization step.

A drought is indicated by a negative SPEI value, which indicates a deficient of available water in a given location. Due to the standardized nature of this drought index, generalized classification systems have been developed. The drought classification system provided by WMO (2012) can be used to interpret the SPEI values (Table A.2). SPEI values are summarized using a set of percentiles for each calendar month. This allows for the distribution of water deficit/surplus across calendar months to be examined.

Table A.2: SPEI Classification System

SPEI Value	Classification
2.0+	extremely wet
1.5 to 1.99	very wet
1.0 to 1.49	moderately wet
-0.99 to 0.99	near normal
-1.0 to -1.49	moderately dry
-1.5 to -1.99	severely dry
-2 and less	extremely dry

A.2.5.5 Wind Speed and Relative Humidity

The closest published climate normals from ECCC (2020) are used to characterize wind speed and relative humidity at the site, and are compared to published literature values, where available. Information on daily mean wind speed trends is obtained from Wan et al. (2010). In this study, wind speed observations are homogenized across Canada using the ECCC digital data archive for the period of 1953 to 2010. Homogenization was carried out by first adjusting for the effects of non-standard anemometer heights, detecting and adjusting for systematic errors (location and exposure of the observation site, anemometer type, instrument malfunctions, etc.), and identification and adjustment for discontinuities in wind speed timeseries. Linear trends were then estimated using the monthly mean series of the homogenized daily mean wind speed data.

A.3 FUTURE CLIMATE PROJECTIONS DEVELOPMENT

Future climate projections are important for understanding how climate is projected to change from the climate baseline. The future climate projections come from publicly available statistical downscaled future climate projections on a daily scale. Recognizing the inherent uncertainty with projections, multiple projections from multiple models and scenarios are included in the analysis. Therefore, the future projections are provided in terms of percentiles.

The following sub-sections describe the methodology to develop future climate change projections and to incorporate these projections to the PMP estimates, IDF curves, and additional climate variables. The methodology presented in these subsections supports the analyses and results for the future projections for PMP and IDF curves presented in Section 4.

A.3.1 DATA SOURCES FOR FUTURE CLIMATE

Future climate projections are important for understanding how climate is projected to change from the climate baseline. The Intergovernmental Panel on Climate Change (IPCC) is generally considered to be the definitive source of information related to past and future climate change as well as climate science. In 1988, the IPCC was formed by the World Meteorological Organization (WMO) and the United Nations Environment Program (UNEP) to review international climate change data. The IPCC is generally considered to be the definitive source of information related to past and future climate change as well as climate science. As an international body, the IPCC provides a common source of information relating to emission scenarios, provides third party reviews of models, and recommends approaches to document future climate projections. Periodically, the IPCC issues assessment reports summarizing the most current state of climate science. The Fifth Assessment Report (AR5) (IPCC 2013) represents the most current complete synthesis of information regarding climate change. The Sixth Assessment report (AR6) is due for release in May 2022 and will include updated climate scenarios and projections (IPCC 2020). The updated projections are anticipated to be in line with the AR5 but will include additional emissions scenarios to be assessed.

A.3.2 GLOBAL CLIMATE CHANGE PROJECTIONS

Future climate is typically projected using general circulation models (GCMs; also used interchangeable with global climate models) that involve the mathematical representation of global land, sea and atmosphere interactions over a long period of time. GCMs are one of the tools available that allows us to estimate and understand changes in climatic conditions for future periods. In order to provide global projections of climate, the spatial and temporal resolution of GCMs (hundreds of kilometers and monthly) is coarse compared to meteorological models (kilometers and hourly).

These GCMs have been developed by various government agencies, but they share a number of common elements described by the IPCC. The IPCC does not run the models but acts as a clearinghouse for the distribution and sharing of the model forecasts. Future climate projection data are available from about 30 GCMs. GCMs require extensive inputs to characterize the physical processes and social development paths that could alter climate in the future. In order to represent the wide range of the inputs possible to global climate models, the IPCC has established a series of RCPs that help define the future levels of radiative forcing terms. The IPCC identified four greenhouse gas (GHG) emission scenarios, namely, RCP 2.6, RCP 4.5, RCP 6.0, and RCP 8.5 (business-as-usual). The pathways are named after the radiative forcing projected to occur by 2100.

Beyond 2100, the radiative forcing is described using extensions of the RCPs called Extended Concentration Pathways (ECPs) that help define the trajectory of greenhouse gas concentrations out to the year 2300. It should be noted that the ECPs (i.e., climate change model projections beyond 2100) contain a high degree of uncertainty. These four RCPs and ECPs have been described more fully by van Vuuren et al. (2011) in their paper "The representative concentration pathways: an overview" and have been summarized in Table A.3. The IPCC identified four RCPs; however, this report focuses on the three RCPs (RCP 2.6, RCP 4.5, and RCP 8.5) currently available from ClimateData.ca (ClimateData.ca 2019).

Table A.3: Characterization of Representative Concentration Pathways

Name	Radiative Forcing in 2100 and 2300	Characterization
RCP 8.5, ECP 8.5	8.5 W/m² (2100) 12 W/m² (2300)	Increasing greenhouse gas emissions over time, with no stabilization, representative of scenarios leading to high greenhouse gas concentration levels (business-as-usual GHG emissions); and comparable to the SRES A2/A1FI scenarios. Past 2100, greenhouse gas emissions stabilize near 2250 at 12 W/m².
RCP 6.0, ECP 6.0	6.0 W/m²	Without additional efforts to constraint emissions (baseline scenarios); and comparable to SRES B2 scenario. Past 2100, greenhouse gas emissions stabilize near 2150 at 6.0 W/m².
RCP 4.5, ECP 4.5	4.5 W/m²	Total radiative forcing is stabilized shortly after 2100, without overshoot. This is achieved through a reduction in greenhouse gases over time through climate policy; and comparable to SRES B1 scenario. Past 2100, greenhouse gas emissions stabilize near 2150 at 4.5 W/m².
RCP 2.6, ECP 3PD	2.6 W/m²	"Peak and decline" scenario where the radiative forcing first reaches 3.1 W/m² by mid-century and returns to 2.6 W/m² by 2100. This is achieved through a substantial reduction in greenhouse gases over time through stringent climate policy. Past 2100, greenhouse gases remain constant at concentrations in 2100.

Note: Summarized from van Vuuren et al. (2011); W/m² = watt per square metre.

A.3.2.1 Regional Climate Change Projections

GCMs resolution is generally too coarse for direct use as it does not resolve weather and extreme weather patterns or climatology at local scales. Outside of using the GCM output directly, there are different options to analyze climate projections at a regional scale. Most downscaled climate datasets include minimum temperature, maximum temperature and precipitation. The focus is on statistical or dynamically downscaled datasets which have a higher temporal and spatial resolution of the data; however, they may have limited variables available. The availability of daily downscaled data allows for better characterization of climate extremes, especially for precipitation. The availability of high spatial resolution (10 km instead of hundreds of km in global climate models or GCMs) provides better data to represent site-specific information for the study.

The climate change impact assessment for this study considers 136 bias-corrected climate projections from two distinct data sources:

- BCCAQ v2: Pacific Climate Impact Consortium (ClimateData.ca) data using Bias Correction/Constructed Analogues with Quantile mapping reordering (BCCAQ) version 2– (ClimateData 2019)
- GDO-DCP LOCA: Bias Correct models using Localized Constructed Analogs (LOCA, Pierce et al. 2014 and Reclamation 2013)

The BCCAQv2 data consists of 24 models (72 projections), using RCP 2.6, RCP4.5, and RCP8.5, and the LOCA data consists of 32 models for RCP 4.5 and RCP 8.5 only (64 projections), for a total of 136 projections for the dataset (hereinafter referred as the ensemble). The GCMs that were incorporated into each downscaling method are shown in Table A.4. Additional information on each model including the associated institution and resolution and methods used for each model component are provided in Appendix A of Flato et al. (2013). The downscaled projections are available for two different horizontal resolutions: 1/8 degree or approximately 12 km (BCCAQv2) and 1/16 degrees or approximately 6 km (LOCA). Both datasets provide downscaled climate model results from 1950 to 2100 for daily total precipitation, minimum temperature, and maximum temperature.

Table A.4: Global Climate Models used in BCCAQv2 and LOCA Downscaling Methods

Dataset Characteristic	ClimateData.ca (BCCAQv2)	GDO-DCP Archive (LOCA)
Climate Models		
ACCESS1-0	—	X
ACCESS1-3	—	X
bcc-csm1-1	X	X
bcc-csm1-1-m	X	X
BNU-ESM	X	—
CanESM2	X	X
CCSM4	X	X
CESM1-BGC	—	X
CESM1-CAM5	X	X
CMCC-CM	—	X
CMCC-CMS	—	X
CNRM-CM5	X	X
CSIRO-Mk3-6-0	X	X
EC-EARTH	—	X
FGOALS-g2	X	X
GFDL-CM3	X	X
GFDL-ESM2G	X	X
GFDL-ESM2M	X	X
GISS-E2-H	—	X

Dataset Characteristic	ClimateData.ca (BCCAQv2)	GDO-DCP Archive (LOCA)
GISS-E2-R	—	X
HadGEM2-AO	X	X
HADGEM2-CC	—	X
HadGEM2-ES	X	X
INMCM4	—	X
IPSL-CM5A-LR	X	X
IPSL-CM5A-MR	X	X
MIROC5	X	X
MIROC-ESM	X	X
MIROC-ESM-CHEM	X	X
MPI-ESM-LR	X	X
MPI-ESM-MR	X	X
MRI-CGCM3	X	X
NorESM1-M	X	X
NorESM1-ME	X	—
Spatial Resolution		
6 km	—	X
12 km	X	—
Years Available		
1950 - 2100	X	X
Climate Variables		
Minimum Temperature	X	X
Maximum Temperature	X	X
Mean Temperature	X	X
Total Precipitation	X	X

Both data sources provide spatially downscaled data; however, the BCCAQv2 approach has some drawbacks that makes it difficult to find good analog days for the entire domain as the domain size increases. It is also more likely that the model can miss days with precipitation and localized extreme precipitation events that are important to capture. These drawbacks are discussed in detail in *Downscaled CMIP3 and CMIP5 Climate Projections* by Bracken (2016). The LOCA approach was developed to address these issues of BCCAQv2 and was therefore used in this analysis.

The ClimateData.ca portal provides statistically downscaled daily Canada-wide climate scenarios, at a gridded resolution of 300 arc-seconds (or roughly 10 km) for the simulated period of 1950-2100 (ClimateData.ca 2019). The climate variables available from ClimateData.ca data include minimum temperature, maximum temperature and precipitation. The selection of data for this project is based on the available temporal and spatial resolution of the data. The availability of daily downscaled data allows for better characterization of the climate extremes, especially for precipitation. The availability of high spatial resolution (10 km instead of hundreds of km in GCMs) provides better representation for site-specific studies like this project.

The LOCA data is retrieved from the GDO-DCP archive, which provides fine spatial resolution translations of climate projections using three downscaling techniques including daily LOCA for the United States. The archive uses global climate projections from the World Climate Research Programme's (WCRP) CMIP3 and CMIP5 multi-model dataset that was used for the IPCC fifth assessment report (GDO-DCP 2019).

GCM projections are downscaled to a finer resolution using the Bias Correction/Constructed Analogues with Quantile mapping reordering version 2 (BCCAQv2) developed by the Pacific Climate Impacts Consortium (PCIC) (ClimateData.ca 2019). This downscaling method is a statistical algorithm that disaggregates the GCM outputs to a finer spatial and temporal resolution; in other words, they take the gridded data and calculate values that reflect the local conditions that cannot be simulated by the GCM. The Bias Correction/Constructed Analogues with Quantile mapping reordering interpolates spatially to a finer scale daily. More detailed description and model performance can be found in Werner and Cannon (2016).

Since no one model or climate scenario can be viewed as completely accurate, the IPCC recommends that climate change assessments use as many models and climate scenarios as possible, or a "multi-model ensemble". For this reason, the multi-model ensemble approach is used in this study to delineate the probable range of results and better capture the actual outcome (an inherent unknown). Best practices recommend using all plausible futures for greenhouse gases that includes to best- and worst-case scenarios (RCP 2.6, 4.5, 6.0, and 8.5) when considering long timescales to address uncertainty. In addition, a multi-model ensemble is also recommended since the mean of an ensemble is generally closer to the observed values for past climate than any given individual model or scenario (Charron 2016).

Before beginning the future climate projections, the 136 potential members of the multi-model ensemble are reviewed to observe whether the general temperature and precipitation ranges reasonably match the observed ranges of climate for the region. Monthly averages are used to capture the known seasonality of the region. From this evaluation, all scenarios from the ensemble demonstrated typical behaviour within the current climate normal for the region and within the monthly averages.

The downscaled data has a daily temporal resolution (GCMs typically have monthly temporal resolution) which allows for the characterization of future climate extremes. In addition, the improved horizontal resolution of 10 km in the downscaled data could better improve the representation of the study area, given the complex terrain in study area.

A.3.2.2 Uncertainty of Climate Change Downscaling Methods

To address the inherent uncertainty associated with climate change projections, multiple projections from multiple models and scenarios are used in this study. ECCC (2016) recommends that multiple climate models and emission scenarios should be used to overcome the range of natural climate variability and uncertainties regarding future greenhouse gas emissions pathways and climate response. Instead of selecting one single projection, projections from all available model runs are used to describe the probable range of results. The future projections are provided in terms of percentiles of the range of future climate projections.

A.3.3 PROJECTING FUTURE RAINFALL STATISTICS (IDF CURVES)

This subsection describes the methodology to estimate IDF curves using modelled data from the ensemble and the methodology to assess changes to future rainfall (i.e., 2050s and 2080s), when compared to model baseline from the ensemble. This section, specifically, describes in detail Golder's IDF curve updating methods, including the Quantile Delta Method (QDM) and the Ratio Method (RM). This section supports the results and analysis presented in Section 4.2 of the main report.

The ensemble approach is used to obtain daily precipitation (1950 to 2100) to develop IDF curves representative of the model baseline (ideally same period as the current climate baseline) and the desired future periods, following the methods described in Section A.2.2. Specifically, IDF curves are developed for multi-day precipitation (methodology described in Section A.2.2.2.) and for sub-daily and daily observations applied only at stations with sub-daily observation records (methodology described in Section A.2.2.1). Statistical distributions (A.2.2.3) and goodness-of fit tests (A.2.2.5) are completed for each IDF developed under this task.

Once the IDF curves are developed for each climatic projection (model baseline and desired future periods), each model within the ensemble (approximately 136 models sourced from ClimateData.ca and LOCA) and each duration (e.g., multi-day precipitation or sub-daily and daily precipitation), future IDF curves are then compared to model baseline IDF curves. The QDM and RM methods are selected to produce a statistical range for the percentage change in absolute values.

The difference in IDF estimates between the QDM and RM models, across the entire ensemble is used to present the changes from the model baseline over a range of percentiles for selected return periods and duration of storm. Percent changes in precipitation associated with the 50th percentile are presented in Section 4.2. Detailed percentile differences across the dataset are presented Appendix B.

The projected change in the IDF curves can be applied to the observed estimates in order to obtain absolute values adjusted for climate change. This is represented by the equation given below:

$$IDF_{future} = IDF_{observed} \cdot (1 + IDF_{change}) \quad \textbf{Equation 41}$$

Where the absolute value for the future IDF estimate (IDF_{future}) is obtained using the observed IDF estimate ($IDF_{observed}$) and the percentage change (IDF_{change}) projected under the selected future conditions. All changes should be applied for the same return periods and durations between the future percentage changes and the observed IDF estimates. For example, if the observed IDF estimate ($IDF_{observed}$) is 109.8 mm for the 1-day 100-year return period and the projected percentage change at the 50th percentile (IDF_{change}) is 14.3% for the 1-day 100-year return period, the estimated future IDF absolute value (IDF_{future}) is 109.8 mm * (1 + 0.143) = 125.5 mm.

A.3.3.1 Quantile Delta Mapping (QDM)

This method is based on the Equidistant Quantile Matching (EQM) algorithm (Li et al. 2010, Piani et al. 2010, Hassanzadeh et al., 2014, Srivastav et al., 2014, Cannon et al. 2015 and Schardong et al. 2018). First, the current climate baseline (based on observations), model baseline, and modelled future annual maximum rainfall datasets are fitted with statistical distributions. This method is generic to any of the four potential statistical distribution to be tested. Next, the current climate baseline annual maximum rainfall and model baseline annual maximum rainfall are equated using a functional relationship. This relationship establishes a mathematical connection between daily modelled and sub-daily observed annual maximum precipitation. Projected changes in climate (Δ_m) are calculated between the quantiles of the model baseline ($IDF_{baseline}$) and future (IDF_{future}) distributions corresponding to selected return periods of the IDF curve. This is done using the following equation for a given sub-daily duration i,

$$\Delta_{m_i} = \frac{IDF_{future_i}}{IDF_{baseline_i}} - 1 \quad \textbf{Equation 42}$$

The projected future sub-daily IDF ($IDF_{projected}$) is then calculated using the functional relationship (f) established previously, along with the projected changes in climate (Δ_m) for each sub-daily duration.

$$IDF_{projected_i} = f\left(IDF_{baseline_i}\right) \cdot \Delta_{m_i} \quad \textbf{Equation 43}$$

After the distribution of the future sub-daily IDF has been obtained, extreme values are then extracted using the inverse cumulative distribution function with the probability of the selected return periods.

Downscaled climate projections from the data portals used here are limited to daily temporal resolutions. Therefore, sub-daily rainfall projections are not available, and it is assumed here that the projected changes in the 1-day modelled IDFs is uniform across the sub-daily durations. This allows for Δ_m to be constant for each sub-daily rainfall duration. Applying changes in daily to sub-daily precipitation extremes has been done in the past; however, it should be noted that changes in atmospheric processes governing rainfall production will unlikely be uniform for short to long time durations (e.g., convective scale processes at shorter durations versus large scale synoptic systems at longer durations) (CSA 2012). Therefore, the projected changes in sub-daily extremes should be interpreted with caution, and values used for design purposes should select a higher percentile to account for uncertainty related to the projected changes in sub-daily precipitation extremes.

The QDM, as well as the EQM, follows the steps presented in the flowchart of Figure A.4.

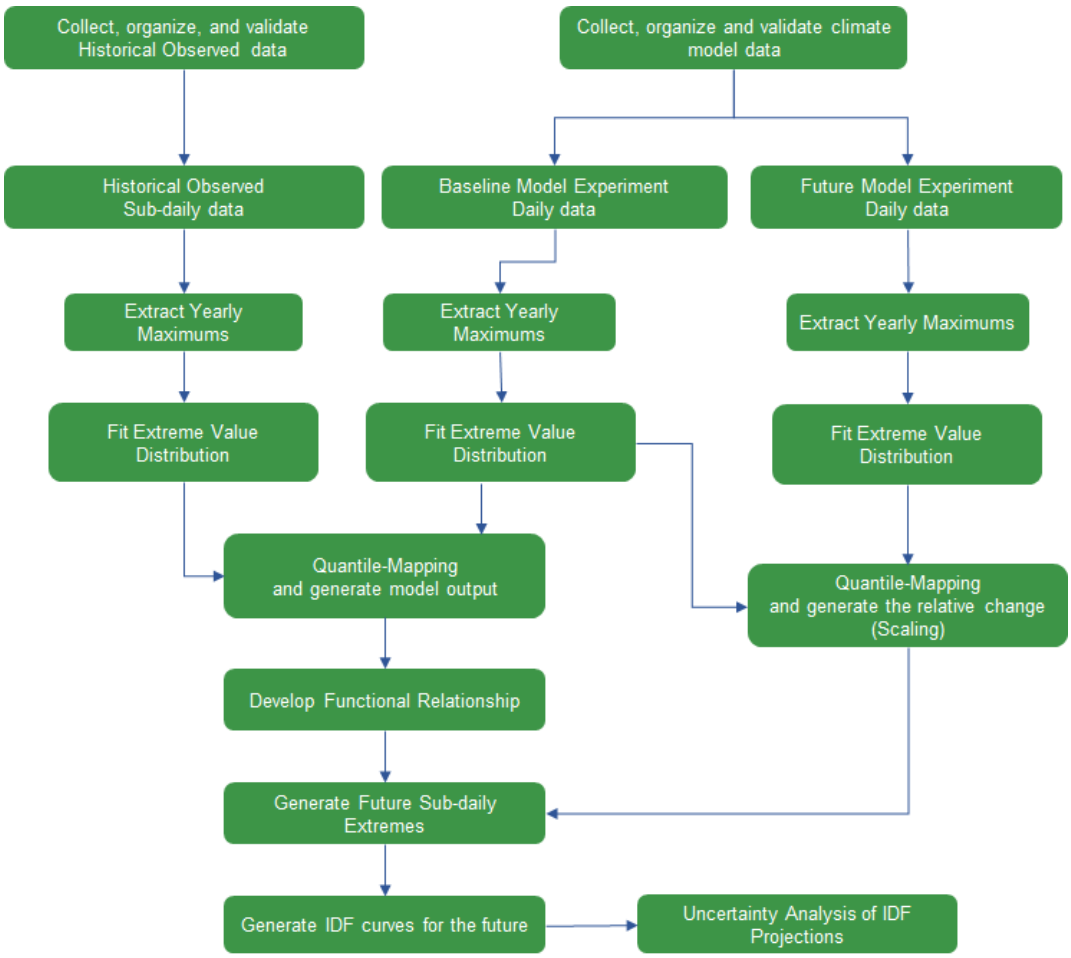

Figure A.4: QDM Method Flowchart (Adopted from Schardong and Simonovic 2019)

A.3.3.2 Ratio Method (RM)

The Ratio Method (RM) (Olsson et al. 2009) is generic for any statistical distribution selected and allows for analysis of any return period, including the 500-year return period. Details on how RM has been used in this work are shown in Figure A.5. Ratios are calculated between the model baseline and future projected IDF curves which signify the projected changes due to climate change. Since this method uses only the daily GCM results to estimate a percentage change between baseline and future conditions, the smallest timestep for which a percent change is generated is one-day. The 1-day changes are then applied uniformly to each sub-daily duration. The inclusion of the RM method in addition to the QDM method captures an additional source of uncertainty pertaining to the method used for updating the IDF curves for climate change, as the results of both methods are used when generating percentile levels from the multi-model ensemble.

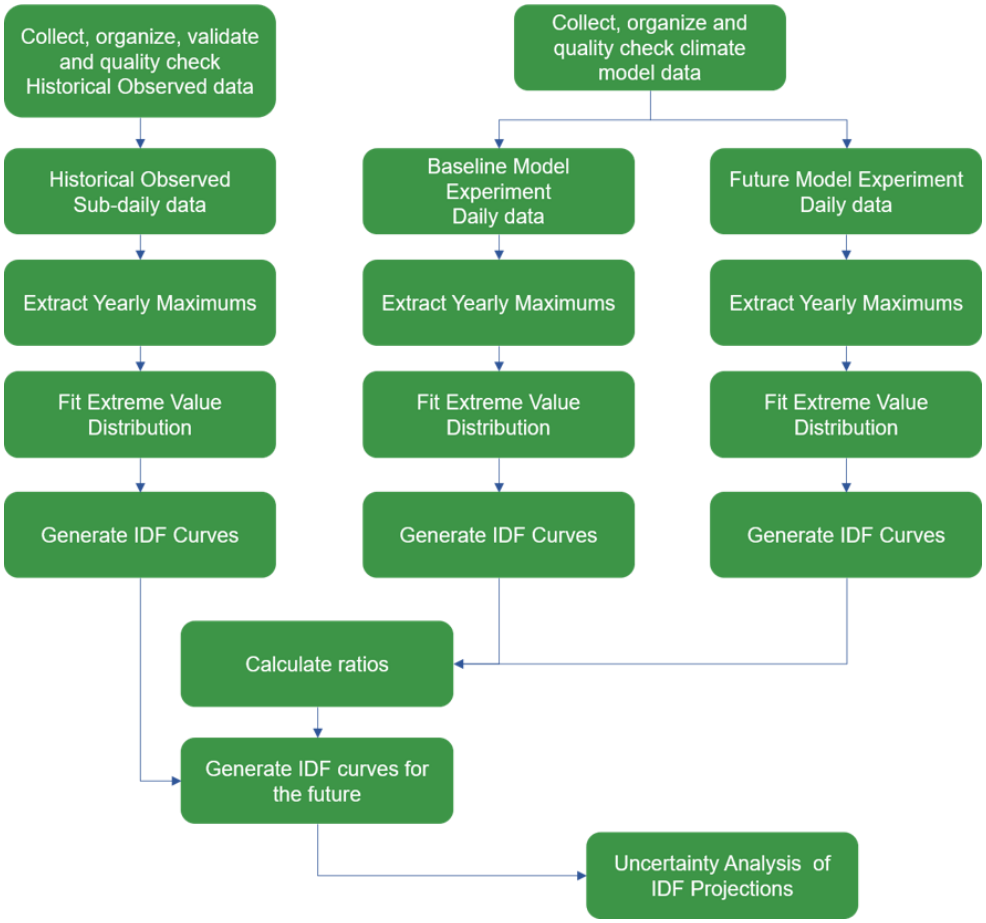

Figure A.5: Ratio Method Flowchart

A.3.4 PROJECTING FUTURE CHANGES IN PMPS

Future climate projections follow the steps outlined in Figure A.2. First, downscaled daily climate projections are obtained (Step 6). Next, variables relevant to the estimation of PMP using the Moisture Maximization and Hershfield methods are extracted which include daily total precipitation and daily minimum temperature (Step 7). The results for the future time periods using these methods are calculated (Step 8). Percentiles are calculated across the results of both methods used for all members of the multi-model ensemble. The percentage changes for each percentile are then applied to the DAD tables for current climate presented in Section 3.3.3 (Steps 9 and 10). All percentiles for the DAD tables are given in Appendix B, which provide an indication of the level of uncertainty associated with the climate projections on the DAD tables (Step 11).

The change in PMP for the future are presented as percent changes between the model baseline period (1950- 1993) and the selected future periods (2050s and 2080s) across all models within the ensemble. The Hershfield method follows the same approach used to develop PMP estimates for current climate (see Section A.2.3).

The Moisture Maximization method requires the moisture content and other variables, which are not readily available from the modelled climate datasets. In order to calculate the moisture content for the model result datasets that do not provide this variable, the daily minimum temperature projections from the multi-model ensemble are used as a proxy for the dew point temperature, which is used to estimate saturation vapor pressure. The saturation vapor is then used as a proxy for the precipitable water. No additional proxies are required to be used to describe other variables. Uncertainty regarding the projected changes in PMP from the multi-model ensemble is shown using percentiles which demonstrate how the PMP projections are distributed. The minimum and maximum projections were calculated, along with those corresponding to the 5th, 25th, 50th, 75th, and 95th percentiles.

The projected change in the PMP values can be applied to the observed estimates in order to obtain absolute values adjusted for climate change. This is represented by the equation given below:

$$PMP_{future} PMP_{future} = PMP_{observed} \cdot (1 + PMP_{change}) \quad \textbf{Equation 44}$$

Where the future value for the PMP estimate (PMP_{future}) is obtained using the observed PMP estimate ($PMP_{observed}$) by the percentage change (PMP_{change}) in the value for the PMP.

A.3.5 PROJECTING FUTURE CHANGES IN RAIN ON SNOW AND SNOWPACK

The method for projecting changes in rain on snow and snowpack follows the method applied to the baseline climate described in Section A.2.4. Daily snowpack and snowmelt is estimated for each of the models in the ensemble methodology adopted by ECCC (Louie and Hogg 1980), and snowmelt is added to assumed rainfall to estimate rain on snow. The method uses a degree-day method, which assumes that in the case of sub-zero temperatures, precipitation falls as snow, which can accumulate to form snowpack. For temperatures above zero, precipitation falls as rain and accumulated snow begins to melt. The resulting annual maximum series for rainfall and snowmelt for each model and baseline/future period is then fitted to a Gumbel distribution to estimate the return period, and the resulting return values are then compared within each model to estimate a percentage change between the baseline and the future periods.

A.3.6 PROJECTING FUTURE CHANGES IN ADDITIONAL CLIMATE VARIABLES

The method for projecting changes in the additional climate variables follows the method applied to the baseline climate described in Section A.2.5. For each of the additional climate variables, projected changes are obtained using the approach outlines in the following sections.

A.3.6.1 Projecting Future Changes in Monthly Mean, Minimum, and Maximum Temperature and Precipitation

Minimum and maximum daily temperature from the multi-model ensemble of climate projections are first averaged into the mean temperature for all calendar months across all years in the model baseline and future time periods corresponding to the 2050s and 2080s. For each calendar month, the difference between the model baseline and future time periods is calculated. In the case of precipitation, the daily precipitation totals are first summed into monthly totals, then the average of the monthly totals is taken for each calendar month. The percentage difference from the model baseline to the future time periods is provided for each calendar month.

Daily future timeseries are provided from the multi-model ensemble for both precipitation and temperature climate variables. For precipitation, a bias correction step is needed to account for artifacts in the modelled daily values. Although statistically downscaled climate models discussed in Section A.3.2.1 have a higher spatial resolution than GCMs (10 km instead of hundreds of km), there are still issues with the statistically downscaled projections including:

- Artifacts from the GCMs, resulting in drizzle (more frequent low intensity precipitation), and under representation of precipitation extremes.
- The data used for bias correction of the statistically downscaled climate products may be inappropriate for the location of the site due to interpolation of point values in the gridded datasets used in the downscaling process.

In the analyses for future climate presented in the previous sections, the changes between the model baseline and future climate periods are calculated to mitigate bias that remains present in the downscaled climate products. Here, a bias correction methodology is presented to obtain the most representative data for the site climate. The bias correction is applied to precipitation only, as temperature is generally well represented by climate models and downscaled climate products.

The Quantile Delta Mapping (QDM) method of Cannon (2015) is used for bias correction, as the correction can be applied to different segments of the precipitation distribution. This allows for the correction of drizzle in days with low amounts of precipitation, as well as days with extreme precipitation amounts. The QDM bias correction is applied using on a monthly timescale, which is interpolated for each day of the year. This allows for seasonal bias to be corrected without introducing additional artifacts near the boundary between months or seasons. The QDM method for bias correction is similar to that used for updating future rainfall statistics in Section A.3.3.1, but there are key differences. First, the relationships are built between the observed and model baseline data and are applied to the future projections to correct for bias. Second, quantiles are extracted from the empirical distribution using linear interpolation, rather than fitting a statistical distribution to each dataset. The method is applied using the following steps:

1. For a calendar month extract data for all years.
2. Extract a set of Q_{m_i} evenly spaced quantiles from the observed and model baseline empirical cumulative distributions across the range of non-exceedance probabilities, P_i.
3. Compute bias-correction factors, CF_{m_i} for each Q_i by taking the difference between those obtained from Step 2.
4. Apply linear interpolation of monthly correction factors to daily correction factors (for each day of the year) from the center day of each month, resulting in the set of correction factors CF_{d_i}.
5. For each day in the future projected dataset, find the closest probability to those in the set of P_i from Step 2, and apply the corresponding CF_{d_i} using addition.
6. Repeat Steps 1 to 4 for each day of the year. The future dataset is now corrected for bias with the fundamental assumption that the difference between observed and model baseline datasets will be preserved in the future (Wang and Chen 2014).

The calculation (Step 3) and application (Step 5) of additive correction factors allows for wet and dry day frequencies to be corrected as multiplicative correction factors will not be applied in regions of the precipitation distribution where there are all zeros for either the observed or model baseline datasets. Anandhi et al. (2011) recommends that when using additive correction factors, the set of evenly spaced quantiles should be greater than 25 to minimize differences between additive and multiplicative correction factors. In this work, 50 evenly spaced quantiles are used in order to correct for bias in precipitation extremes.

The corrected daily timeseries of precipitation and derived variables including rain, snow, and snow depth are provided. Daily timeseries for temperature and potential evapotranspiration are included but are not bias corrected as mentioned above.

A.3.6.2 Projecting Future Changes in WMO Climate Indices

The WMO climate indices are first calculated for the model baseline and future periods using the method described in Appendix A.3.6.2. Projected changes in the WMO climate indices are obtained by taking the difference in the maximum, minimum, mean, and median values calculated across years between the model baseline and the 2050s and 2080s future time periods.

A.3.6.3 Projecting Future Changes in Potential Evapotranspiration

Projected change in potential evapotranspiration are estimated by first calculating potential evapotranspiration using the statistically downscaled minimum and maximum temperature projections from the multi-model ensemble. Monthly totals are then taken and averaged across calendar months. The percentage change between the monthly values between the model baseline and future time periods is calculated for each member of the multi-model ensemble. The distribution of percentage changes across the multi-model ensemble is then provided using a set of percentiles. Daily future timeseries are provided for potential evapotranspiration using the downscaled temperature projections from the multi-model ensemble, using the same methodology as Appendix A.2.5.3.

A.3.6.4 Projecting Future Changes in the Drought Index

The drought index is first calculated with the method describes in Appendix A.2.5.4 using statistically downscaled precipitation and temperature projections for each member of the multi-model ensemble. The percentage change is taken for each month and percentile between the model baseline and future time periods.

A.3.6.5 Qualitative Changes in Wind Speed and Relative Humidity

Changes in windspeed and relative humidity are provided using the best available information applicable to the Ignace study area. Both windspeed and relative humidity climate variables are not available in the set of statistically downscaled climate projections from Climatedata.ca. However, the ECCC provides projected surface wind speed changes based on an ensemble of 29 global climate models from the CMIP5 on a 1°x1° grid across Canada (ECCC 2018). The projected changes from the grid cell closest to the Ignace study area are extracted, and percentiles across the multi-model ensemble are presented for each future period and climate scenario available. This information should be interpreted qualitatively, as the global climate models have a very course spatial resolution and may not be representative of the study area.

In the absence of literature values, relative humidity can be estimated using the August-Roche-Magnus approximation, which implies that saturation vapor pressure changes approximately exponentially with temperature under typical atmospheric conditions (Alduchov and Eskridge 1996).

$$Relative\ Humidity = \frac{\exp\left(\frac{17.625 \cdot t_D}{243.04 + t_D}\right)}{\exp\left(\frac{17.625 \cdot t}{243.04 + t}\right)} * 100\% \qquad \textbf{Equation 45}$$

Where t is the mean daily temperature and t_D corresponds to the dewpoint temperature, which is assumed to be the minimum daily temperature (all in °C).). This assumption was also made for storm maximization in DAD curve development (Appendix A.2.3.2). Relative humidity is calculated using this equation for each member of the multi-model ensemble. Monthly mean values are then calculated and summarized using a set of percentiles.

REFERENCES

Alduchov, O. A. and R. E. Eskridge. 1996: Improved Magnus' form approximation of saturation vapor pressure. Journal of Applied Meteorology, 35, 601–609.

Anandhi, A., F. Allan, D.C. Pierson, E.M. Schneiderman, M.S. Zion, D. Lounsbury and A.H. Matonse. Examination of change factor methodologies for climate change impact assessment. Water Resources Research, 47(3). doi: 10.1029/2010WR009104.

Bracken, C. 2016. Downscaled CMIP3 and CMIP5 Climate Projections – Addendum, Release of Downscaled CMIP5 Climate Projections (LOCA) and Comparison with Preceding Information. Bureau of Reclamation. Retrieved from https://gdo-dcp.ucllnl.org/downscaled_cmip_projections/techmemo/Downscaled_Climate_Projections_Addendum_Sept2016.pdf.

Canadian Standards Association (CSA). 2012. Draft Standard Plus 4013-12 Technical Guide Development, Interpretation and Use of Rainfall Intensity-Duration-Frequency (IDF) Information: Guideline for Canadian Water Resources Practitioners. Toronto, Canada.

Cannon, A.J., S.R. Sobie and T.Q. Murdock. 2015. Bias Correction of GCM Precipitation by Quantile Mapping: How Well Do Methods Preserve Changes in Quantiles and Extremes? Journal of Climate, 28(17), 6938-6959. DOI: 10.1175/JCLI-D-14-00754.1.

Charron, I. 2016. A Guidebook on Climate Scenarios: Using Climate Information to Guide Adaptation Research and Decisions, 2016 Edition. Ouranos, 94 pages.

Cunnane, C. 1989. Statistical Distributions for Flood Frequency Analysis. Operational Hydrology Report no. 33, World Meteorological Organization.

Environment and Climate Change Canada (ECCC). 2020. Canadian Climate Normals. Government of Canada. Available at: https://climate.weather.gc.ca/climate_normals/.

Environment and Climate Change Canada (ECCC). 2019a. Engineering Climate Datasets. Available at https://climate.weather.gc.ca/prods_servs/engineering_e.html. Accessed June 15, 2019.

Environment and Climate Change Canada (ECCC). 2019b. Historical Climate Data. Available at: http://climate.weather.gc.ca/historical_data/search_historic_data_e.html. Accessed June 15, 2019.

Environment and Climate Change Canada (ECCC). 2018. Projected Surface Wind Speed Change Based on CMIP5 Multi-Model Ensembles. Government of Canada. Available at: https://open.canada.ca/data/en/dataset/e0c71149-db7a-4700-acfd-1c8f9d778354.

Environment and Climate Change Canada (ECCC). 2016. Climate Data and Scenarios for Canada: Synthesis of Recent Observation and Modelling Results. Environment and Climate Change Canada. Available at: https://www.canada.ca/en/environment-climate-change/services/climate-change/publications/data-scenarios-synthesis-recent-observation.html.

FAO (Food and Agriculture Organization). 2006. FAO Irrigation and Drainage Paper NO. 56 Crop Evapotranspiration. Available at http://www.fao.org/docrep/X0490E/X0490E00.htm.

Flato, G., J. Marotzke, B. Abiodun, P. Braconnot, S.C. Chou, W. Collins, P. Cox, F. Driouech, S. Emori, V. Eyring, C. Forest, P. Gleckler, E. Guilyardi, C. Jakob, V. Kattsov, C. Reason and M. Rummukainen. 2013: Evaluation of Climate Models. In: Climate Change 2013: The Physical Science Basis. Contribution of Working Group I to the Fifth Assessment Report of the Intergovernmental Panel on Climate Change [Stocker, T.F., D. Qin, G.-K. Plattner, M. Tignor, S.K. Allen, J. Boschung, A. Nauels, Y. Xia, V. Bex and P.M. Midgley (eds.)]. Cambridge University Press, Cambridge, United Kingdom and New York, NY, USA.

GDO-DCP. Downscaled CMIP3 and CMIP5 Climate and Hydrology Projections. Accessed 2019. Retrieved from https://gdo-dcp.ucllnl.org/downscaled_cmip_projections/#Welcome.

Guo, J.C.Y, B. Urbonas and K. Stewart. 2001. Rain Catch under Wind and Vegetal Cover Effects. Journal of Hydrologic Engineering, Vol. 6, Issue 1. https://doi.org/10.1061/(ASCE)1084-0699(2001)6:1(29).

Hassanzadeh, E., A. Nazemi and A. Elshorbagy. 2014. Quantile-Based Downscaling of Precipitation using Genetic Programming: Application to IDF Curves in the City of Saskatoon. J. Hydrology. Eng., 19(5), 943-955.

Hogg, W. D., D. A. Carr and B. Routledge. 1989. Rainfall Intensity–Duration–Frequency Values for Canadian Locations. Ottawa: Environment Canada, Atmospheric Environment Service.

Hosking, J.R.M. and J.R. Wallis. 1997. Regional Frequency Analysis. Cambridge University Press, Cambridge, U.K.

Intergovernmental Panel on Climate Change (IPCC). 2013. Climate Change 2013: The Physical Science Basis. Contribution of Working Group I to the Fifth Assessment Report of the Intergovernmental Panel on Climate Change. Retrieved on March 15, 2017 from https://www.ipcc.ch/report/ar5/wg1/.

Intergovernmental Panel on Climate Change (IPCC). 2020. The IPCC and the Sixth Assessment Cycle. Retrieved on May 8th, 2020 from https://www.ipcc.ch/site/assets/uploads/2020/05/2020-AC6_en.pdf.

Li, H., J. Sheffield and E.F. Wood. 2010. Bias Correction of Monthly Precipitation and Temperature Fields from Intergovernmental Panel on Climate Change AR4 Models Using Equidistant Quantile Matching. Journal of Geophysical Research, 115(D10), D10101.

Louie, P. Y. T. and W. D. Hogg.1980. Extreme Value Estimates of Snowmelt. Proceedings of Canadian Hydrology Symposium 80 (Toronto, ON: 64-78 National Research Council Canada).

Mekis, É. and L.A. Vincent. 2011. An Overview of the Second Generation Adjusted Daily Precipitation Dataset for Trend Analysis in Canada. Atmosphere-Ocean 49, 163–177. https://doi.org/doi: 10.1080/07055900.2011.583910.

Millington, N., S. Das and S.P. Simonovic. 2011. The Comparison of GEV, Log-Pearson Type 3 and Gumbel Distributions in the Upper Thames River Watershed under Global Climate Models. Water Resources Research Report no. 077, Facility for Intelligent Decision Support, Department of Civil and Environmental Engineering, London, Ontario, Canada, 53 pages. ISBN: (print) 978-0-7714-2898-2; (online) 978-0-7714-2905-7.

National Aeronautics and Space Administration (NASA). 2019. Modern-Era Retrospective analysis for Research and Applications, Version 2. Retrieved from https://gmao.gsfc.nasa.gov/reanalysis/MERRA-2/.

Olsson, J., K. Berggren, M. Olofsson and M. Viklander. 2009. Applying Climate Model Precipitation Scenarios for Urban Hydrological Assessment: A Case Study in Kalmar City, Sweden. Atmos. Res., 92:364–375, doi:10.1016/j.atmosres.2009.01.015.

Ontario Ministry of Natural Resources (OMNR). 2006. PMP for Ontario. Prepared by IBI Group. December 2006.

Overeem, A., A. Buishand and I. Holleman. 2007. Rainfall Depth-Duration-Frequency Curves and Their Uncertainties. Journal of Hydrology. 348(1-2), 124-134. DOI:10.1016/j.jhydrol.2007.09.044.

Piani, C., G.P. Weedon, M. Best, S.M. Gomes, P. Viterbo, S. Hagemann and J.O. Haerter. 2010. Statistical Bias Correction of Global Simulated Daily Precipitation and Temperature for the Application of Hydrological Models. Journal of Hydrology, 395(3-4), 199–215.

Pierce, D. W., D. R. Cayan and B. L. Thrasher. 2014. Statistical Downscaling Using Localized Constructed Analogs (LOCA), Journal of Hydrometeorology, 15(6), 2558-2585.

Pysklywec, D.W., K.S. Davar and D.I. Bray. 1968. Snowmelt at an Index Plot, Water Resource, 4(5), 937-946.

Reclamation, 2013. Downscaled CMIP3 and CMIP5 Climate Projections: Release of Downscaled CMIP5 Climate Projections, Comparison with Preceding Information, and Summary of User Needs. U.S. Department of the Interior, Bureau of Reclamation, Technical Service Center, Denver, Colorado, 116 p. Available at: http://gdo-dcp.ucllnl.org/downscaled_cmip_projections/techmemo/downscaled_climate.pdf.

Salmi, T., A. Määttä, P. Anttila, T. Ruoho-Airola and T. Amnell. 2002. Detecting Trends of Annual Values of Atmospheric Pollutants by the Mann-Kendall Test and Sen's Slope Estimates – The Excel Template Application MakeSens. Publications on Air Quality, No. 31.

Schardong A., A. Gaur, S.P. Simonovic and D. Sandink. 2018. Computerized Tool for the Development of Intensity-Duration-Frequency Curves under a Changing Climate: Technical Manual v.3. Water Resources Research Report no. 103, Facility for Intelligent Decision Support, Department of Civil and Environmental Engineering, London, Ontario, Canada, 67 pages. ISBN: 978-0-7714-3107-4.

Schardong, A. and S.P. Simonovic. 2019. Application of Regional Climate Models for Updating Intensity-Duration-Frequency Curves under Climate Change. International Journal of Climate Change. 9(5): 311-330. DOI: 10.9734/ijecc/2019/v9i530117.

Srivastav, R.K., A. Schardong and S. P. Simonovic. 2014. Equidistance Quantile Matching Method for Updating IDF Curves under Climate Change, Water Resources Management, 28(9): 2539-2562.

van Vuuren, D.P., J. Edmonds and M. Kainuma et al. 2011. The Representative Concentration Pathways: An Overview. Climatic Change 109, 5. https://link.springer.com/article/10.1007/s10584-011-0148-z.

Werner, A.T. and A.J. Cannon. 2016. Hydrologic Extremes – An Intercomparison of Multiple Gridded Statistical Downscaling Methods. Hydrology and Earth System Sciences. 20: 1483-1508. doi: 10.5194/hess-20-1483-2016.

Wood. 2019. Climate Change Impacts Review and Method Development. Nuclear Waste Management Report NWMO-TR-2019-05. Toronto, Canada. Available at: http://rms.nwmo.ca/Sites/APM/Reports/NWMO-TR-2019-05.pdf.

World Meteorological Organization (WMO). 2009a. Manual on Estimation of Probable Maximum Precipitation (PMP). World Meteorological Organization (WMO). WMO-No. 1045. Geneva, Switzerland.

World Meteorological Organization (WMO). 2009b. Guidelines on Analysis of Extremes in a Changing Climate in Support of Informed Decisions for Adaptation. World Meteorological Organization (WMO). Climate Data and Monitoring WCDMP-No. 72. Geneva, Switzerland.

World Meteorological Organization. 2012. Standardized Precipitation Index: User Guide. Washington, DC: World Meteorological Organization. Technical report: WMO No. 1090. Geneva, Switzerland

APPENDIX B: ADDITIONAL FUTURE CLIMATE STATISTICS

Additional climate statistics tables are provided in the companion spreadsheet for this report. This format was selected in order to allow for the results to be more readily accessible and improve the readability of the report. The minimum, maximum, mean, standard deviation, and a set of percentiles provide information on the distribution of the projected changes in climate from the multi-model ensemble. These statistics are provided for daily, and multi-day IDF curves, PMP, combined rainfall and snowmelt, peak snowpack accumulation for the multi-model ensemble climate projections. Projections for both the 2050s and 2080s time periods for all the statistics are included.

APPENDIX C: DAILY CLIMATE TIME SERIES

Daily current climate timeseries are provided for the baseline period of 1914 to 1992. This includes the daily infilled dataset discussed in Section 3.1.2 of the main report, which includes the infilled daily precipitation, and minimum, maximum, and mean daily temperatures. Derived variables for potential evapotranspiration, rain, snow, and snow depth are also included.

Daily future timeseries are provided for the bias corrected precipitation and derived variables including rain, snow, and snow depth. Minimum, maximum and mean daily temperatures are also provided as well as potential evapotranspiration. For the climate variables, a daily timeseries is provided for each member of the multi-model ensemble for the period of 1950 to 2100. This corresponds to a total of 136 daily timeseries for each of the climate variables. It should be noted that for the period that overlaps the daily current climate timeseries, the daily current climate timeseries should be preferred as it is based on observations instead of modelled results.

If possible, it is recommended each member of the multi-model ensemble be used to capture the full range of uncertainty in the climate projections. If this is not possible (due to computational time constraints for example), a subset of the daily timeseries may be selected in a way that reasonably captures the range of uncertainty in the impact model. For example, if rainfall on snow in the month of April is a critical design parameter for a flood management model, a subset of the daily timeseries that captures the range of rainfall and snowmelt in the month of April may be selected if it is not possible to run all of the climate scenarios. For water balance assessments, an example of scenario selection may focus on combinations of wet, dry, warm, and cold scenarios such as:

- Wet-Cold Climate with a higher precipitation rate and lower evapotranspiration rate (i.e., low air temperature). These conditions may lead to a **net-positive-water-balance**.
- Wet-Warm Climate with a higher precipitation rate and higher evaporation rate.
- Dry-Cold Climate with a lower precipitation rate and a lower evaporation rate.
- Dry-Warm climate with a lower precipitation rate and a higher evaporation rate. These conditions may lead to a **net-negative-water-balance**.

The selection of climate scenarios for use in climate impact assessments that are not able to utilize the full ensemble (136 scenarios) will need to be assessed on a case-by-case basis. The examples provided above may not be applicable to all types of climate change impact assessments. The goal of climate scenario selection is to attempt to select a subset of climate scenarios that may reasonably capture the range of impacts likely be obtained if the full ensemble were utilized.